From the
DEPARTMENT OF MOLECULAR MEDICINE AND SURGERY
Karolinska Institutet, Stockholm, Sweden

LEFT VENTRICULAR REMODELING AND FUNCTION IN ISCHEMIC HEART DISEASE AND AORTIC VALVE DISEASE

Jonas Jenner

Karolinska Institutet

Stockholm 2021

Published by Karolinska Institutet.
Printed by Universitetsservice US-AB, 2021

ISBN 978-91-8016-082-7
Cover illustration: Schematic illustration of a 3D echocardiographic acquisition

LEFT VENTRICULAR REMODELING IN ISCHEMIC HEART DISEASE AND AORTIC VALVE DISEASE

THESIS FOR DOCTORAL DEGREE (Ph.D.)

By

Jonas Jenner, MD

Principal Supervisor:
Professor Kenneth Caidahl
Karolinska Institutet
Department of Molecular Medicine and Surgery
Unit of Clinical Physiology

Co-supervisor(s):
Associate Professor Maria J Eriksson
Karolinska Institutet
Department of Molecular Medicine and Surgery
Unit of Clinical Physiology

Professor Per Eriksson
Karolinska Institutet
Department of Medicine Solna
Unit of Cardiovascular Medicine

Professor Martin Ugander
Karolinska Institutet
Department of Molecular Medicine and Surgery
Unit of Clinical Physiology;
Kolling Institute, Royal North Shore Hospital;
University of Sydney, Sydney Medical School, Sydney, Australia

Opponent:
Professor Eva Nylander
Linköping University
Department of Health, Medicine and Caring Sciences
Division of Diagnostics and Specialist Medicine

Examination Board:
Professor Carl-Johan Carlhäll
Linköping University
Unit for Cardiovascular Sciences, Department of Health, Medicine and Caring Sciences
Division of Diagnostics and Specialist Medicine

Professor Per Lindqvist
Umeå University
Department of Surgical and Perioperative Sciences
Unit of Clinical Physiology

Associate Professor Carl Meurling
Lund University
Department of Clinical Sciences Lund,
Unit of Cardiology

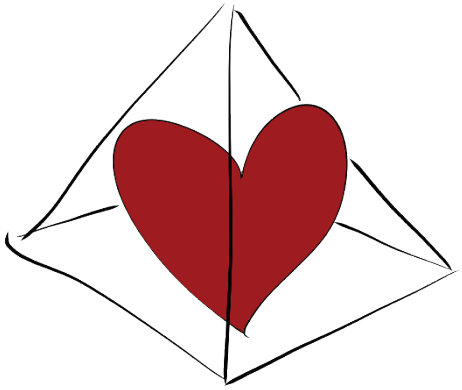

To my family

POPULÄRVETENSKAPLIG SAMMANFATTNING

Hjärtats funktion är att pumpa syrerikt blod till kroppens alla organ och distribuera det återvändande syrefattiga blodet genom lungorna. Hjärtat har en fantastisk förmåga att ständigt tillgodose kroppens omedelbara och långvariga behov. När förutsättningarna och kraven förändras under en längre period, som exempelvis vid träning, graviditet och andra fysiologiska påfrestningar, anpassar hjärtat sin struktur specifikt efter den typ av påfrestning det utsätts för. De förändringar som hjärtat genomgår i relation till förändrade krav eller förutsättningar kallas med ett samlingsbegrepp för remodellering (eng. *remodeling*).

När kraven på hjärtat inte längre är fysiologiska utan beror på sjukdom eller extrem påfrestning kan hjärtats anpassningsmekanismer vara otillräckliga eller till och med inadekvata, vilket i sin tur kan leda till en sviktande hjärtfunktion. Ett sådant tillstånd är aortaklaffläckage, vilket innebär att blod rinner tillbaka från stora kroppspulsådern till hjärtat mellan varje hjärtslag. För att kompensera för detta backflöde måste hjärtat pumpa ut en större blodvolym–vilket leder till en *volymsbelastning*. Ett annat tillstånd är aortastenos–förträngning av aortaklaffen–vilket genererar ett högt blodflödesmotstånd och en *tryckbelastning*. Ett tredje exempel är sjukdomar som direkt påverkar hjärtats pumpfunktion, som exempelvis ischemisk hjärtsjukdom, som beror på syrebrist i hjärtmuskeln på grund av förträngningar i kranskärlen.

Hjärtats struktur och funktion kan studeras med olika metoder, varav den vanligast förekommande är 2D-hjärtultraljud. Under senare år har utvecklingen av 3D-hjärtultraljud tagit fart, med möjliga fördelar jämfört med 2D-hjärtultraljud. Två andra bildgivande metoder för att studera hjärtat är magnetisk resonanstomografi, vilken betraktas som referensmetod för att mäta hjärtvolym, samt *single-photon emission cardiac tomography (*SPECT) som används vid undersökningar av patienter med ischemisk hjärtsjukdom.

Syftet med denna avhandling var att utvärdera värdet av 3D-hjärtultraljud i jämförelse med andra avbildningsmetoder, samt att studera remodellering vid aortaklaffläckage och aortaklaffstenos och vilka faktorer som har betydelse för hjärtats återhämtning efter det att klaffsjukdomen åtgärdats kirurgiskt.

Vi fann att 3D-hjärtultraljud hade högre mätsäkerhet och bättre reproducerbarhet än 2D-hjärtultraljud för bestämning av vänster kammares volym och funktion. Användandet av kontrastmedel förbättrade mätsäkerheten och reproducerbarheten för både 2D- och 3D-hjärtultraljud, där största nyttan sågs för 2D-hjärtultraljud.

Patienter med aortaklaffläckage hade förstorade hjärtan med tecken på försämrade fyllnadsegenskaper (diastolisk dysfunktion). Efter klaffoperation förbättrades den diastoliska funktionen, hjärtvolymen minskade och hjärtfunktionen förbättrades hos de flesta, men inte alla. Hjärtats volym före operation och vänstra förmakets funktion var faktorer som var associerade med huruvida hjärtfunktionen normaliserades eller ej. Hos patienter med aortastenos fann vi att rörligheten i hjärtmuskelväggen (global longitudinell strain) samt hjärtmuskelmassa före operation var associerade med sannolikheten för att återfå normal vänsterkammarmassa efter operation, samt att bestämning av global longitudinell strain med 2D-ultraljud var känsligare för förändringar än motsvarande mätning med 3D-ultraljud.

Dessa fynd har betydelse för valet av undersökningsmetod vid uppföljning av patienter med aortaklaffsjukdom och bidrar med kunskap kring faktorer som påverkar utfallet efter aortaklaffkirurgi.

ABSTRACT

Background: Cardiac remodeling is a broad term that refers to structural and functional alterations of the heart in response to chronic changes in loading conditions or left ventricular (LV) contractile performance. Different loading conditions will affect the heart in different ways, some leading to impaired heart function, symptoms of heart failure, or even death. However, the process of remodeling may not be permanent. If the heart is relieved of the underlying cause of the remodeling, the heart function and structure may normalize in a process referred to as reverse remodeling. The complex interplay of factors that determine the process of reverse remodeling is not fully elucidated. Cardiac remodeling can be evaluated by many different diagnostic modalities, but the most widely used diagnostic tool is two-dimensional echocardiography (2DE). In recent years, three-dimensional echocardiography (3DE) has emerged with possible advantages in the assessment of LV volume and function.

The thesis aimed to evaluate 3DE in the assessment of LV function and remodeling, and to study different aspects of remodeling in response to pressure and volume overload in patients with aortic stenosis (AS) and aortic regurgitation (AR), respectively.

Methods: Studies I and II investigated patients with ischemic heart disease (n = 15 and n = 32, respectively). In Study I, the assessments of LV volume and ejection fraction (EF) were compared using 3DE, cardiac magnetic resonance (CMR), and single-photon emission computer tomography (SPECT). Study II compared the performance of 2DE, contrast-enhanced 2DE, 3DE, and contrast-enhanced 3DE in the assessment LV volumes and EF, using CMR as a reference standard. In Studies III and IV, 65 patients with severe AR and 120 patients with severe AS, respectively, were examined using 2DE and 3DE before and at one year after aortic valve replacement (AVR). In Study III, LV volumes, systolic and diastolic LV function, and left atrial strain (LAS) were analyzed to identify predictors of impaired LV reverse remodeling in AR. Study IV assessed LV functional indices, including 2D global longitudinal strain (GLS) and 3D strain, to assess predictors of incomplete reverse remodeling in AS.

Results and conclusions: There were significant differences among 3DE, SPECT and CMR regarding the measurement of LV volumes. However, the estimation of EF showed good agreement. 3DE was more accurate and showed more favorable reproducibility than 2DE for the assessment of EF and LV volumes. Contrast enhancement improved accuracy and reproducibility for both 2DE and 3DE. One-third of patients with AR had signs of impaired LV diastolic function. After AVR, diastolic LV functional indices improved, LV and left atrial (LA) volumes decreased, and indices of LA function increased. LA conduit strain had an incremental prognostic value for the prediction of impaired LV functional and structural recovery. In patients with AS, AVR was associated with a decrease in LV mass, an improvement in 2D GLS, and a decrease in LV twist. 2D GLS and left ventricular mass index were predictive of incomplete reverse remodeling during the follow-up period. 3D GLS did not add discriminatory or predictive information over 2D GLS.

LIST OF SCIENTIFIC PAPERS

I. Beitner N[*], **Jenner J**[*], Sörensson P. Comparison of Left Ventricular Volumes Measured by 3DE, SPECT and CMR. *J Cardiovasc Imaging*. 2019 Jul;27(3):200-211.

II. **Jenner J**, Sörensson P, Pernow J, Caidahl K, Eriksson MJ. Contrast Enhancement and Image Quality Influence Two- and Three-dimensional Echocardiographic Determination of Left Ventricular Volumes: Comparison With Magnetic Resonance Imaging. *Clinical Medicine Insights: Cardiology.* 2019 Mar 5;13:1–12.

III. **Jenner J,** Ilami A, Petrini J, Eriksson P, Franco-Cereceda A, Eriksson MJ[*], Caidahl K[*]. Pre- and postoperative left atrial and ventricular volumetric and deformation analyses in severe aortic regurgitation. *Cardiovasc Ultrasound.* 2021 Feb 14;19(1):14.

IV. **Jenner J**, Ilami A, Eriksson P, Franco-Cereceda A, Caidahl K[*], Erikson MJ[*]. Prediction of incomplete reverse remodeling by 2D and 3D speckle-tracking echocardiography in severe aortic stenosis. *Submitted*.

---

* Equal contributions

CONTENTS

ABBREVIATIONS

2DE	Two-dimensional echocardiography
3DE	Three-dimensional echocardiography
AR	Aortic regurgitation
AS	Aortic stenosis
AVR	Aortic valve replacement
BSA	Body surface area
CE2DE	Contrast-enhanced two-dimensional echocardiography
CE3DE	Contrast-enhanced three-dimensional echocardiography
CI	Confidence interval
CMR	Cardiovascular magnetic resonance
DD	Diastolic dysfunction
ECG	Electrocardiogram
EDV	End-diastolic volume
EF	Ejection fraction
ESV	End-systolic volume
GCS	Global circumferential strain
GLS	Global longitudinal strain
GRS	Global radial strain
IRR	Incomplete reverse remodeling
IQR	Interquartile range
LA	Left atrium/left atrial
LAS	Left atrial strain
LAScd	Left atrial strain conduit phase
LASct	Left atrial strain contraction phase
LASr	Left atrial strain reservoir phase
LAVi	Left atrial volume index
LOA	Limits of agreement
LV	Left ventricle/left ventricular
LVMi	Left ventricular mass index
MAPD	Mean absolute percentage deviation
MI	Myocardial infarction
OR	Odds ratio
PTS	Principal tangential strain
SPECT	Single-photon emission computer tomography
SV	Stroke volume
TR	Tricuspid regurgitation

1 INTRODUCTION

1.1 LEFT VENTRICULAR REMODELING

The heart functions as a pump to deliver oxygenated blood to the body and propel the returning deoxygenated blood through the pulmonary circulation. Under normal physiological loading conditions, the heart's work is highly effective, and the heart chambers retain their normal size and function. However, when loading conditions change due to either intrinsic factors, such as diseases affecting the heart muscle or the valves, or extrinsic factors, the structure and function of the heart are altered in a process referred to as remodeling. Left ventricular (LV) remodeling is a broad term that refers to structural and functional alterations of the LV in response to chronic changes in loading conditions or LV contractile performance. There are various patterns of LV remodeling and the underlying causes are complex. However, based on the gross morphological features of the LV, the alterations can be divided into three main categories with respect to the LV wall thickness and the presence or absence of increased LV mass: (i) concentric hypertrophy, (ii) concentric remodeling, and (iii) eccentric hypertrophy (Figure 1).[1]

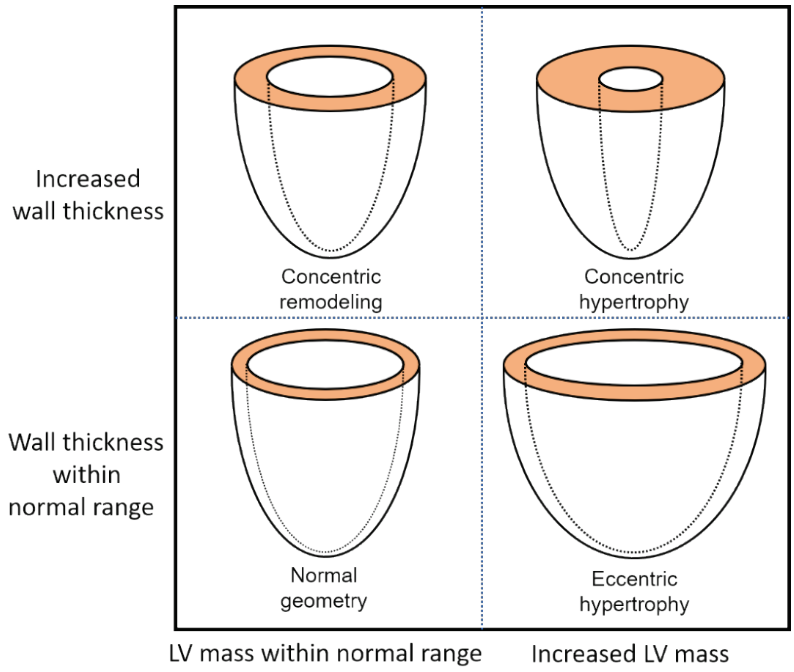

Figure 1 *Morphological patterns of left ventricular remodeling*

Concentric remodeling and concentric hypertrophy refer to increased LV wall thickness, the former associated with preserved LV mass and the latter with increased LV mass. These patterns are typically found in ventricles that have been subjected to sustained pressure overload, which is commonly caused by hypertension or, as in the present thesis, by aortic stenosis (AS). Eccentric hypertrophy refers to increased LV mass with normal or decreased wall thickness, commonly accompanied by an increase in LV volume. This pattern is the hallmark of the volume-overloaded LV, which is represented by aortic regurgitation (AR) in the present thesis. Remodeling might also occur secondary to loss of LV contractile function,

constituting the fourth category. This pattern is seen in ischemic heart disease, where depressed regional or global LV function results in loss of regional or global contractile function and progressive LV dilatation (Figure 2).

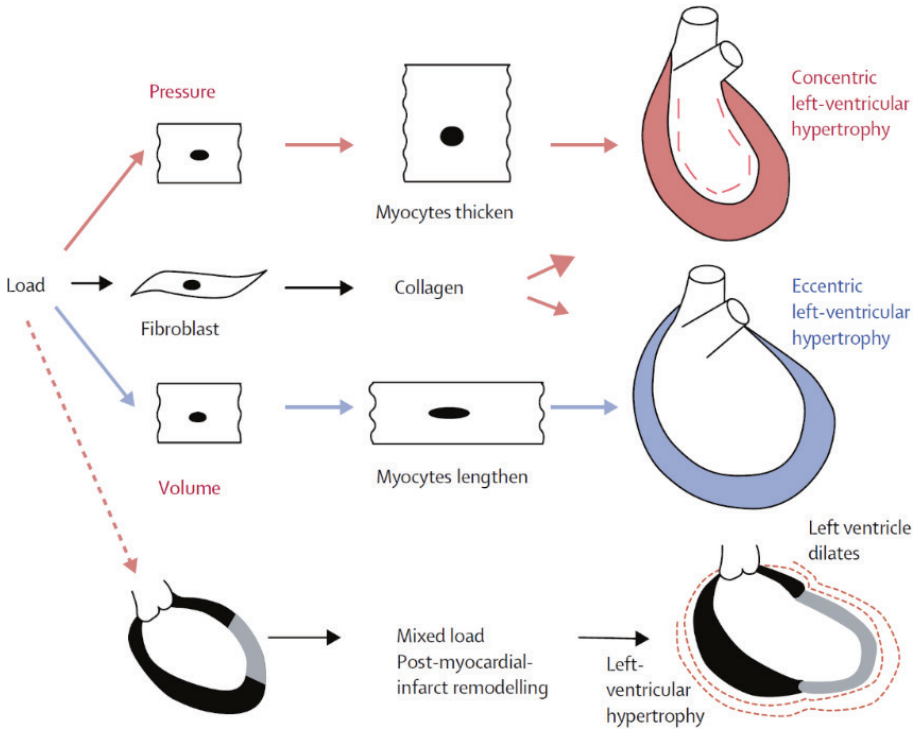

Figure 2 *Three patterns of left ventricular remodeling; concentric hypertrophy in pressure overload, eccentric hypertrophy in volume overload, and remodeling post-infarct in ischemic heart disease.* Reprinted from The Lancet, 367, Opie *et al*. Controversies in ventricular remodelling, 356–67, copyright (2006), with permission from Elsevier

1.2 THE CARDIAC CYCLE IN THE NORMAL LEFT VENTRICLE

LV function dynamics are perhaps best illustrated by the pressure–volume loop (Figure 3). This diagram is generated using invasively acquired LV pressures and volume measurements through the heart cycle and provides a comprehensive overview of the LV contraction and relaxation phases. Time runs counterclockwise in the diagram. The cardiac cycle consists of four phases: (a) ventricular filling, (b) isovolumetric contraction, (c) ejection, and (d) iso-volumetric relaxation.

The first phase is the ventricular filling phase. The curve that defines the filling is the end-diastolic pressure–volume relationship or passive filling curve. The slope of the passive filling curve represents the LV stiffness ($\Delta P/\Delta V$) or inversely, the LV compliance ($\Delta V/\Delta P$). Consequently, the steeper the slope, the lower the compliance and the higher the stiffness. Furthermore, the passive filling curve slope increases with increasing LV volume, meaning that the LV becomes progressively stiffer with increasing volumes. The pressure at the end of the filling phase is the end-diastolic pressure (LVEDP). The LV volume at the end of the filling phase is the LV end-diastolic volume (EDV).

LVEDP and EDV determine LV preload, defined as the load that the cardiac myocytes must overcome at the beginning of contraction. Because LVEDP cannot be quantified non-invasively, EDV is often used as an estimate of preload because it represents the initial stretching of cardiac myocytes before contraction.[2] After the filling phase, the mitral valve closes, and the LV starts its contraction phase, initiating LV systole. During the isovolumetric contraction phase, the LV pressure increases rapidly while the aortic valve is still closed; hence there is no change in LV volume. The aortic valve opens when the LV pressure exceeds the aortic pressure, and blood is ejected from the LV to the aorta and arteries. In the normal heart, the open aortic valve does not impose a significant resistance to flow, so the systolic pressure difference between the LV and aorta is low. The LV relaxes in late systole, and the LV pressure falls slightly below the aortic pressure; blood flow continues due to its inertial energy. When the LV pressure and the inertial energy of the ejected blood fall below the aortic pressure, the aortic valve closes. The residual volume of the LV after the ejection phase is the end-systolic volume (ESV). The width of the loop represents the stroke volume (SV). The following phase is isovolumetric relaxation, which initiates the LV diastole. During this phase, both the aortic and the mitral valves are closed, and the LV pressure falls rapidly without a change in LV volume. The mitral valve opens when the LV pressure falls below the left atrial (LA) pressure, initiating the next ventricular filling phase.

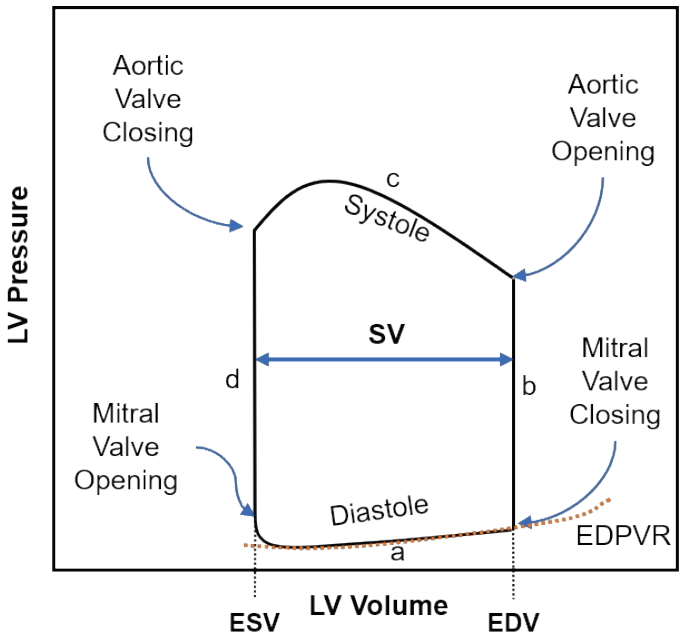

Figure 3 *Normal left ventricular (LV) pressure–volume loop, the end-diastolic volume (EDV) is the maximum volume after LV filling, end-systolic volume (ESV) is the residual volume of the LV at the end of ejection; the difference between EDV and ESV represents the stroke volume. See text for details. EDPVR, end-diastolic pressure–volume relationship.*

Changes in loading conditions or LV contractility lead to characteristic alterations in the pressure–volume loop, as illustrated in Figure 4 and commented on in the next three paragraphs with reference to AS, AR, and ischemic disease.

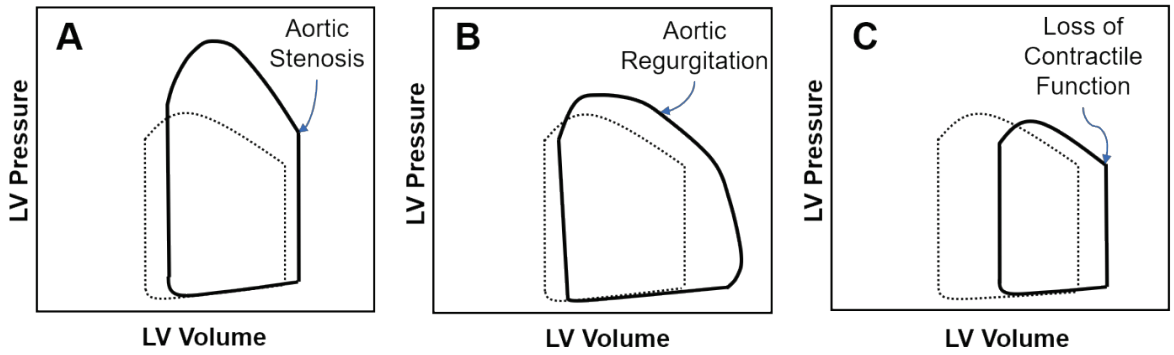

Figure 4 *Effects on the pressure–volume loop from pressure overload in aortic stenosis (A), volume overload in aortic regurgitation (B), and loss of contractile function (C). Note that the effects include compensatory adaptations. Normal dashed pressure-volume loops for reference, see text for details.*

1.3 EFFECTS OF PRESSURE OVERLOAD

The hallmark of LV pressure overload is an increased afterload. Afterload is the impedance (load) against which the LV must work to eject blood. In the absence of LV outflow obstruction, afterload is mainly dependent on the properties of the arterial tree, denoted as arterial load. The interaction between the LV and arterial tree is complex. Several invasive and noninvasive approaches are used to assess afterload, taking into account the relations of pressure and flow in the LV and arterial tree, the systemic vascular resistance, and the total arterial compliance.[3] The effective arterial elastance (E_a), calculated as the LV end-systolic pressure divided by the SV, is regarded as a reliable method to assess total arterial load.[4] However, this approach requires invasive pressure measurements, limiting its practical use. A noninvasive estimation of E_a using systolic arterial pressure as a surrogate for LV pressure has been proposed.[5]

In the present thesis, the pathophysiological alterations associated with LV pressure overload were studied in patients with AS. AS is characterized by a reduced opening of the aortic valve, leading to increased resistance to flow through the valve. Consequently, the severity of valve disease must be considered when assessing LV afterload in patients with AS. Accordingly, the valvulo-arterial impedance (Z_{va}) has been proposed as a noninvasive measure of afterload.[6] The Z_{va} is calculated by dividing the estimated LV systolic pressure by the stroke volume index:

$$Z_{va} = \frac{SAP + AVMPG}{SVi},$$

where SAP is systolic arterial pressure, AVMPG is the aortic valve mean pressure gradient, and SVi is the stroke volume indexed to body surface area (BSA). To overcome the increased afterload, the LV must generate higher systolic pressure during systole, which leads to an increased ESV and a decreased SV. The reduced SV leads to increased EDV (i.e., increased preload) as a secondary mechanism. Increased preload results in an increased contraction force, referred to as Starling's law, which will act to preserve SV (Figure 4A).

Furthermore, increased LV pressure will result in increased LV wall stress (σ), which is proportional to the intraventricular pressure (*P*) and ventricular radius (*r*) and inversely related to wall thickness (*h*) according to the law of Laplace:

$$\sigma \propto \frac{P \times r}{h},$$

LV wall stress can be described as the afterload experienced by the individual muscle fibers in the myocardium, as compared with the arterial afterload imposed on the whole LV as a pump in the description above. Increased LV wall stress acts as a stimulus for LV hypertrophy (i.e., increased LV wall thickness and mass), increasing *h* in the equation above, which will counteract the increased wall stress. However, LV hypertrophy also contributes to decreased relaxation and increased LV stiffness, resulting in an increased slope of the passive filling curve, associated with diastolic dysfunction, and eventually increased LV filling pressure.[1,7]

1.4 EFFECTS OF VOLUME OVERLOAD

In the present thesis, AR serves as a model for the effects of volume overload on the heart. In AR, the LV receives blood from both the mitral inflow and the AR during the filling phase, leading to increased EDV, i.e., increased preload. When the ventricle starts to contract and generate pressure, blood is still entering from the aorta, so there is no proper isovolumic contraction phase.[2] Increased preload leads to increased contraction force by Starling's law, resulting in increased SV (Figure 4B). The increase in SV compensates for the regurgitant volume and preserves cardiac output. Increased SV also leads to increased systolic pressure and increased afterload. ESV might only be increased a small amount in the early stage. The increase in EDV leads to a concomitant increase in diastolic wall stress by increasing *r* in the equation above, acting as a stimulus for a compensatory increase in wall thickness. As long as LV compliance remains normal, it will accommodate the increased volume with normal diastolic pressures, and the patient may not experience any symptoms.[1] However, after prolonged exposure to volume overload, LV dilatation progresses. At a certain point, this process results in increased stiffness, elevated LV filling pressures, and eventually to a decompensated state.[8]

1.5 EFFECTS OF DECREASED CONTRACTILITY

Changes in LV contractility refer to changes in the force of contraction of the myocytes, independent of changes in preload and afterload.[2] When contractility decreases, e.g., in ischemic heart disease, the ESV increases. This change causes a secondary increase in EDV, with a net effect of decreased ejection fraction (EF) calculated as SV/EDV (Figure 4C).

1.6 AORTIC STENOSIS

AS is the most common primary valve disease in North America and Europe.[9] The incidence rate in Sweden is 37.8 and 24.2 per 100,000 person-years in men and women, respectively, and constitutes 47% of the country's total incidence of valvular heart disease.[10] While calcific degeneration in a congenitally bicuspid or normal trileaflet valve is the most common cause of AS in Europe and North America, rheumatic AS is still prevalent worldwide.

Calcific AS was traditionally regarded as a degenerative process. However, it is now considered an active disease process, where the early process of calcific change is characterized by lipid accumulation, inflammation, and punctuate calcification. In end-stage disease, bone formation ensues and the valve becomes progressively more rigid and stenotic.[11] The most common symptom of severe AS is exertional dyspnea. Other symptoms include angina due to an increased oxygen demand by the myocardium and syncope. Once symptoms develop, the disease carries a mortality rate of about 25% per year.[12-14] The treatment for AS is aortic valve replacement (AVR), either surgically or by transcatheter valve replacement. The current indications for intervention are (i) symptomatic severe AS (valve area < 1 cm^2, flow velocity > 4 m/s, transvalvular mean gradient > 40 mmHg), (ii) asymptomatic severe AS with evidence of systolic LV dysfunction or abnormal exercise testing, (iii) symptomatic severe low-flow/low-gradient AS (valve area < 1 cm^2, mean gradient < 40 mmHg) with evidence of contractile reserve.[9] AVR relieves symptoms and has a profound impact on short-term and long-term survival.[15]

1.7 AORTIC REGURGITATION

AR results from disease of the aortic valve or the aortic root that prevents the normal apposition of the aortic valve leaflets, resulting in retrograde blood flow from the aorta to the LV during diastole. Calcific degeneration in a tricuspid or bicuspid valve is the most common underlying etiology in Europe.[16] Other causes of AR include infective endocarditis, rheumatic valvular heart disease, connective tissue disorders, aortic dissection, trauma, and ventricular septal defect. The incidence rate of AR in Sweden is 20.2 and 10.8 per 100,000 patient-years in males and females, respectively, and AR constitutes 18% of the total incidence of valvular heart disease in Sweden.[10] The gender difference in incidence rate may be attributed to a higher prevalence of bicuspid aortic valve and also a higher incidence of aneurysm of the ascending aorta in men, both associated with increased risk of AR.[10,17]

The symptoms of chronic severe AR include exertional dyspnea and sometimes angina due to decreased diastolic perfusion pressure of the LV. There is often a long latency period, and symptoms might occur at a late stage of the disease.[18] The treatment for severe AR is aortic valve surgery, with AVR being the standard procedure in most cases. However, valve repair and valve-sparing aortic root surgery are also considered depending on the valve morphology and the presence of an aortic root aneurysm. The timing of the intervention depends on the presence of symptoms or evidence of LV dilatation or systolic functional impairment. Current guidelines recommend AVR for severe AR in (i) symptomatic patients, (ii) asymptomatic

patients with EF ≤ 50%, and (iii) asymptomatic patients with an end-diastolic left ventricular diameter of 70 mm, end-systolic diameter > 50 mm, or indexed 25 mm/m^2 BSA.[9]

1.8 ECHOCARDIOGRAPHY

Cardiac ultrasound was pioneered by Swedish cardiologist Dr. Inge Edler and Swedish-German engineer Helmut Hertz in the mid-'50s. Dr. Edler was able to evaluate mitral stenosis, pericardial effusion, and left atrial mass using an industrial ultrasound machine.[19,20] Cardiac ultrasound was later named echocardiography, and there has been a remarkable development of the technique over the decades. Today, echocardiography is established as the principal diagnostic tool for noninvasive cardiac structure and function assessment due to its ability to provide real-time imaging, wide availability, and portability.

A hand-held transducer emits pulses of high-frequency soundwaves by electronically activating elements of piezo-electric crystals. The emitted soundwaves have a frequency of typically 1.5–12 MHz . Wavelength and frequency are inversely related, and this relationship depends on the sound propagation velocity through tissue according to the equation:

$$c = \lambda \cdot f,$$

where λ is the wavelength, f is frequency, and c is propagation speed. As an example, ultrasound with a frequency of 3 MHz will have a wavelength of 0.5 mm, given that the propagation speed of sound through bodily tissue is approximately 1540 m/s. The axial resolution of ultrasound, i.e., the ability to discern two separate objects in the longitudinal direction of the ultrasound beam, is dependent on the pulse length according to the equation:

$$axial\ resolution = \frac{1}{2} \times pulse\ length,$$

where the pulse length is the number of cycles in each pulse multiplied by the wavelength. With an ultrasound frequency of 3 MHz and a pulse length of 4 cycles, the axial resolution equals 1 mm. A higher ultrasound frequency results in improved axial resolution but as the ultrasound frequency increases, so does the attenuation of the ultrasound in tissue, meaning that there is a trade-off between resolution and penetration in echocardiographic imaging. Lateral resolution—the ability to discern side-by-side structures in the image—is primarily dependent on the ultrasound beam width and shape, which in turn is dependent on the distance from the probe. Lateral resolution is typically four times worse than the axial resolution and can be improved by increasing the number of scan lines. However, increasing the number of scan lines results in lower time resolution, i.e., the frame rate of the acquired cine-loop will decrease.

Sound waves propagate through tissue and are partially reflected when they meet tissue boundaries with different acoustic impedances. The reflected sound waves are registered by the probe and converted into electrical signals, which are processed and visualized by the ultrasound machine. Dr. Edler's ultrasound machine generated a one-dimensional image

consisting of dots on an oscilloscope. Today's echocardiography equipment uses electronically steered phased-array transducers with thousands of piezo-electrical elements. The transducer scans a sector by emitting ultrasound pulses in an orderly sequence in a fan-like shape, generating a tomographic two-dimensional (2D) image. Images are in turn acquired in a rapid sequence, typically 10 to 70 frames per second, generating cine-loops that enable observation of the real-time motion of the heart. An echocardiographic examination comprises a series of predefined tomographic cut-planes, termed echocardiographic views. The standard echocardiographic examination starts with the transducer at the left parasternal position, followed by apical views, and then images are acquired from the subcostal view, with additional views incorporated as necessary.[21] The image of the heart is described and displayed in relation to the LV. A long-axis view describes a plane that sections the heart from the base to the apex through the mitral valve. There are three standard long-axis views of the heart: the four-, three-, and two-chamber views. A short-axis view describes a plane that is perpendicular to a long-axis view (Figure 5).

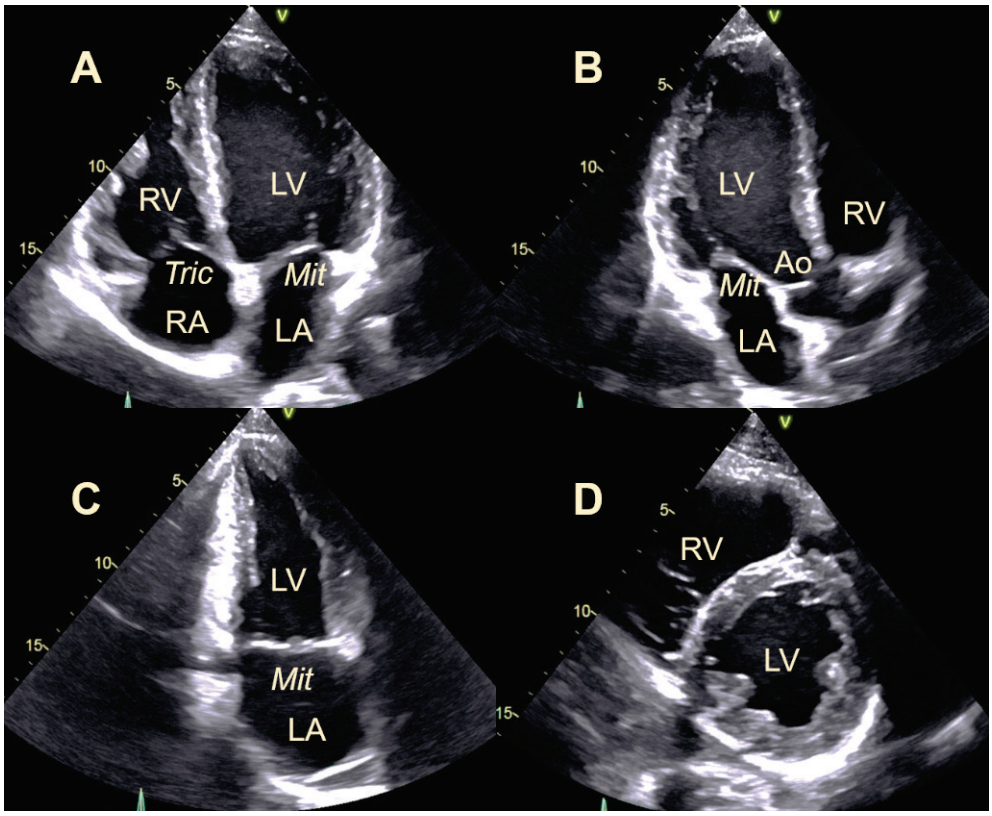

Figure 5 *Echocardiographic long-axis and short-axis views of the heart. Four-chamber view (A), three-chamber view (B), two-chamber view (C), short-axis view (D). Ao, aortic valve; LA, left atrium; LV, left ventricle; Mit, mitral valve; RA, right atrium; RV, right ventricle; Tric, tricuspid valve*

1.8.1 Doppler echocardiography

Doppler echocardiography allows the assessment of blood flow and myocardial wall motion. The Doppler principle states that a wave frequency will be altered when reflected from a moving object. The difference between received frequency and emitted frequency is denoted the Doppler shift and can be measured using an ultrasound machine. Using this technique, the

direction and velocity of the blood flow within the heart, through vessels, and across valves can be measured. Pulsed-wave (PW) Doppler echocardiography measures velocities by emitting and receiving wave-pulses. The pulse-wave technique enables the measurement of velocity at a specific depth. However, because it is a sampling technique, it is susceptible to aliasing artifacts that occur when the Doppler shift exceeds half the pulse-repetition frequency.[22] Thus, PW-Doppler is used to measure relatively low-velocity flow at a specific location within the heart or vessels, e.g., inflow velocities over the mitral valve or the velocity in the LV outflow tract. On the other hand, continuous-wave Doppler measures velocities continuously along the ultrasound beam. While this technique enables the measurement of the maximum velocity, the location of the maximum velocity cannot be determined. Color flow Doppler is a technique whereby multiple PW-Doppler measurements are made within an image sector. The velocity information is color-coded based on the direction and velocity of flow within each sample, generating a live color map of the blood flow.

Velocity measurements within the heart are not restricted to blood flow. Myocardial tissue is also in motion. Tissue-Doppler imaging (TDI) uses the PW-Doppler technique to measure the velocity of the myocardium through the cardiac cycle. TDI can be interrogated at a specific location in the myocardial wall analogous to PW-Doppler blood flow measurements or measured and color-coded using multiple sample volumes, generating a color TDI image.[23,24] TDI provides comprehensive information about the systolic and diastolic movement and deformation of the myocardium.[25]

1.8.2 Three-dimensional echocardiography

2D echocardiography provides a detailed assessment of cardiac structure and function. However, because it relies on tomographic cut-planes through the heart, 2D images cannot fully represent the 3D space. The investigator must synthesize the 2D images to appreciate the 3D relationships and the shape of cardiac structures. To address this problem, the concept of 3D echocardiography (3DE) was proposed in the 1980s. The early prototypes relied on freehand 2D acquisitions using external spatial tracking systems. These images were then merged off-line to generate 3D echocardiograms as wire-frame images of ventricular chambers.[26,27] Further development resulted in automated rotational acquisitions, that enabled more detailed imaging of anatomical structures.[28] Accurate calculations of LV volume and mass were reported using these early 3D techniques.[29,30] However, the 3D acquisitions were time-consuming and relied on off-line reconstruction, which limited the use of 3DE in clinical practice. Real-time 3DE became a reality in the early 1990s with the development of the matrix array transducer capable of steering the ultrasound beam in any direction.[31] Further technical advancements in transducer design, beamforming, and computing over the next decade resulted in the first commercially available 3DE system in the early 2000s, which prompted the development of analysis software that could perform accurate 3D assessments of the LV.[32] The first generations of 3DE transducers were large compared with their 2D counterparts, and some required internal liquid cooling systems. Today, several vendors have incorporated 3D

capability into their standard echocardiographic transducers, making the technique readily available and easier to incorporate into standard examination protocols.

There are two principal methods for 3DE data acquisition, real-time 3DE and gated acquisition. Using real-time 3DE, multiple pyramidal data sets are acquired in a single heartbeat, generating a live view of a 3D sector that can be adjusted in size and position to enable visualization of the structures of interest. Gated acquisition refers to the acquisition of multiple narrow volume subsets over two or more heartbeats. These volumes are then stitched together by the software, generating a complete pyramidal 3D data set. Gated acquisition produces data sets with higher temporal and spatial resolution than real-time 3DE for any given volume size. However, the technique is prone to stitching artifacts that arise from misalignment between subsets of volumes, and for this reason, gated acquisition cannot be used when there is considerable variation in the heart rhythm, e.g., in atrial fibrillation. Figure 6 demonstrates the principal differences between 2DE, real-time 3DE, and gated 3DE image acquisitions.

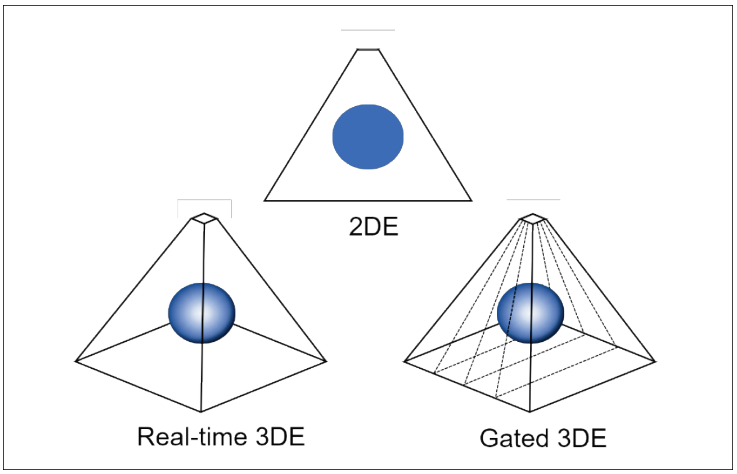

Figure 6 *Two-dimensional echocardiography (2DE) generates a tomographic cut-plane; real-time three-dimensional echocardiography (3DE) generates live 3D data during the cardiac cycle; gated 3DE acquires subvolumes over two or more heartbeats that are stitched together to generate a full-volume data set.*

1.8.3 Ultrasound contrast agents

Ultrasound contrast agents consist of an emulsion of gas-filled microbubbles that are injected intravenously. The microbubbles typically have a diameter of 3 µm. The diameter of a red blood cell is 7 µm in comparison, which means that the microbubbles are small enough to distribute freely throughout the vascular bed and the capillaries in the body. Microbubbles work by resonating with an ultrasound beam. When exposed to ultrasound, the microbubbles will rapidly contract and expand in response to the ultrasound pressure variation, making them significantly more reflective than body tissues.[33] Moreover, the microbubbles exhibit nonlinear oscillation, which means that the vibration of the microbubbles produces multiple harmonic signals or overtones. Ultrasound scanners detect these harmonic signals, producing preferential imaging of the microbubbles in an image.

Microbubble contrast agents make blood–tissue boundaries much clearer. In echocardiography, this translates to an improvement in delineation of the endocardial border, which helps in the assessment of wall motion abnormalities, detecting thrombus, and estimating LV volumes. Good endocardial definition is critical, and contrast agents are beneficial for studies with poor image quality using standard techniques. Indeed, the use of contrast agents has been shown to reduce the percentage of non-diagnostic studies from 12% to <1% by improving the endocardial delineation.[34]

Other uses for microbubble contrast agents in echocardiography include the assessment of myocardial perfusion. Contrast-specific technologies allow real-time imaging of perfusion by applying intermittent high-power pulses to destroy microbubbles within the scan plane and subsequently assess the replenishment of contrast in the myocardium, which is a measure of microcirculatory flow.

1.9 ASSESSMENT OF LV VOLUMES AND SYSTOLIC FUNCTION

The EF is the most widely used quantitative measure of LV systolic function. EF is expressed as a percentage and is calculated as the SV relative to the EDV:

$$EF = \frac{SV}{EDV} = \frac{EDV - ESV}{EDV} \times 100\%.$$

As discussed above, a reduction in LV contractility will result in increased ESV and EDV, with reduced or preserved SV and consequently reduced EF. Hence the rationale for EF as a measure of systolic LV function. There is abundant literature on the prognostic implications of EF, and the EF is included in diagnostic decision-making in several cardiovascular diseases including valvular disease and heart failure.[9,35-40] Furthermore, LV volumes and EF carries prognostic implications in the general population, regardless of symptoms or the presence of underlying cardiac disease.[41,42] Importantly, the EF is not a measure of contractility *per se* because it is dependent on loading conditions and LV geometry, the EF might be within the normal range in small ventricles and hypertrophied ventricles, despite reduced SV.[43] In the volume-overloaded LV, both EDV and SV increase, whereas the EF might remain within the normal range despite diminished contractile performance.[44]

EF can be assessed by measuring EDV and ESV using various imaging techniques, including 2DE and 3DE. In 2DE, the recommended method for quantification of LV volumes is the biplane method of disks.[45] This method requires two cine-loops from orthogonal long-axis views of the LV. The LV geometry is defined by manual or semiautomated tracings of the LV cavity borders at end-diastole and end-systole. Analysis software then quantifies the EDV and ESV by approximating the LV cavity volume as the summed volume of a stack of disks. Sources of error in these measurements include foreshortening of the LV in the long-axis views and geometrical assumptions that may not be accurate in asymmetrically remodeled ventricles.

In 3DE, LV volumes are quantified from full-volume data sets using semiautomated or fully automated analysis software. The software employs feature-tracking or speckle-tracking algorithms to delineate the LV cavity border in 3D space, thus creating an LV cast. The volume enclosed by the cast at end-diastole and end-systole is calculated, yielding the EDV and ESV (Figure 7).

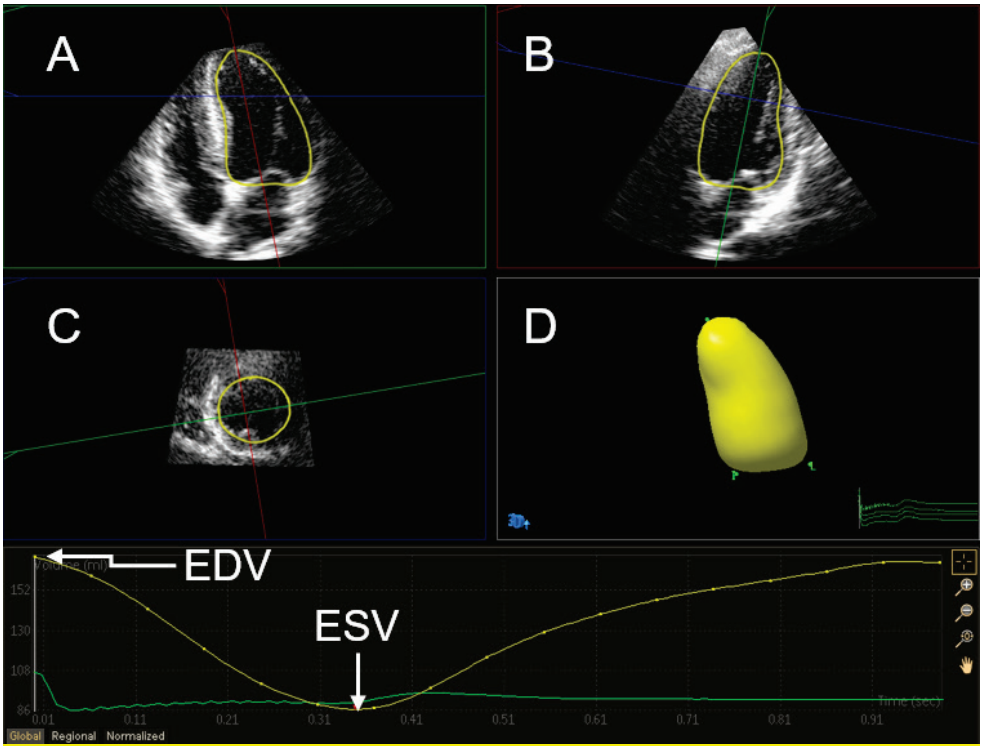

Figure 7 *Left ventricular volume assessed by 3DE. Gray-scale images are two reference long-axis views (A and B) and one short-axis view (C) of the left ventricle with the endocardial delineation shown in yellow. Panel D shows the resulting 3D "cast" of the LV cavity. Bottom panel shows the time–volume curve generated by endocardial tracking throughout the cardiac cycle. EDV, end-diastolic volume; ESV, end-systolic volume.*

1.9.1 LV strain

The LV myocardium is composed of myofiber layers from two helices arranged in opposing directions and mechanically interconnected.[46] The LV systolic motion is a complex interplay between these fiber layers resulting in the atrioventricular plane moving toward the LV apex (longitudinal function) and a simultaneous twisting motion of the apex relative to the LV base. The myocardium is virtually incompressible; therefore, the ventricular wall volume remains constant during the cardiac cycle[47] resulting in deformation of the LV in three dimensions. Using the LV long-axis as a reference, the systolic deformation can be expressed in three ventricular coordinates: a longitudinal shortening, a radial thickening, and a circumferential shortening (Figure 8). The longitudinal function is most important for cardiac function because it contributes 60–75% of the SV regardless of LV size.[47,48]

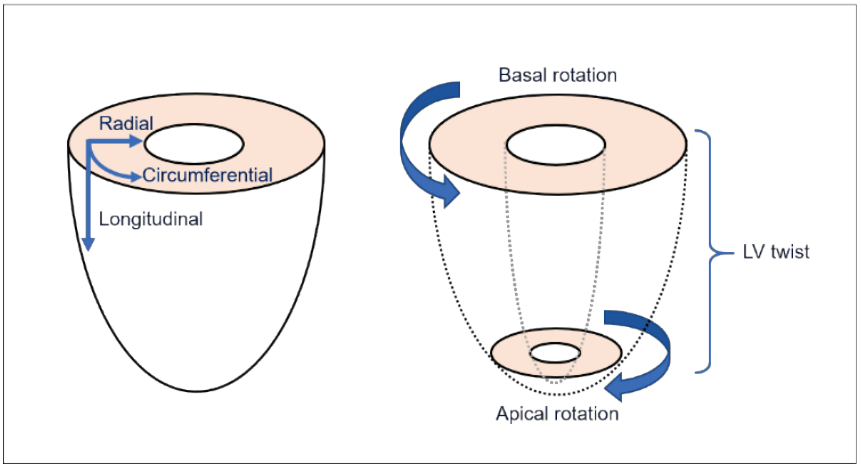

Figure 8 *Myocardial deformation coordinates (left panel) and twisting motion (right panel)*

The amount of shortening and thickening can be quantified by measuring regional strain. Strain is a dimensionless quantity, expressed in percent and defined as a deformation of an object relative to its original dimension. In the one-dimensional case, the deformation can be illustrated as a shortening or lengthening of a thin bar (Figure 9).

Figure 9 *Strain describes the deformation of an object relative to its initial length*

A lengthening is expressed as a positive strain value by convention, while shortening is expressed as a negative strain value. Myocardial strain can be calculated in two principal ways. Lagrangian strain (ε_L) is defined as the change in length (ΔL) relative to the initial length (L_0) by the equation:

$$\varepsilon_L = \frac{\Delta L}{L_0}$$

Natural strain (ε_N) represents the instantaneous length change (dl) relative to the instantaneous length (l), described by the integral equation:

$$\varepsilon_N = \int_{L_0}^{L} \frac{dl}{l}$$

Lagrangian strain and natural strain both describe deformation, but they do not yield identical results; hence, it is recommended to define which type of strain is measured.[49] The strain values reported in Studies III and IV are Lagrangian strain.

Strain can be assessed using echocardiography either by tissue-Doppler imaging or by speckle-tracking echocardiography. Tissue-Doppler imaging measures velocity gradients within the myocardium, which are then integrated to obtain strain curves.[23,50] Tissue-Doppler imaging has an excellent temporal resolution. The main disadvantage is that it is angle-dependent, i.e., it can only accurately measure velocity directions that are parallel or near parallel to the

ultrasound beam. Speckle-tracking echocardiography, which was used in Studies III and IV, uses automated tracking of myocardial "features" (speckles) from frame to frame throughout the cardiac cycle in 2D cine-loops, yielding regional strain curves.[51] Speckle-tracking echocardiography allows measurement of strain in any direction in the 2D image. The main disadvantages of speckle-tracking echocardiography are its dependence on good image quality for accurate measurements and differences in strain estimates between different software vendors. Importantly, the latter problem is being addressed with recent guidelines governing the definitions and measurement of strain.[52] Another source of error in speckle-tracking echocardiography is through-plane tissue motion, which might be significant, particularly in short-axis views.

Three-dimensional strain analysis employs block-matching algorithms to assess deformation of the LV myocardium analogous to 2D speckle-tracking echocardiography.[53] The strain values obtained by 3D analysis are generally expressed in the same directional components as in 2D-derived strain, i.e., in longitudinal, circumferential, and radial strain components. By assessing rotational motion in short-axis slices at the LV apex and base, 3D strain analysis also allows LV twist to be measured.

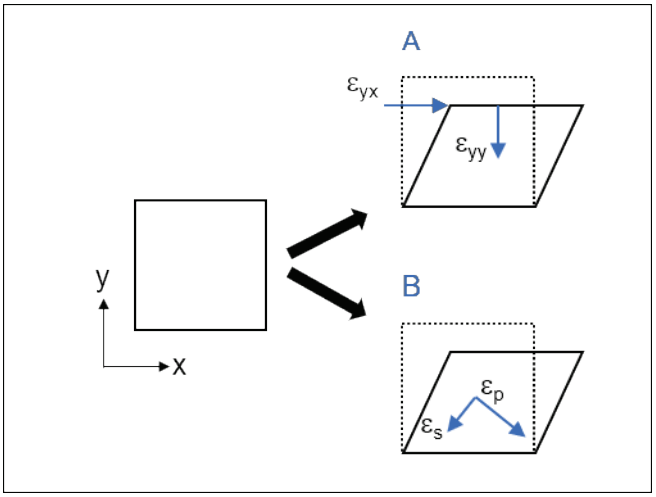

Figure 10 *Example of deformation of a 2D object. The deformation can be described in (A) as a normal strain along the y-axis (ε_{yy}) and a shear strain parallel to the x-axis (ε_{yx}). Using a relative coordinate system (B), the same deformation can be described as a strain along the principal direction (ε_p) and a perpendicular smaller secondary strain (ε_s).*

A deformation process can be described in a Cartesian coordinate system by a composition of the strain along each axis (normal strain) plus shear strain parallel to each axis. For the 2D case, this means that the full description of the deformation of an object requires up to four strain components, two normal strains (ε_{xx}, ε_{yy}) and two shear strains (ε_{xy}, ε_{yx}). Correspondingly, for deformation in 3D, up to nine strain components are required. However, using a relative coordinate system, the shear components can be eliminated. The deformation is then described by its principal strain (PS) in the principal direction, and a smaller secondary strain perpendicular to the principal direction. In cardiac deformation analysis, PS might be interpreted as the main direction and magnitude of contraction (Figure 10).[54] The analysis

software used in Study IV was capable of determining the endocardial tangential PS, denoted principal tangential strain (PTS). Thus, PTS describes the deformation of a 2D curved surface moving in 3D space, rather than 'true' 3D PS. We used the term 3D PTS in Study IV because it was derived from 3D data to separate it from 2D-derived strain.

In contrast to 2D derived strain, full-volume 3D data sets enable tracking of myocardial motion in any direction without the need for multiple plane acquisitions and without errors caused by through-plane motion. However, 3D strain analysis is hampered by lower spatial and temporal resolution in 3DE compared with 2DE. Furthermore, differences in tracking algorithms and technical approaches by different vendors limit the generalizability of 3D strain measurements. Figure 11 demonstrates 2D and 3D longitudinal strain measurements on echocardiographic data from the same patient.

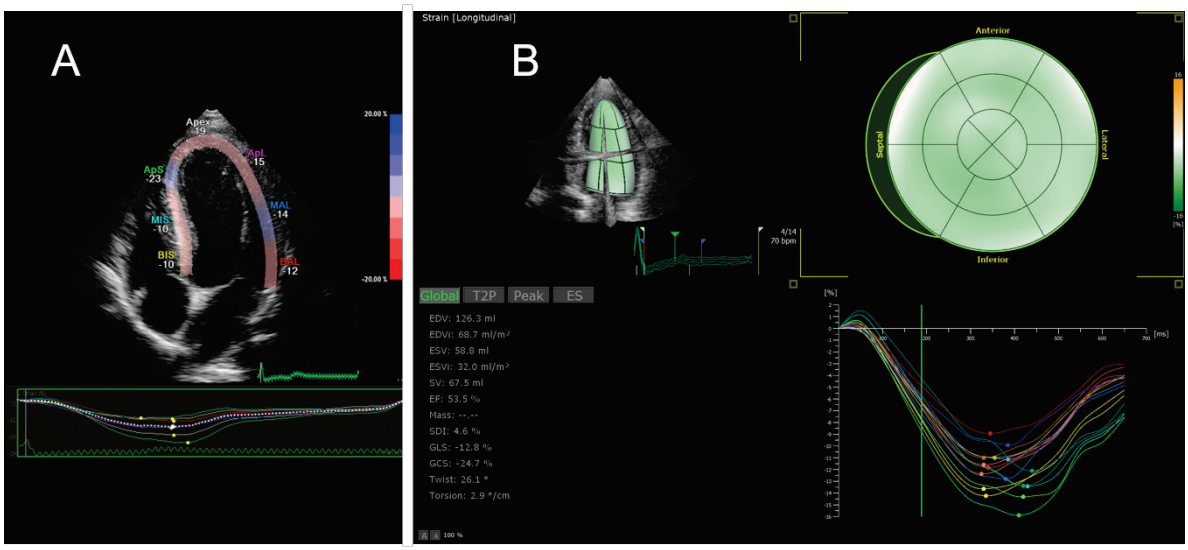

Figure 11 *Longitudinal LV strain assessment by 2D analysis (A) and 3D analysis (B) with regional strain curves. Note that the 2D image shows a single long-axis view; two additional long-axis views are required for complete coverage of the LV.*

1.10 ASSESSMENT OF LV DIASTOLIC FUNCTION

Diastolic dysfunction (DD) is an important aspect of LV dysfunction that may be present in patients with signs of heart failure despite having normal EF.[55-57]

Diastole is defined as the period of the cardiac cycle between aortic valve closure and mitral valve closure. At the cellular level, the process of relaxation starts in late systole with the uncoupling of actin–myosin filaments in the myocardium.[58] In early diastole, restoring forces within the LV myocardium create an elastic recoil of the LV.[59] The following phase is the diastasis, characterized by passive LV filling during which the LV and LA pressures are equalized. The last phase is the atrial systole, or LA contraction phase, which contributes to LV filling in late diastole. The most significant LV diastolic function determinants are active ventricular relaxation and passive viscoelastic stiffness (or inversely compliance).[60] DD is present when there is an impairment in one or both factors. The main physiological

consequence of DD is elevated filling pressure, which is associated with symptoms of congestive heart failure, e.g., dyspnea and reduced exercise capacity.[61] The term filling pressure is ambiguous, because it can refer to LVEDP, mean LA pressure, LV pre-A pressure, or pulmonary capillary wedge pressure. The quantitative assessment of these pressures requires invasive procedures using pressure catheters.

The noninvasive determination of diastolic function using Doppler-echocardiography is complex; DD and elevated filling pressure are determined by several factors, associated with different echocardiographic indices.[61,62] Accordingly, current guidelines recommend an integrative approach that considers the ratio between the early (E) and atrial (A) mitral inflow Doppler velocities (E/A ratio), tissue-Doppler derived velocity of the LV wall (e′), pulmonary artery pressure estimated from tricuspid regurgitation maximal velocity, and LA volume.[7] An increased E/A ratio is associated with increased LA pressure. The early diastolic velocity of the LV wall (e′) is related to LV relaxation, and an increased E/e′-ratio is related to increased LV filling pressure. Pulmonary artery pressure is usually elevated in DD, and increased LA volume is a sign of chronically elevated LA pressure. It is important to bear in mind that each of these parameters has limitations regarding accuracy and feasibility and can be altered in conditions other than DD. Moreover, the assessment of DD and LV filling pressure remains challenging in patients with atrial fibrillation, mitral valve disease, atrioventricular block, and pacemakers, and there is limited data on the assessment of DD in aortic regurgitation.[7] Nevertheless, the diagnostic algorithm proposed in the guidelines was validated in a study on 450 patients and was shown to predict elevated LV filling pressure with 87% accuracy and 91% positive predictive value.[63]

1.11 ASSESSMENT OF LEFT ATRIAL SIZE AND FUNCTION

The function of the left atrium (LA) is to modulate LV filling. The left atrial volume and function are determined by an interplay between LA loading conditions and LV systolic and diastolic properties. Increased LA afterload, for example in mitral stenosis, increased LV stiffness, or increased LV filling pressures, will result in an increase in LA size. An increase in LA preload, such as occurs secondary to mitral regurgitation, will also lead to an increase in LA volume. Accordingly, LA size and function are associated with adverse outcomes in various cardiovascular conditions and in the general population.[64] LA volume is usually determined with echocardiography but can also be assessed with other imaging modalities, including cardiovascular magnetic resonance (CMR) and computed tomography (CT).

LA function is divided into three phases during the cardiac cycle: the reservoir phase during LV systole, the conduit phase during early LV diastole, and the contraction phase during late LV diastole. During the reservoir phase, the LA volume increases while it accommodates blood entering from the pulmonary veins. This process is regulated by the LV systolic function through the movement of the mitral annular plane and modulated by the compliance of the atrium.[65] The next phase is the conduit phase, during which blood is passively transferred to the LV. The conduit phase is influenced by LV relaxation and compliance. During the

contraction phase, the LA acts as a pump and contributes to the late filling of the LV. The contraction phase is dependent on atrial contractility, LV end-diastolic pressure, and atrial preload. LA function can be assessed by echocardiography using various methods, such as volumetric analysis, Doppler analysis, and deformation analysis (strain and strain rate). Deformation analysis, in turn, can be performed using tissue-Doppler or by speckle-tracking echocardiography.

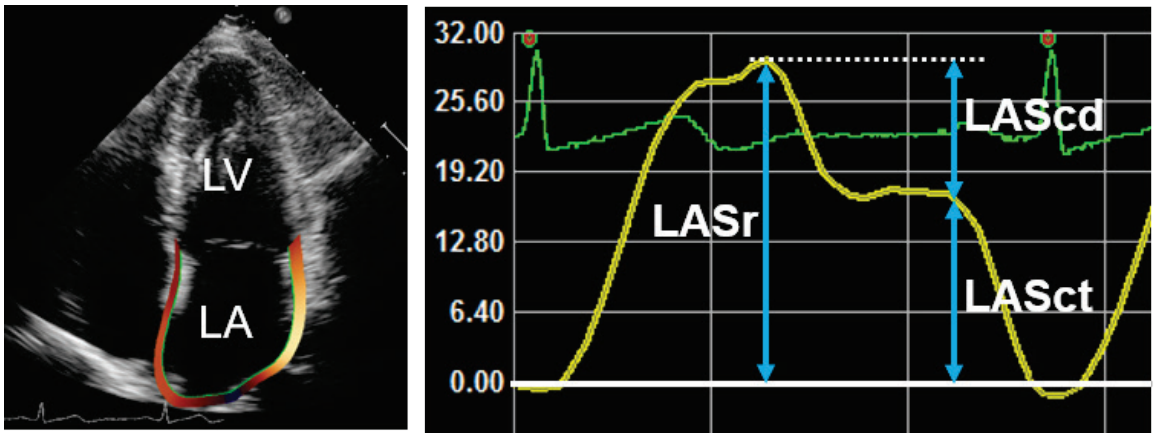

Figure 12 Left panel*: apical four-chamber view; LV left ventricle; LA left atrium;* Right panel*: Left atrial strain (LAS) curve (yellow); ECG recording in green for reference; time on the x-axis and strain values in percentage on the y-axis; dashed line represent strain value at end-systole, blue arrows demonstrate the LAS phases: LASr, reservoir phase; LAScd, conduit phase; LASct, contraction phase.*

In this thesis, LA function was assessed using speckle-tracking echocardiography, which is performed similarly to LV strain assessment. The LA endocardial border is tracked throughout the cardiac cycle in a 2D cine-loop using dedicated semiautomated software, generating a longitudinal strain curve. The zero-strain reference point is set at LV end-diastole. The peak LA strain represents the reservoir phase, denoted LASr. The contraction phase starts at atrial contraction and is denoted LASct. Strain during the conduit phase is the difference between LASr and LASct. An example of a LAS curve with the phasic function components is shown in Figure 12 along with an echocardiographic image of the LV and left atrium.

1.12 CARDIOVASCULAR MAGNETIC RESONANCE IMAGING

CMR imaging is well-established in clinical practice as a versatile technique for assessing cardiac anatomy, cardiac function, valve function, myocardial tissue characteristics, and myocardial perfusion.[66] Furthermore, CMR imaging has emerged as the *de facto* reference standard for determining LV volume and mass, owing in significant part to its excellent reproducibility.[67,68] There is no ionizing radiation in CMR, making it a suitable imaging modality when there is a need for repeated examinations. However, the strong magnetic field used in CMR scanners can displace ferromagnetic objects such as certain implants and affect the function of pacemakers. Furthermore, claustrophobia may pose a problem for some patients in the scanner.

LV volume and function are assessed in time-resolved cine images, most commonly acquired with a balanced steady-state free precession sequence. This sequence facilitates rapid image acquisition and generates images with excellent contrast between myocardium and blood. The cine images are acquired using retrospective ECG gating and require breath-hold to minimize the translational movement of the heart during image acquisition. This means that LV volume quantification using this sequence is less accurate in patients with arrhythmia and in patients that have difficulties holding their breath. Real-time imaging sequences offer an alternative in these cases; however, its spatial and temporal resolution is generally worse than in ECG-gated sequences. The cine images are oriented in the long-axis and short-axis planes of the heart, using the same anatomical representation and nomenclature as in echocardiography. Short-axis cine images are acquired in a stack covering the whole LV during the cardiac cycle. The endocardial border is delineated in the end-diastolic and end-systolic frames in each short-axis. The volume in each slice is calculated as the delineated area multiplied by the slice thickness. The LV volume is calculated as the sum of all slice volumes (Figure 13).

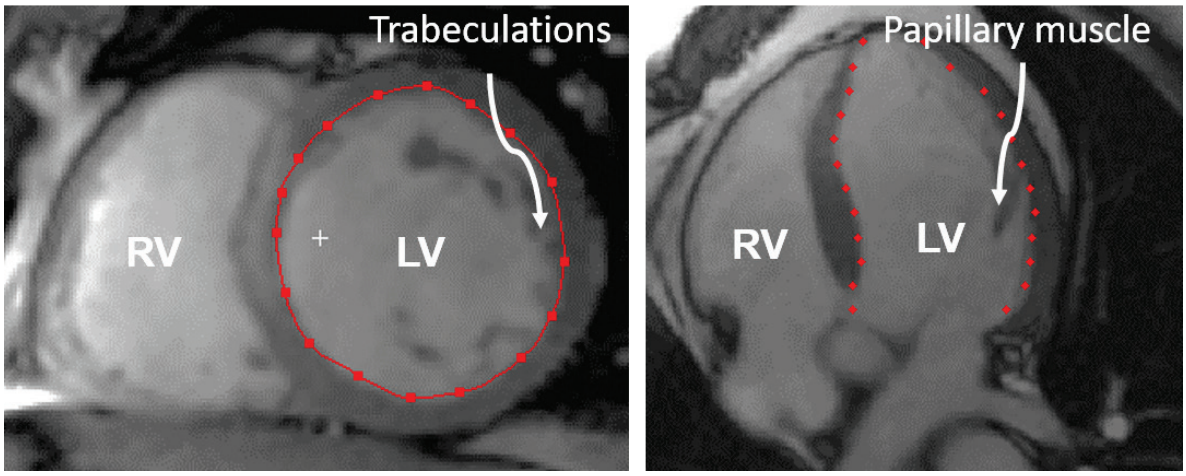

Figure 13 *CMR images from a patient included in Study I, short-axis view (left) and four-chamber long-axis view (right). The red line in the short-axis view represents the endocardial delineation in end-diastole. Note that trabeculations and papillary muscles are included in the LV cavity. Delineation is carried out in all the short-axis slices, and the enclosed volume is calculated by the summation of disks method. The long-axis view is used to confirm correct delineation; LV, left ventricle; RV, right ventricle.*

A CMR scanner consists of a large cylindrical gantry that accommodates the patient during the scan. The gantry houses an electromagnet that generates a strong static magnetic field (B_0) along the scanner's longitudinal direction with a field strength typically of 1.5 or 3 T. There are also gradient coils that generate transient magnetic field gradients and radiofrequency (RF) coils that emit and receive RF pulses.

CMR is based on the detection of protons in hydrogen nuclei in tissues. Hydrogen is abundant in the human body in water, fat, and proteins. Protons have an intrinsic magnetic property referred to as *spin* or magnetic moment. When the protons are exposed to an external magnetic field, their magnetic momentum vector will precess, or rotate, around the axis of the external

magnetic field. The precession frequency is dependent on the strength of the magnetic field according to the equation:

$$f = \gamma \cdot B_0$$

where f is the precession frequency referred to as the Larmor frequency, γ is the gyromagnetic ratio, and B_0 is the strength of the static magnetic field. When the patient is outside the magnetic field, the magnetic moments of all the protons are randomly distributed, so the net magnetization is zero. However, when the patient is placed in the gantry, the strong external magnetic field will cause a fraction of the protons in the body to align with the magnetic field, generating a net magnetization vector along the direction of B_0. This direction is denoted the Z-axis, and the plane perpendicular to the Z-axis is denoted the XY-plane. To generate a signal, the net magnetization of the protons needs to be manipulated and this is accomplished by transmitting RF pulses into the patient. Given that the gyromagnetic ratio of hydrogen is 42.6 MHz/T, the Larmor frequency for hydrogen is 64 MHz at 1.5 T. By sending RF pulses with this frequency, a secondary magnetic field perpendicular to B_0 is induced, causing the net magnetization to deviate from the Z-axis toward the XY-plane. When the RF pulse is switched off, the net magnetization vector will return to its equilibrium state along the Z-axis. The recovery of net magnetization along the Z-axis follows an exponential curve, and the time constant that describes this curve is denoted the T_1 relaxation time. Conversely, the time constant that describes the exponential *decrease* of the net magnetization in the XY-plane is denoted the T_2 relaxation time. T_1 and T_2 both vary depending on the local environment of the protons (i.e., the specific molecule and the tissue surroundings), which enables the tissue discrimination seen in CMR images. While returning to equilibrium after an RF pulse, the net magnetization in the XY-plane will emit radiofrequency signals at the Larmor frequency, which are registered by RF coils placed close to the patient's chest during the examination. Image formation requires information regarding the origin of a particular signal, which is achieved by applying magnetic field gradients while transmitting and receiving RF signals. The raw data acquired are stored in a data matrix called the K-space. The data from K-space are subsequently analyzed using complex mathematical processes, including Fourier transformation to yield images or functional information.

1.13 SINGLE-PHOTON EMISSION COMPUTER TOMOGRAPHY

Myocardial perfusion single-photon emission computer tomography (SPECT) evaluates myocardial perfusion and LV volume and function. It is widely used in clinical practice in patients with known or suspected ischemic heart disease and remains the most commonly used procedure in nuclear cardiology.[69] A perfusion tracer with an affinity for the myocardium, labeled with a radioactive substance (^{201}Tl or ^{99m}Tc for cardiac imaging), is administered intravenously. The extraction of tracer from the blood to the myocardium is linearly related to the regional myocardial blood flow, thereby enabling the assessment of regional LV perfusion.

Following the tracer injection, the patient is examined in a gamma-camera system that registers the emitted electromagnetic radiation (gamma radiation) at a specific energy (140 keV for ^{99m}Tc). A conventional dual-detector SPECT for cardiac imaging uses two cameras mounted at 90° that are rotated to register planar projections from multiple angles around the body. The raw data are transformed using reconstruction algorithms followed by filtering to reduce noise, and then tomographic images of the heart are produced. The images are oriented along the LV short- and long-axes to review the tracer distribution in the LV wall.

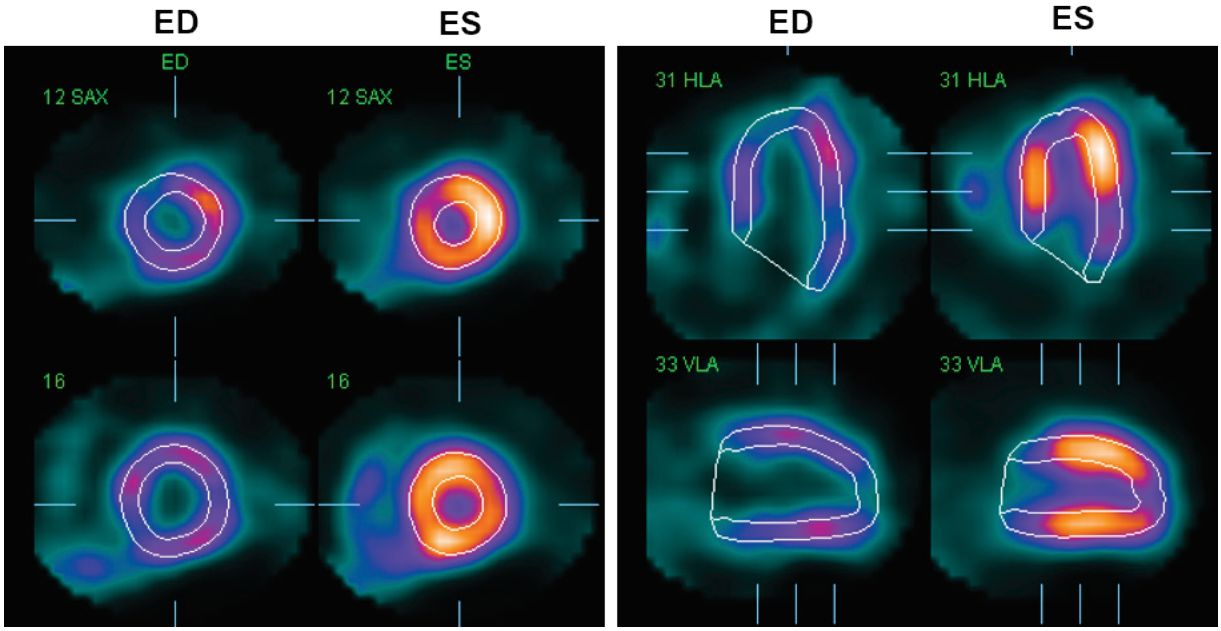

Figure 14 *Gated SPECT images showing short-axis views (left panel) and long-axis views (right panel) of the left ventricle. Using semi-automated quantification software, the endocardial and epicardial borders are delineated in end-diastole (ED) and end-systole (ES); SAX, short-axis, HLA, horizontal long-axis; VLA, vertical long-axis.*

The ability to perform gated acquisitions facilitates the assessment of LV volumes and EF, which adds diagnostic and prognostic information.[37,70,71] Using ECG gating, images are acquired at multiple time points throughout the cardiac cycle. The cardiac cycle is usually divided into 8 or 16 time bins, based on the relative timing from the R-wave in the ECG. Data from each time bin are reconstructed, producing image sets that allow visual or quantitative assessment of functional parameters such as myocardial motion, and thickening. LV volumes

are assessed using dedicated software that operates in three-dimensional space, using gated short-axis images. The algorithm consists of three steps: segmenting of the LV myocardium, extracting the LV's mid-myocardial surface, and determining the endocardial and epicardial surfaces based on Gaussian fitting of the count profiles across the mid-myocardial surface.[71] The software then calculates the volume enclosed by the endocardial surface in end-diastole and end-systole and derives the EF (Figure 14).

The spatial and temporal resolution in SPECT is limited compared with other imaging modalities. The reconstructed images typically have a resolution of 5 mm in all directions. Gated SPECT cine images acquired using 8 bins per cardiac cycle in a patient with heart rate 60 beats/min will have a frame rate of 8 frames/s.

2 RESEARCH AIMS

The overall aims of the thesis were:

- to evaluate the value of 3D echocardiography in the assessment of left ventricular function and remodeling in comparison with other modalities, and
- to study different aspects of remodeling in response to pressure and volume overload in aortic stenosis and aortic regurgitation, respectively, and to examine the determinants of reverse remodeling following aortic valve surgery.

The specific aims were:

Study I

To assess the level of agreement between 3DE, SPECT, and CMR on left ventricular volume and ejection fraction assessment.

Study II

To evaluate the impact of image quality and contrast enhancement on the assessment of left ventricular volume and ejection fraction by 2DE and 3DE, using CMR as a reference standard.

Study III

To assess structural and functional effects of severe aortic regurgitation on the left ventricle and left atrium before and at one year after aortic valve surgery.

Study IV

To assess structural and functional effects of severe aortic stenosis on the left ventricle and to evaluate determinants of incomplete reverse remodeling following aortic valve surgery.

3 SUBJECTS AND METHODS

3.1 SUBJECTS IN STUDIES I AND II

The study groups for Studies I and II were recruited from a study on patients with acute myocardial infarction performed at the Karolinska University Hospital in Stockholm, Sweden, in 2007.[72] This study was a prospective, randomized clinical trial that aimed to compare standard percutaneous coronary intervention (PCI) with an extended protocol that included postconditioning. Patients admitted for acute myocardial infarction and planned for primary PCI were eligible for inclusion. Exclusion criteria were previous myocardial infarction, previous coronary bypass surgery, cardiogenic shock, cardiac arrest, contraindications for CMR, known renal insufficiency, persistent atrial fibrillation, and treatment with metformin. A total of 89 patients were randomized, and 68 patients completed the full study protocol. The imaging protocol included CMR and 2D-, and 3D-echocardiography one week after the initial event and at follow-up visits at 3 months and 12 months.

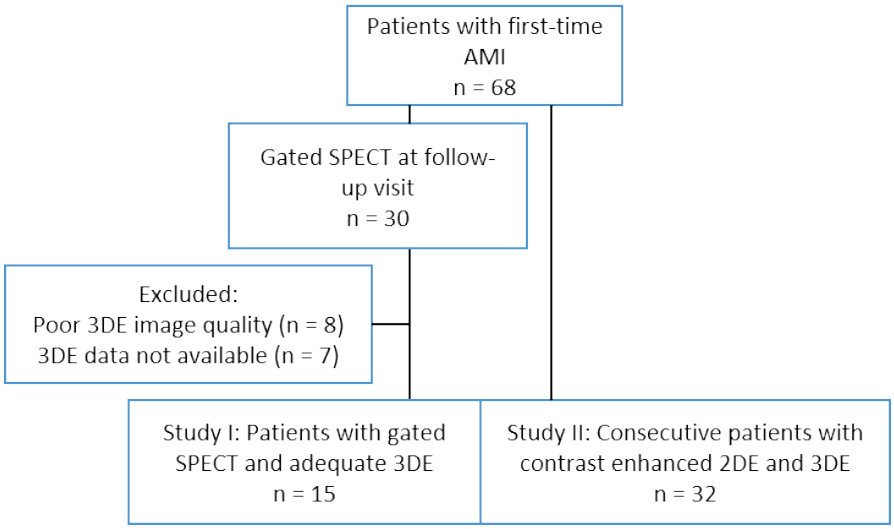

Figure 15 *Study group selection for Studies I and II. 2DE, two-dimensional echocardiography; 3DE, three-dimensional echocardiography; AMI, acute myocardial infarction, SPECT, single-photon emission computer tomography.*

A subgroup of 30 patients underwent gated SPECT at the three-month visit, and these patients were eligible for inclusion in Study I. 3D-echocardiograms were missing in two patients, and five patients had 3D data stored in a format that was incompatible with the analysis software. Eight patients were excluded due to insufficient image quality, defined as two or more adjacent LV wall segments not visualized in the 3D images. Hence, the study group consisted of 15 patients. Their median age was 61 (IQR 58–70) years, and there were two females.

For Study II, the echocardiographic protocol was extended to include contrast enhancement echocardiography, which was performed on 32 consecutive patients. Low image quality was not an exclusion criterion for Study II because one of the study objectives was to assess the impact of image quality on the accuracy of echocardiographic LV volume determination. The

median age was 64 (IQR 52–70) years, and there were two females in the study group. Four of the patients had previously been included in Study I; however, data from different time points were used for the two studies (3-month visit for Study I and 12-month visit for Study II), so there was no overlap in the imaging data. Figure 15 demonstrates the study group selection for Studies I and II.

3.2 SUBJECTS IN STUDIES III AND IV

The study groups for Studies III and IV were recruited from a prospective observational cohort study performed at the Karolinska University Hospital in Stockholm, Sweden, from 2007 to 2013.[73] The study included adult patients scheduled for elective open-heart surgery for severe aortic valve disease or aneurysm of the aortic root or ascending aorta. Exclusion criteria were significant coronary artery disease assessed by coronary angiogram, previous cardiac surgery, and other significant valve disease requiring surgical intervention. The final study cohort comprised 573 patients. Of these patients, 556 had 2D and 3D echocardiograms performed within one week before surgery and at a follow-up visit one year after surgery. The echocardiographic data were incomplete or uninterpretable due to technical reasons in 32 cases. Hence, there were 524 patients with complete echocardiographic data eligible for inclusion in the present studies. Studies III and IV included patients with isolated AR and AS, respectively. Isolated AR was defined as severe AR and an aortic transvalvular mean gradient < 20 mmHg. Isolated AS was defined as severe AS (aortic transvalvular mean gradient ≥ 40 mmHg, and/or aortic valve area ≤ 1.0 cm^2) and no or mild concomitant AR. Hence, patients with mixed aortic valve disease or isolated aneurysm of the ascending aorta were excluded (n = 170). Patients with atrial fibrillation were excluded due to the inability to measure LV volume and strain reliably in these patients (n = 24). Adequate echocardiographic image quality for 2D and 3D LV volume and strain measurements were required at baseline and at the follow-up examination in each patient. For this reason, 145 patients were excluded due to two or more adjacent LV wall segments not visualized in either the 2D or 3D echocardiogram at either the baseline or the follow-up examination.

The final study group of Study III comprised 65 patients with isolated severe AR. In Study IV, the final study group comprised 120 patients with isolated severe AS. Demographic data for the study populations are listed in Table 1. Patient selection is shown in Figure 16.

For Study III, a control group was selected comprising 20 consecutive patients with aneurysm of the aortic root or ascending aorta and no or mild concomitant aortic valve disease, defined as an aortic transvalvular mean gradient < 20 mmHg and no or mild AR, who underwent open thoracic aneurysm surgery without valve replacement during the same period. The same control group was used in Study IV, with the addition of seven patients with isolated aneurysm of the ascending aorta, who received aortic root grafts with a valve prosthesis (due to the native valve not being suitable for reimplantation).

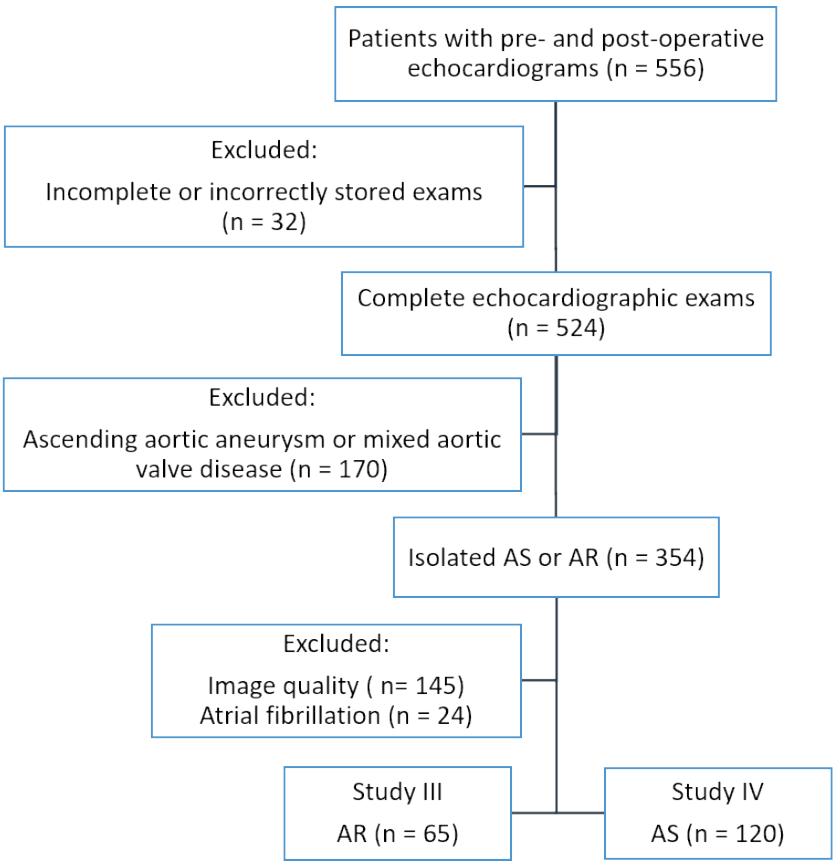

Figure 16 *Patients selection for Studies III and IV. AS, aortic stenosis; AR, aortic regurgitation*

Table 1 Patient characteristics in Studies III and IV

	Study III AR (n = 65)	**Study IV AS (n = 120)**	***P***
Age (years), median (IQR)	54 (46–63)	68 (62–74)	< 0.001
Gender, males (%)	56 (86%)	67 (56%)	< 0.001
BMI (kg/m^2)	26.1 ± 4.0	26.8 ± 3.7	0.21
BSA (m^2)	2.0 ± 0.2	1.9 ± 0.2	0.004
Systolic BP (mmHg)	145 ± 16	141 ± 21	0.17
Diastolic BP (mmHg)	70 ± 11	83 ± 12	< 0.001
Diabetes, n (%)	1 (1,5%)	15 (13%)	0.01
Hypertension, n (%)	30 (46%)	73 (61%)	0.048
NYHA functional class, n (%)			0.005
I	16 (25%)	8 (7%)	
II	39 (60%)	85 (71%)	
III	10 (15%)	27 (22%)	
IV	0	0	
Bicuspid aortic valve, n (%)	38 (58%)	72 (60%)	0.84
NTproBNP (NPX-units)	4.4 ± 1.7	5.0 ± 1.3	0.001

P-values are for the differences between the study groups. AR, aortic regurgitation; AS, aortic stenosis; BMI, body mass index; BP, blood pressure; BSA, body surface area; IQR, inter-quartile range; NPX, Normalized protein expression; NTproBNP, N-terminal pro-B-type natriuretic peptide; NYHA, New York Heart Association

3.3 2D ECHOCARDIOGRAPHY

Comprehensive echocardiographic examinations were performed following current recommendations[45] by experienced examiners using commercially available equipment (Philips iE33 or Philips Epic 7; Philips Medical Systems, Bothell, WA, USA). The 2D echocardiographic data were analyzed using a dedicated software package (IntelliSpace Cardiovascular 2.3; Philips Medical Systems Nederland B.V., Best, The Netherlands).

LV EDV and ESV were measured using the biplane method of disks from four- and two-chamber 2DE views.

Diastolic and systolic LV dimensions and wall thickness were measured in the parasternal long-axis view. Relative wall thickness was calculated as (2 × posterior wall thickness)/(LV internal diameter at end-diastole). LA volume was calculated using the biplane method of disks in the apical 4- and 2-chamber views at the end of the LV systole. LA volume index (LAVi) was calculated as LA volume/BSA. Aortic transvalvular velocity was measured using CW Doppler in the apical 5-chamber view or 3-chamber view. The mean transvalvular pressure gradient was calculated by applying the Bernoulli equation and averaging the instantaneous gradients over the ejection period. LV outflow tract velocity was measured using PW Doppler in the apical 5-chamber view. The aortic valve area was calculated according to the continuity equation.[74]

AR was assessed using a semiquantitative, integrative approach according to current guidelines incorporating pressure half-time, color flow jet area, vena contracta, jet density, and diastolic flow reversal in the descending aorta.[75]

3.3.1 Left ventricular diastolic function (Study III)

Diastolic LV inflow was recorded from the apical 4-chamber view using PW Doppler at the level of the mitral leaflet tips. Early diastolic (E) and atrial (A) peak velocity and deceleration time (DT) of the E-wave were measured. The peak jet velocity of the tricuspid regurgitation (TR V_{max}) was measured when possible. Early diastolic myocardial velocities (e′) were measured using PW tissue-Doppler. The sample volume was placed at the mitral valve insertion level in the LV septum and lateral wall in the apical 4-chamber view yielding septal and lateral e′, respectively. The average of septal and lateral e′ was used to calculate the E/e′ ratio. DD was evaluated in accordance with current guidelines incorporating the E/A ratio, E/e′ ratio, TR velocity, and LA volume.[7] The cases were classified into three categories, (i) no or grade 1 DD, (ii) grade 2 DD, and (iii) grade 3 DD. Cases that could not be assigned a DD grade were deemed indeterminate (Figure 17).

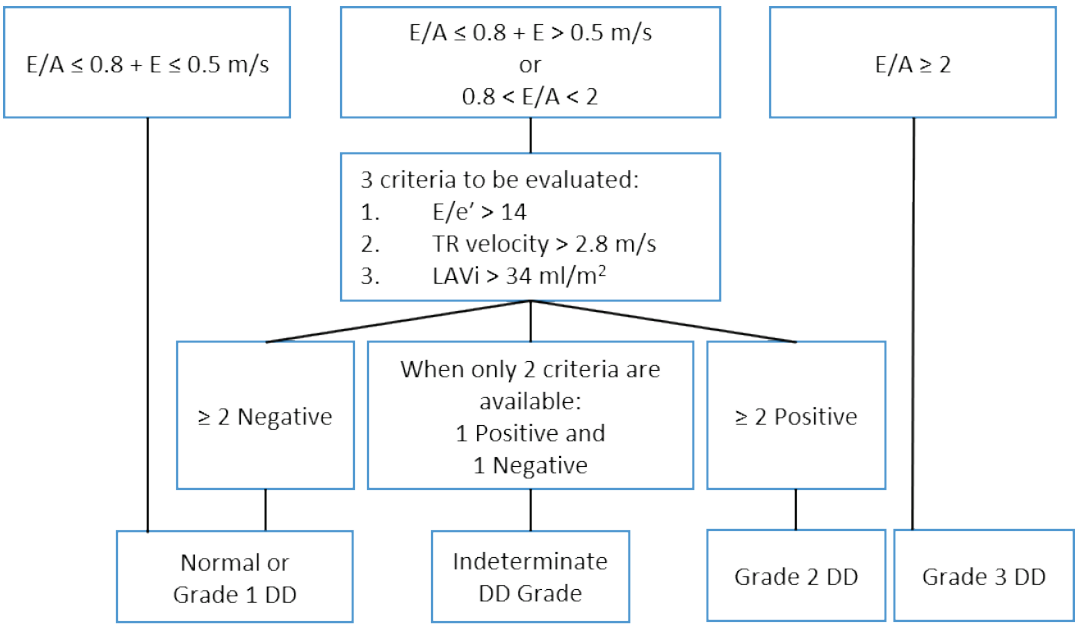

Figure 17 *Algorithm for diastolic dysfunction (DD) assessment. E/A, ratio between early and late diastolic filling velocities; E/e', ratio between mitral early filling velocity and annular tissue velocity; LAVi, left atrial volume index; TR, tricuspid regurgitation.* From Nagueh *et al.*[7], copyright (2016), with permission from Elsevier.

3.3.2 Left ventricular global longitudinal strain (Studies III and IV)

Global longitudinal LV strain (GLS) was measured using dedicated software (QLab 10.7 with aCMQ module, Philips Medical Systems Nederland B.B., The Netherlands). Four-, three-, and two-chamber views were used for the analysis. The LV wall was automatically tracked throughout the cardiac cycle in each view using a speckle-tracking algorithm. The region of interest was manually adjusted if needed after visual inspection of the tracking results, and the width of the region of interest was adjusted to the myocardial wall thickness, carefully avoiding the inclusion of pericardium in the tracing. A longitudinal myocardial strain value was computed for each segment according to a 17-segment model.[76] GLS was calculated by averaging the peak systolic longitudinal strain from all segments and is expressed as an absolute percentage (|%|).

3.3.3 Left atrial strain analysis (Studies III and IV)

LA strain (LAS) was calculated using dedicated software (TomTec-Arena with 2D Cardiac Performance Analysis 1, TomTec Imaging Systems GmbH, Germany). Four- and two-chamber views were used for the analysis. Two points were manually placed at the mitral annulus and a third point at the LA roof in each view. The software then tracked the LA wall through the cardiac cycle and generated a global longitudinal strain curve. The tracking result was inspected, and the atrial wall delineation was manually corrected at end-systole and end-diastole if needed. The zero-strain reference point was set to the end-diastolic frame immediately following mitral valve closure. The resulting LA strain curve was subdivided into three phases, (i) reservoir phase (LASr), (ii) conduit phase (LAScd), and (iii) contraction phase

(LASct).[77] LASr was measured as the peak strain value at end-systole. LASct was measured at the end of the plateau phase following early diastolic filling, where the p-wave in the ECG recording and visual assessment of the 2D image for the start of atrial contraction was used to assure correct measurement. LAScd was calculated as LASr – LASct. Results are reported as the average of measurements obtained from 4- and 2-chamber views and are presented as an absolute percentage (|%|).

3.4 3D ECHOCARDIOGRAPHY

3D full-volume data sets were acquired using commercially available equipment (Philips iE33 or Philips Epic 7, as above) equipped with a dedicated 3D transducer (X3-1, Philips) or a combined 2D- and 3D transducer (X5-1, Philips). The 3D data were obtained from the apical transducer position using gated acquisitions over four or seven cardiac cycles during breath-hold, and care was taken to include the whole LV in the data set.

3.4.1 Left ventricular volume (Studies I, II, III, and IV)

Measurements of LV volume was performed using dedicated software (QLab 10.7 with options 3DQ Advanced, Philips Medical Systems Nederland B.B., The Netherlands). The end-diastolic (first frame) and end-systolic (smallest cavity) frames were identified. Five points were placed manually at the lateral, medial, anterior, and inferior aspects of the mitral valve annulus, and one point at the apex. The endocardial surface was then delineated by the software using an automated contour detection algorithm. The surface was examined in multiple sagittal and transverse planes and manually adjusted if necessary. Papillary muscles and trabeculations were included in the cavity. The volume enclosed by the generated surface was computed by the program, yielding the EDV and ESV. SV was calculated as EDV–ESV.

3.4.2 Left ventricular mass (Studies III and IV)

LV mass was calculated using the biplane method of disks in images extracted from 3D data sets.[78] The long-axis and rotational angle of two orthogonal planes were adjusted to yield nonforeshortened four- and two-chamber views. Endocardial and epicardial contours were traced manually with the papillary muscles included in the LV cavity. The software calculated the mass of the enclosed volume representing LV myocardium. Measurements were made at end-diastole and end-systole; the LV mass was estimated as the average of the two measurements. LV mass index (LVMi) was calculated as LV mass/BSA.

3.4.3 3D strain (Study IV)

Assessment of LV 3D strain was performed using dedicated software (4D LV Analysis 21.05, TomTec Imaging Systems GmbH, Unterschleissheim, Germany). The 3D data sets were displayed as reconstructed long-axis views and a short-axis view. The long-axis views were adjusted to ascertain nonforeshortened views in end-diastole, and the mitral annular plane and the LV apex were manually defined in each view. The endocardial surface was then

automatically delineated in the end-diastolic and end-systolic frames. The reconstructed delineations were manually adjusted when needed to optimize the identification of the endocardial boundary. The software then tracked the endocardial surface throughout the cardiac cycle using a three-dimensional speckle-tracking algorithm, yielding endocardial strain curves. The longitudinal strain, circumferential strain, radial strain, and principal tangential strain were calculated for each segment of a 16-segment model. The global values of each strain component were calculated as the average of all segments, yielding global longitudinal strain (3D GLS), global circumferential strain (3D GCS), global radial strain (3D GRS), and 3D principal tangential strain (3D PTS), where 3D PTS describes myocardial deformation by its principal direction tangential to the endocardial surface. All strain variables are presented as absolute percentages (|%|). The software measured the rotation of the apical and basal short-axis slices, and the LV twist was calculated as the difference in peak rotation between the slices.

3.5 ECHOCARDIOGRAPHIC IMAGE QUALITY ASSESSMENT (STUDY II)

Echocardiographic image quality was assessed in each segment of a 17-segment model on a 0–4 grade scale as follows: (0) no visible endocardium, (1) the endocardial border not visible in the whole segment, (2) the endocardial border just visible, (3) the endocardial border easily visible, and (4) the endocardium visible, including clearly defined trabeculations. For 2DE studies, only the two- and four-chamber views were evaluated because these are the two views used in the biplane volume calculation. The LV image quality index was calculated as the average of the segmental scores.

3.6 CONTRAST-ENHANCED ECHOCARDIOGRAPHY (STUDY II)

A commercially available contrast agent containing sulfur hexafluoride microbubbles (SonoVue; Bracco Imaging S.p.A., Milan, Italy) was prepared according to the manufacturer's recommendations and administered intravenously as a bolus injection of 1 mL. The injection was repeated if needed to achieve optimal opacification of the LV cavity. Contrast-enhanced 2DE and 3DE images were acquired using a contrast-specific acquisition program on the ultrasound scanner.

LV volumes and EF were assessed in the same manner using the same software as for the nonenhanced studies described above (Figure 18). However, the 3D quantification software was not optimized for contrast-enhanced images, necessitating manual tracings of the endocardial surface.

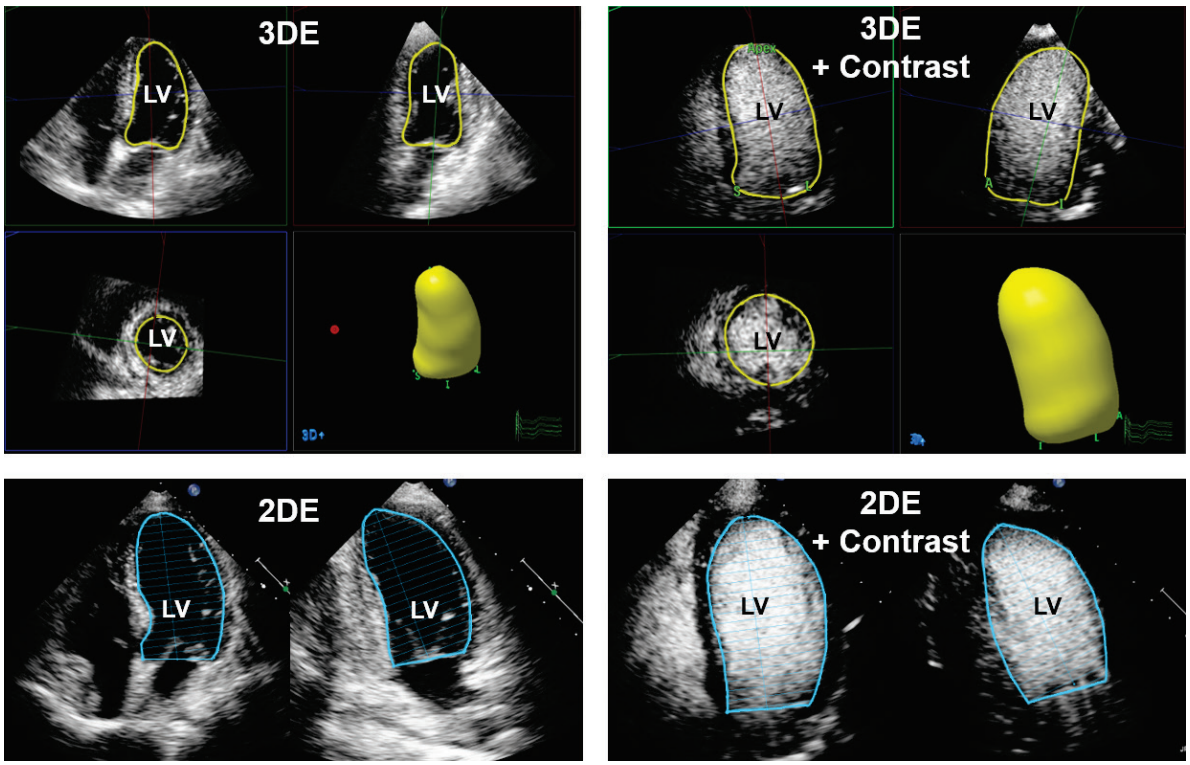

Figure 18 *Example of LV volume assessment in nonenhanced (left column) vs. contrast-enhanced echocardiography (right column) in 3D echocardiographic (3DE) data (upper row) and 2D echocardiographic (2DE) images (lower row). 3DE data sets were analyzed using dedicated software, yielding a 3D cast of the LV cavity. 2D data were analyzed using the biplane method of disks. All images are acquired from the same patient in Study II. LV, left ventricle.*

3.7 CARDIAC MAGNETIC RESONANCE IMAGING (STUDIES I AND II)

The patients were scanned on a 1.5 T CMR system (Signa Excite Twin Speed, General Electric Healthcare, Waukesha, WI, USA) using an 8-channel phased-array radiofrequency receiver cardiac coil. ECG-gated images were acquired during end-expiratory breath-hold. The LV was covered with retrospectively gated cine steady-state free precession images. Ten to twelve short-axis planes and two-, three-, and four-chamber views were obtained. Typical scanner parameters were: echo time 1.58 ms, repetition time 3.61 ms, flip angle 60°, 25 phases, 8-mm slice, no gap, matrix 226 × 226.

The CMR data were analyzed off-line using semiautomatic, freely available segmentation software (Segment V.1.8 R1405).[79] In short-axis image stacks, endocardial borders were delineated in end-diastole and end-systole. Papillary muscles and trabeculations were included in the LV volume. The basal short-axis slice was identified by simultaneously observing long-axis views of the LV while performing the tracings; specifically, the three-chamber view where the LV outflow tract is visible. This way, the LV outflow tract was included in the volume, and inclusion of the left atrium was avoided.

3.8 SINGLE-PHOTON EMISSION COMPUTER TOMOGRAPHY (STUDY I)

Patients received an injection of 600 MBq of ^{99m}Tc sestamibi (Cardiolite®, Lantheus MI UK Ltd) intravenously at rest. ECG-gated images were acquired one to four hours after injection using a dual-head gamma camera (DST-XL, Sopha Medical Vision, Bue Cedex, France). The protocol included imaging in steps of 5.6° using a 64 × 64 matrix, with a typical size of 5 mm × 5 mm and a slice thickness of 5 mm. A 20% energy window and 140 keV photopeak were used. Images were gated at eight frames per cardiac cycle using an R-wave trigger and 60 s per projection over a 180° orbit. The total acquisition time was 16 min. No attenuation or scatter correction was applied. The SPECT images were reconstructed with a filtered back-projection using a Wiener filter with a power of 4.5. The reconstructed voxel size was $3 \times 3 \times 3$ mm^3. To obtain LV volumes and EF, the images were analyzed off-line on a Vision workstation (IBM RS/6000) using semiautomated and commercially available software (QGS; Cedars-Sinai Health System, Los Angeles, CA, USA).

3.9 IMMUNOASSAY ANALYSIS (STUDIES III AND IV)

N-terminal pro-B-type natriuretic peptide (NTproBNP) in plasma samples were analyzed using a multiplex immunoassay (Olink Cardiovascular III; Olink Proteomics, Uppsala, Sweden). NTproBNP concentration is reported as normalized protein expression (NPX) units. NPX is a $\log_2$ scale; hence, an increase of 1 NPX unit means a doubling of protein concentration. NPX values are valid for relative quantification across samples but cannot be converted into absolute plasma concentration.

3.10 STATISTICAL ANALYSIS

Continuous variables are expressed as the mean ± standard deviation (SD) or the median and interquartile range (IQR) depending on the data distribution. A two-tailed P-value < 0.05 was considered statistically significant. The normal distribution of continuous variables was tested using the Shapiro–Wilk test. Correlation between variables was assessed by calculating Pearson's correlation coefficient r and by linear regression analysis. Between-group comparisons of means of continuous variables were performed using Student's t test. Between-group comparisons of skewed or ordinal data were performed using Wilcoxon signed ranks test for related samples and the Mann–Whitney U test for unrelated samples. The relationship between categorical variables was assessed using the chi-squared test or Fisher's exact test where appropriate.

In Studies I and II, the degree of concordance between imaging modalities was assessed by calculating the intraclass correlation coefficient (ICC) for a two-way random-effects model with absolute agreement. The strength of the agreement was deemed as poor (ICC < 0.20), fair (ICC 0.21–0.40), moderate (ICC 0.41–0.60), good (ICC 0.61–0.80), or very good (ICC > 0.80).[80] Bland–Altman plots were generated to assess the bias between measurements and the 95% limits of agreement (LOA) calculated as the mean bias ± 2SD.[81] One-way

repeated-measures analysis of variance was used to assess overall differences between groups in Studies I and III. In Study II, overall differences in related means were assessed using a general linear mixed model and *post hoc* analyses with a Bonferroni correction.

In Studies III and IV, logistic regression analysis was used to assess the association between variables measured at baseline and outcome variables. Variables with *P*-values < 0.10 in the simple logistic regression analysis were assessed for collinearity and entered in multiple logistic regression models. To avoid overfitting, only two variables were entered in each model. The likelihood ratio test was used to assess the contribution of a variable to the model. All combinations were tested, and the models were evaluated for their predictive performance using classification tables and Nagelkerke R^2 values. The discriminatory ability of variables and models was assessed by receiver operating characteristics (ROC) analyses.

Measurement variability was evaluated in randomly selected samples from the respective study population (n = 10 in Study I, n = 15 in Study II, n = 20 in Studies III and IV). Intra- and interobserver agreement was assessed by calculating the ICC (two-way random-effects model with absolute agreement). Variability was evaluated by calculating the coefficient of variation (CV), expressed as the within-subject SD as a percentage of the mean (Studies I and II), and by calculating the mean absolute percentage deviation (MAPD) expressed as the overall mean of the absolute percentage deviation from the mean of paired measurements (Study IV).

Statistical analyses were performed using IBM SPSS Statistics (versions 24–26; IBM Corp., Armonk, NY, USA) and Statistica (versions 9.0–10.0, Statsoft Inc., Tulsa, OK, USA).

3.11 ETHICAL CONSIDERATIONS

The patients included in the studies gave informed written consent, and all studies were approved by the Regional Ethics Review Board in Stockholm, Sweden.

Ethical principles for medical research involving human subjects are defined by the Declaration of Helsinki, which was adopted in its original form by the World Medical Association in 1964 and last revised in 2013. The declaration's first principle states that the health of the patient is the physician's first and most important consideration. This principle was met in the larger studies from which the study samples in the present thesis were recruited. All patients received the conventional treatment for their specific condition (PCI in patients with myocardial infarction in Studies I and II, and aortic valve surgery in patients with aortic valve disease in Studies III and IV). No patient was denied a well-proven treatment, and the extended treatment protocol used in conjunction with PCI in Studies I and II had shown promising results in animal studies before introduction in humans.

Another principle states that medical research involving human subjects must be preceded by careful assessment of predictable risks and burdens to the individuals involved in the research. In the present thesis, we used echocardiography as our primary diagnostic tool, which poses no known medical risk to the patients, although contrast administration may, on rare occasions,

cause allergic reactions. The patients in Study I underwent SPECT examination, which involves exposure to radiation, but gives valuable information also on LV volumes when SPECT is performed for other reasons. In this case, SPECT was performed as part of another study to determine area at risk for myocardial damage in patients with an acute myocardial infarction. The exposure to radiation and other potential health risks involved in the studies were stated in the written information given to the participants.

4 RESULTS

4.1 STUDY I

4.1.1 Left ventricular volumes

In study I, LV volumes and EF were measured using 3DE, SPECT, and CMR in patients with ischemic heart disease (n = 15). Results are presented in Table 2 and Figure 19. EDV and ESV were both underestimated by 3DE and SPECT compared with CMR (overall $P < 0.001$). The *post hoc* analyses demonstrated no difference between SPECT and 3DE ($P > 0.1$). The agreement between SPECT and 3DE on EDV and ESV measurements was good or moderate (ICC = 0.66 and 0.62, respectively). There was a moderate agreement on EDV determination between SPECT and CMR (ICC = 0.49) and a good agreement on ESV determination (ICC = 0.73). 3DE showed a fair agreement with CMR on EDV determination (ICC = 0.28) and a moderate agreement on ESV determination (ICC = 0.44). Bland–Altman plots of the agreement on LV volumes between methods are presented in Study I, Figures 2 and 3.

4.1.2 Ejection fraction

No significant difference was found in the EF estimates by 3DE, SPECT, and CMR (overall $P = 0.82$; Table 2). The agreement between CMR and SPECT was very good (ICC = 0.89), good between 3DE and CMR (ICC = 0.71), and moderate between 3DE and SPECT (ICC = 0.51). Bland–Altman plots of the agreements between methods are presented in Figure 20.

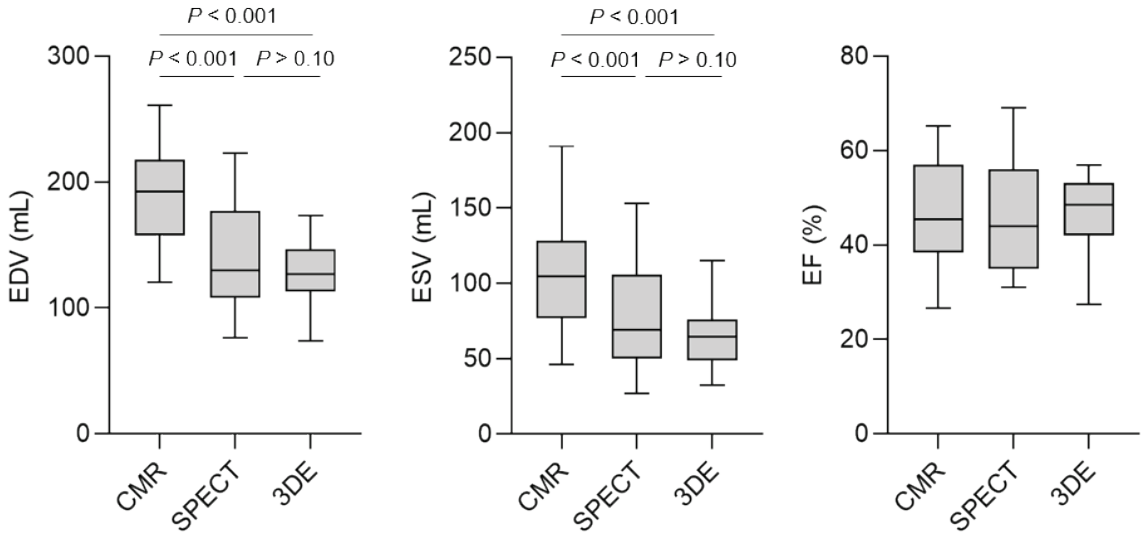

Figure 19 *Box plots of end-diastolic volume (EDV, left), end-systolic volume (ESV, middle), and ejection fraction (EF, right) measured using CMR, SPECT, and 3DE. Overall P = 0.84 for comparisons of EF estimates*

Table 2 LV volumes and EF determined using CMR, SPECT, and 3DE (n = 15)

	CMR	SPECT	3DE	Overall *P*
EDV (mL)	191 ± 42	137 ± 41[a]	127 ± 26[a,b]	< 0.001
ESV (mL)	105 ± 40	77 ± 36[a]	68 ± 22[a,b]	< 0.001
EF (%)	47 ± 11	46 ± 12	47 ± 8	0.82

Values are mean ± SD. 3DE, three-dimensional echocardiography; CMR, cardiac magnetic resonance; EDV, end-diastolic volume; EF, ejection fraction; ESV, end-systolic volume; SPECT, single-photon emission computed tomography. [a]$P < 0.001$ for 3DE and SPECT vs. CMR; [b] nonsignificant for 3DE vs. SPECT

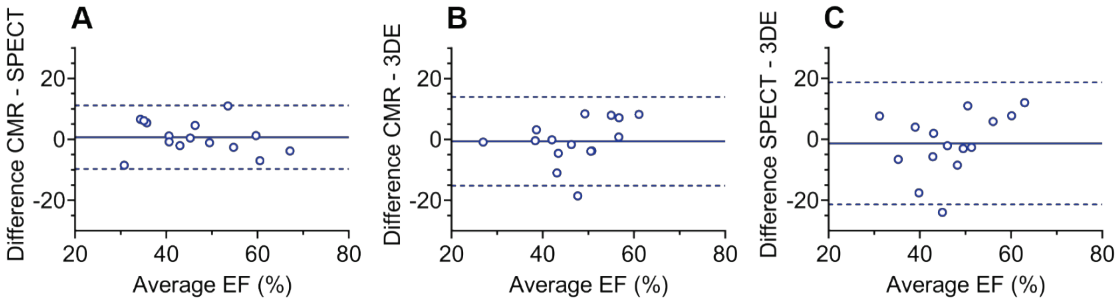

Figure 20 *Bland–Altman plots demonstrating the agreement for the measurement of EF between CMR and SPECT (A), CMR and 3DE (B), and SPECT and 3DE (C). The solid line represents the mean difference, and the dashed lines represent the 95% limits of agreement. 3DE, three-dimensional echocardiography; CMR, cardiac magnetic resonance imaging; EF, ejection fraction; SPECT, single-photon emission computed tomography.*

Table 3 Intra- and interobserver agreement on LV volumes and EF

		Intraobserver		Interobserver	
		ICC	CV (%)	ICC	CV (%)
3DE	ESV	0.95	7.44	0.54	26.6
	EDV	0.92	7.34	0.66	14.2
	EF	0.86	8.27	0.55	15.3
SPECT	ESV	1.00	2.0	1.00	1.76
	EDV	1.00	1.46	1.00	1.57
	EF	1.00	1.55	1.00	1.20
CMR	ESV	1.00	2.91	0.99	3.60
	EDV	0.99	1.62	0.99	1.96
	EF	0.99	2.96	0.99	2.90

3DE, three-dimensional echocardiography; CMR, cardiovascular magnetic resonance; EDV, end-diastolic volume; EF, ejection fraction; ESV, end-systolic volume; ICC, intraclass correlation; CV, coefficient of variation

4.1.3 Intra- and interobserver agreement

The intra- and interobserver agreement on the measurements of EDV, ESV, and EF for all three modalities are presented in Table 3. For CMR and SPECT, the intra- and interobserver agreements on EDV, ESV, and EF were very good, with ICC ranging from 0.99 to 1.00 and CV ranging from 1.5% to 2%. For 3DE, the intraobserver agreement was very good with ICC ranging from 0.86 to 0.95 and CV ranging from 7.4% to 8.3%; the interobserver agreement was moderate with ICC 0.54 to 0.66, and the CV was high, ranging from 15% to 27%.

4.2 STUDY II

4.2.1 Left ventricular volumes and ejection fraction

Study II aimed to study the impact of image quality and contrast enhancement on the assessment of LV volume and ejection fraction by 2DE and 3DE, using CMR as a reference standard. The study group consisted of patients with ischemic heart disease (n = 32).

LV volumes obtained using CMR were consistently greater than those obtained using 2DE, contrast-enhanced 2DE (CE2DE), 3DE, and contrast-enhanced 3DE (CE3DE; Table 4). There was no overall difference in the mean of the EF estimates between the modalities ($P = 0.12$).

The agreements on LV volumes and EF between CMR and 2DE and 3DE with and without contrast enhancement are presented in Table 5. For 2DE, the agreement with CMR on EDV and ESV was fair to moderate (ICC = 0.34 and ICC = 0.53 respectively). After contrast enhancement, the volume estimates increased, and the agreement with CMR improved (ICC 0.49 without contrast, ICC = 0.57 with contrast). Conversely, for EF determined by 2DE, the agreement was not increased with the addition of contrast (ICC = 0.73 without contrast, ICC = 0.69 with contrast); however, the limits of agreement (LOA) were comparable between the two methods (± 14.4 and ± 12.2 percentage units for 2DE and CE2DE, respectively). For 3DE, there was a moderate to a good agreement with CMR on EDV and ESV estimates (ICC = 0.56 and ICC = 0.70, respectively), which improved after contrast enhancement (ICC = 0.71 and ICC = 0.80, respectively). For the determination of EF by 3DE, the agreement with CMR was similarly good with and without contrast enhancement (ICC = 0.86 and ICC = 0.85, LOA ± 8.6 and ± 9.2 percentage units, respectively).

Table 4 LV volumes and EF measured using 2DE and 3DE with and without contrast enhancement compared with CMR (n = 32)

	CMR	2DE	CE2DE	3DE	CE3DE	Overall *P*
EDV (mL)	181 ± 42	122 ± 31[a]	144 ± 32[a,c]	150 ± 35[a]	164 ± 33[b]	< 0.001
ESV (mL)	91 ± 31	63 ± 22[a]	69 ± 20[a,c]	74 ± 23[a]	80 ± 26[b]	< 0.001
EF (%)	50.7 ± 8.3	48.6 ± 12	52.1 ± 7.2	51.3 ± 8.2	52.1 ± 8.6	0.12

Values are expressed as mean ± SD; [a] $P < 0.001$ vs CMR, [b] $P < 0.01$ vs CMR, [c] CE2DE nonsignificant vs 3DE. CMR, cardiac magnetic resonance imaging; 2DE, two-dimensional echocardiography; 3DE, three-dimensional echocardiography; CE2DE, contrast-enhanced two-dimensional echocardiography; CE3DE, contrast-enhanced three-dimensional echocardiography; EDV, end-diastolic volume; ESV, end-systolic volume; EF, ejection fraction

Table 5 Agreement with CMR on LV volumes and EF measured using 2DE and 3DE, with and without contrast enhancement (n = 32)

		ICC	Bias	95% LOA
2DE	EDV (mL)	0.34	-59	[-109, -9.0]
	ESV (mL)	0.53	-28	[-60, 4.0]
	EF (%)	0.73	-2.1	[-16, 12]
CE2DE	EDV (mL)	0.49	-37	[-91, 17]
	ESV (mL)	0.57	-22	[-58, 14]
	EF (%)	0.69	1.3	[-11, 13]
3DE	EDV (mL)	0.56	-31	[-87, 25]
	ESV (mL)	0.70	-17	[-47, 13]
	EF (%)	0.86	0.55	[-8.0, 9.2]
CE3DE	EDV (mL)	0.71	-17	[-67, 33]
	ESV (mL)	0.80	-11	[-41, 19]
	EF (%)	0.85	1.4	[-7.8, 11]

2DE, two-dimensional echocardiography; 3DE, three-dimensional echocardiography; CE2DE, contrast-enhanced two-dimensional echocardiography; CE3DE, contrast-enhanced three-dimensional echocardiography; EDV, end-diastolic volume; ESV, end-systolic volume; EF, ejection fraction; ICC, intraclass correlation; LOA, limits of agreement.

4.2.2 Image quality

The image quality index was 2.03 ± 0.53 for 2DE and 1.96 ± 0.48 for 3DE ($P = 0.35$). The image quality index increased for both modalities after contrast enhancement: to 2.47 for CE2DE and to 2.20 for CE3DE ($P < 0.001$ and $P = 0.02$ for the change). The segmental image quality scores with and without contrast enhancement are presented in Figure 21. Note that in 2DE, the three-chamber view was not evaluated because it is not included in the biplane volume quantification method, hence the dropouts in the diagram. In the 3DE studies, there was an

increase in the segmental image quality index of mainly the apical segments, whereas there was a decrease in the basal inferoseptal, inferior, and inferolateral segments following contrast enhancement; which was due to a contrast-shadowing effect.

The 2DE and 3DE studies were classified into two groups based on the image quality index, using a cut-off value of 2. For the estimation of EF with 2DE, the agreement with CMR was borderline moderate (ICC = 0.64) in the group with image quality index < 2 and very good in the group with image quality index ≥ 2 (ICC = 0.81). Regarding EF estimation with 3DE, the agreement was very good in both groups (ICC = 0.84 and ICC = 0.87, respectively).

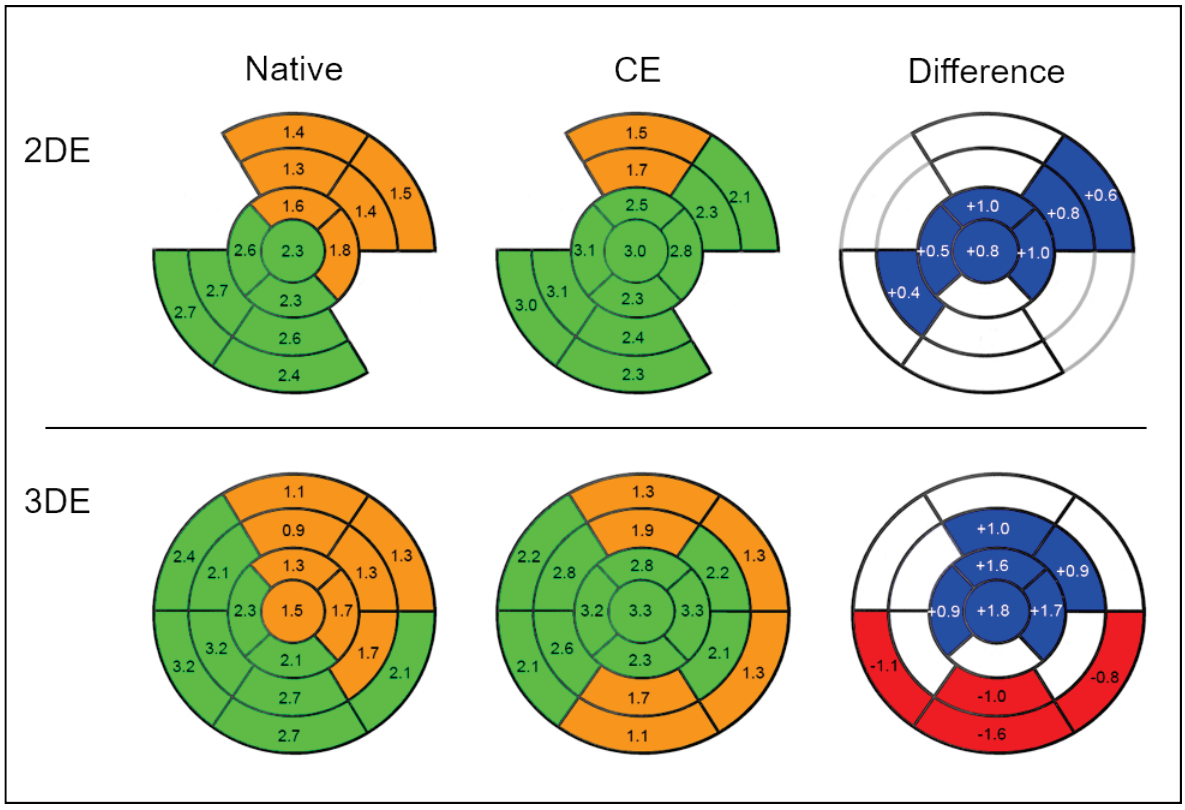

Figure 21 *Average segmental image quality scores on a scale from 0 to 4. 2D echocardiography (upper row) and 3D echocardiography (lower row), green: score ≥ 2, brown: score < 2. The left column represents nonenhanced (native) images and the middle column represents contrast-enhanced (CE) images. The right column demonstrates segments with a significant difference between nonenhanced and contrast-enhanced images, blue: increase, red: decrease.* Figure modified from Study II and published under the terms of Creative Commons Attribution-NonCommercial 4.0 License.

4.2.3 Intra- and interobserver agreement

The intra- and interobserver agreements of LV volumes and EF measurements are presented in Table 6. Figure 22 shows Bland–Altman plots for the interobserver agreement of EF measurements. For 2DE, the ICC increased and the CV decreased for all measured parameters after contrast enhancement. A similar pattern regarding interobserver agreement was observed for 3DE and contrast-enhanced 3DE.

Table 6 Intra- and interobserver agreement on LV volume and EF measurements obtained using 2DE and 3DE with and without contrast enhancement (n = 15)

		Intraobserver		Interobserver	
		ICC	CV (%)	ICC	CV (%)
2DE	EDV	0.90	8.9	0.86	10
	ESV	0.94	10	0.85	17
	EF	0.87	10	0.61	16
CE2DE	EDV	0.96	5.4	0.87	10
	ESV	0.92	9.9	0.91	12
	EF	0.87	6.6	0.84	6.9
3DE	EDV	0.86	9.1	0.60	17
	ESV	0.91	11	0.80	16
	EF	0.93	4.8	0.76	8.3
CE3DE	EDV	0.82	9.4	0.65	16
	ESV	0.87	13	0.81	17
	EF	0.86	6.8	0.86	6.7

2DE, two-dimensional echocardiography; 3DE, three-dimensional echocardiography; CE2DE, contrast-enhanced two-dimensional echocardiography; CE3DE, contrast-enhanced three-dimensional echocardiography; EDV, end-diastolic volume; ESV, end-systolic volume; EF ejection fraction; ICC, intraclass correlation; CV, coefficient of variation.

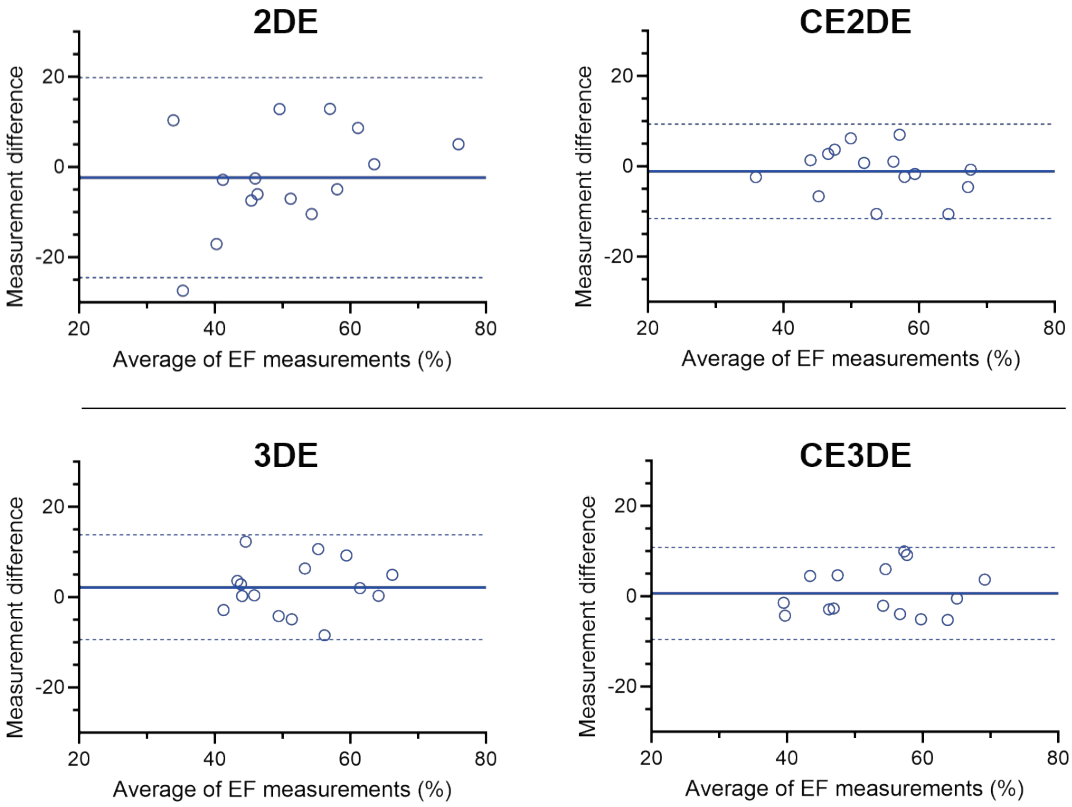

Figure 22 *Bland–Altman plots demonstrating the interobserver agreement for EF measurements. The solid line represents the mean difference, and the dashed lines represent the 95% limits of agreement. 2DE, two-dimensional echocardiography; 3DE, three-dimensional echocardiography; CE2DE, contrast-enhanced 2DE; CE3DE, contrast-enhanced 3DE*

4.3 STUDY III

Study III aimed to assess structural and functional effects of severe aortic regurgitation on the left ventricle and left atrium before and at one year after aortic valve surgery.

4.3.1 Left ventricular dimensions and systolic function

At baseline, the patients with AR had increased EDV, ESV, LVMi, and larger SV compared with the controls (Study III, Table 2). The patients with AR had lower EF than the controls (55 ± 7.3% vs 60 ± 4%, $P < 0.001$). There was no difference in GLS estimates (19.0 ± 3.0|%| vs 19.9 ± 2|%|, $P = 0.24$).

At the follow-up examination one year after valve surgery, decreases were observed in LV volumes, LVMi, and SV, whereas the EF had increased (from 55 ± 7.3% to 57 ± 7.1%, $P = 0.03$) in the patients with AR. No change was observed in GLS.

4.3.2 Diastolic function and left atrial function

At baseline, none of the controls and 21 (32%) of the patients with AR were classified as DD grade ≥ 2. In the AR patients, LASct was lower in the whole group compared with the controls (11.0 ± 4.7|%| vs 12.8 ± 5.6|%|, $P = 0.049$), but after Bonferroni correction only in AR patients with DD grades ≥ 2 (8.0 ± 3.7|%| vs 12.8 ± 5.6|%|, $P = 0.001$) (which was not clearly expressed in the Discussion in the published Study III). The AR patients stratified to DD grade < 2 and grade ≥ 2 differed in LAS phasic function parameters and NTproBNP levels, with lower LASr and LASct estimates and higher NTproBNP levels in the group with DD grades ≥ 2.

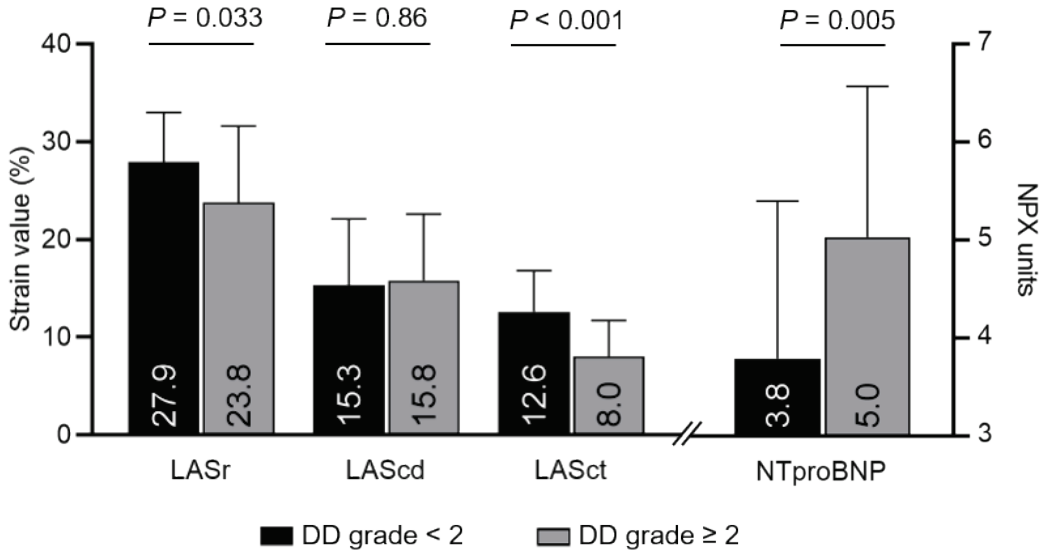

Figure 23 *Left atrial strain (LAS) phasic function and NTproBNP levels in AR patients stratified according to diastolic dysfunction grade. DD, diastolic dysfunction; LASr, reservoir phase; LAScd, conduit phase; LASct, contraction phase; NPX, normalized protein expression*

At follow-up, indices of diastolic function improved with 7 (11%) of AR patients classified as DD grade ≥ 2 and 55 (85%) classified as DD grade ≤ 1 ($P = 0.003$ for the distribution difference), LAVi decreased, and increases were observed in the LASr and LASct estimates (Figures 24 and 25).

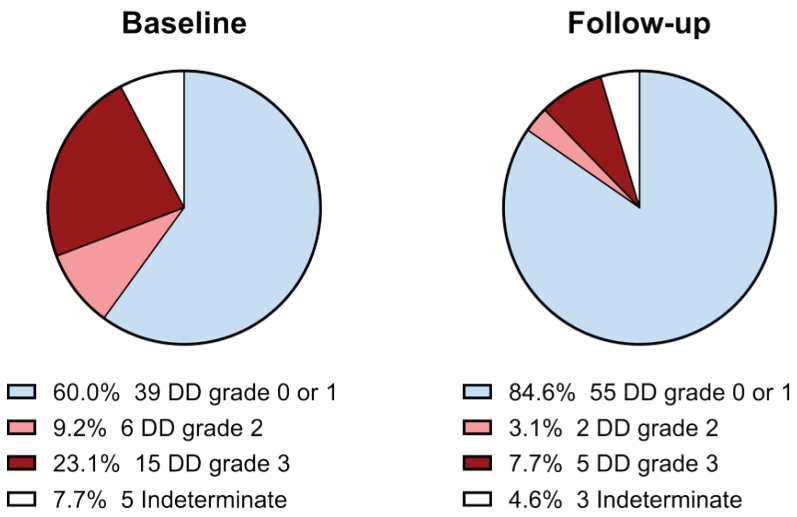

Figure 24 *Diastolic dysfunction grades in patients with AR at baseline and at one year after valve surgery (n = 65), P = 0.003 for the distribution difference; DD, diastolic dysfunction*

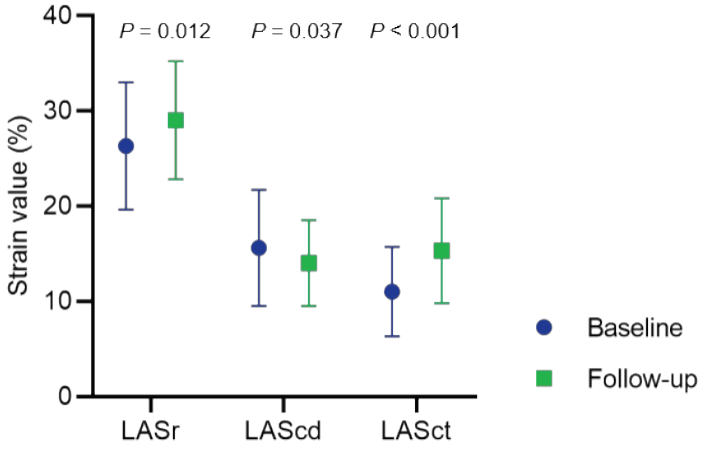

Figure 25 *Left atrial strain (LAS) phasic function in patients with AR at baseline and at one year after valve surgery. LASr, reservoir phase; LAScd, conduit phase; LASct, contraction phase*

4.3.3 Determinants of impaired LV functional and structural recovery

At the follow-up examination, 27 AR patients fulfilled one or more of the following criteria: EF < 50%, DD grade ≥ 2, EDVi above the gender-specific upper normal limit according to current guidelines (79 mL/m^2 for men, 71 mL/m^2 for women).[45] These patients were considered as having an impaired LV functional and structural recovery. Baseline variables were entered in logistic regression analyses with impaired LV functional and structural recovery as the dependent variable (Study III, Table 4). In the unadjusted analysis, end-systolic volume index

(ESVi) had the best predictive performance (OR 1.07, 95% CI [1.03, 1.12]; accuracy 70%). In multiple regression analyses, LAScd was the only variable that added significantly to ESVi in the predictive model (likelihood ratio test $P = 0.006$). The model with ESVi and LAScd combined had better discriminatory ability than ESVi alone (AUC 0.83 vs. 0.78, $P = 0.046$; Study III, Table 5).

4.4 STUDY IV

The aims of Study IV were to assess structural and functional effects of severe aortic stenosis on the left ventricle and to evaluate determinants of incomplete reverse remodeling following aortic valve surgery.

4.4.1 Left ventricular and left atrial dimensions and function

Compared with controls at baseline, patients with AS had increased LV wall thickness, increased LVMi, lower 2D GLS, lower 3D GLS, and increased LV twist. There was no difference in EF. LAVi was increased, LASr and LAScd were decreased. The patients with AS had increased mitral DT, higher E/e′ ratio, and higher TR peak velocity (Study IV, Table 2). 2D GLS and all 3D strain variables correlated with EF, LVMi, and NTproBNP at baseline (Study IV, Table 3).

At the follow-up examination one year after aortic valve surgery, LVMi had decreased (from 60.5 ± 15.4 g/m^2 to 53.6 ± 12.8 g/m^2, $P < 0.001$), 2D GLS had increased (from $18.8 \pm 2.6|\%|$ to $19.5 \pm 2.7|\%|$, $P = 0.002$), and LV twist had decreased (from $19.7 \pm 10.4°$ to $15.4 \pm 8.8°$, $P < 0.001$). There were no changes observed in EF or any of the 3D strain variables, 3D GLS, 3D GCS, or 3D PTS. There were no significant changes in E/e′, LA volume, or TR peak velocity (Study IV, Table 2).

Patient–prosthesis mismatch (PPM), defined as an indexed aortic valve area ≤ 0.85 cm^2 and aortic valve mean pressure gradient >20 mmHg, was present in 16 (13%) of the patients at the follow-up examination.

4.4.2 Incomplete LV reverse remodeling

Incomplete reverse remodeling (IRR) was defined as an LVMi estimate at the follow-up examination above the gender-specific reference upper limit (Figure 26). The reference upper limit was derived from the control group, calculated as the LVMi average plus 2 × SD, which was equal to 68 g/m^2 in males and 58 g/m^2 in females. Based on this criterion, 24 (20%) of the patients with AS were categorized as having IRR. Logistic regression analyses were performed to assess predictors of IRR (Study IV, Table 4). The most predictive variable in unadjusted analysis was LVMi (OR 1.15, 95% CI [1.1, 1.2]; accuracy 84%). Female gender was associated with a lower risk of IRR (OR 0.19, 95% CI [0.06,0.60]); however, the effect was not significant after adjustment for LVMi ($P = 0.48$). Conversely, age, E/e′, LAVi, postoperative systolic blood pressure, valve size, and PPM were not associated with IRR. In

multiple logistic regression analysis, 2D GLS was the only baseline parameter that significantly added to LVMi to predict IRR (likelihood ratio test $P = 0.042$; Study IV, Table 5). A model with LVMi and 2D GLS predicted IRR with 87% accuracy (model $P < 0.001$, AUC 0.93).

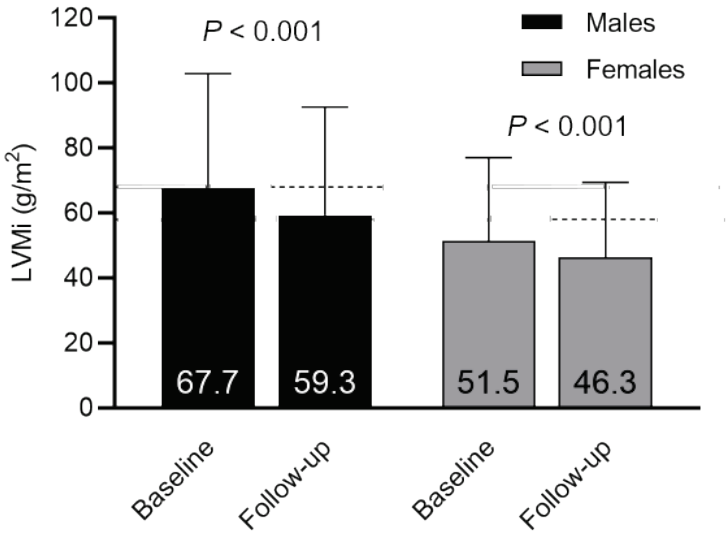

Figure 26 *Left ventricular mass index (LVMi) at baseline and after aortic valve surgery in patients with aortic stenosis. Dotted lines represent the cut-off values for incomplete left ventricular reverse remodeling at the follow-up examination for men and women.*

4.4.3 Observer agreement

Intra- and interobserver agreement on the 2D and 3D strain measurements are presented in Study IV, Table 6. The 2D GLS measurements showed a very good interobserver agreement (ICC = 0.86). There were good interobserver agreements on 3D GLS and 3D GRS measurements (ICC = 0.79 and 0.73, respectively), whereas the interobserver agreement on the 3D GCS and 3D PTS measurements were moderate (ICC = 0.50 and ICC = 0.58, respectively). The LV twist measurements showed a fair interobserver agreement (ICC = 0.34) with high variability (MAPD 23%).

4.5 SUMMARY OF LV AND LA ALTERATIONS IN AS AND AR

Figure 27 summarizes observed structural and functional LV and LA alterations in AS and AR patients before surgery compared with controls. The AS patients showed a concentric remodeling pattern with increased LVMi and increased relative wall thickness. Conversely, the AR patients showed an eccentric remodeling pattern with increased LVMi, but lower relative wall thickness.

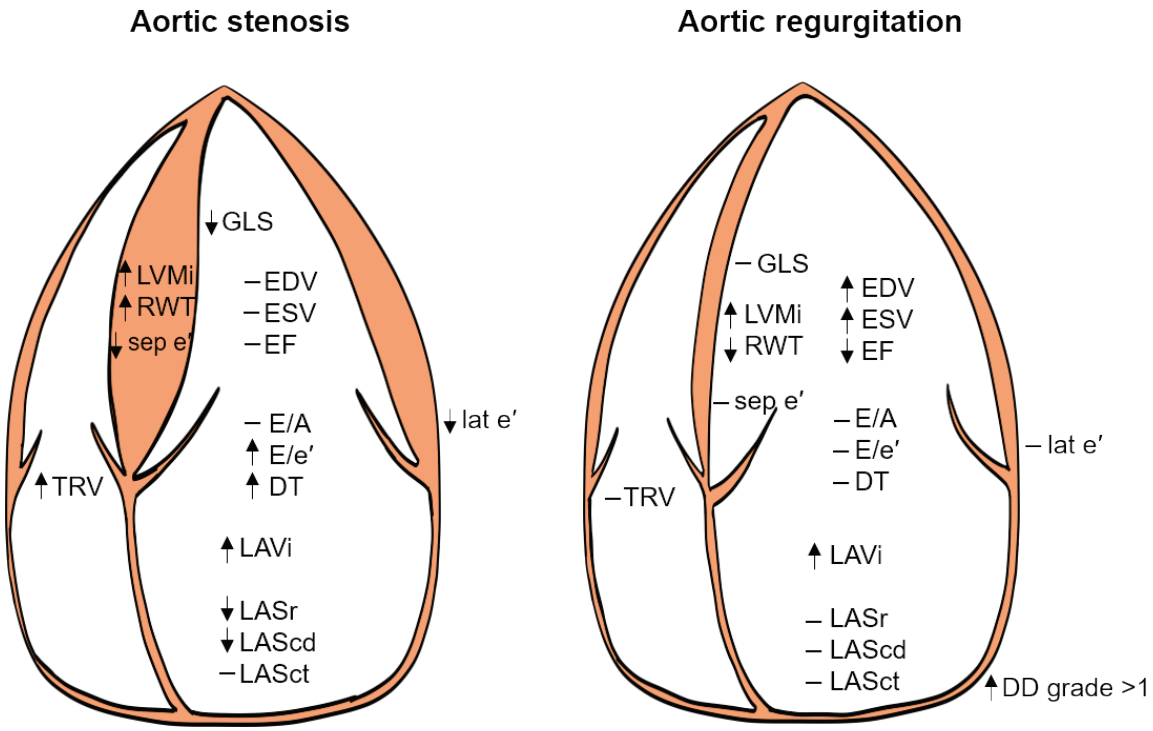

Figure 27 *Summary of LV and LA alterations in AS and AR observed in Studies III and IV. Arrows denote increased or decreased values compared with controls, and a dash denotes no difference. DD, diastolic dysfunction; DT, mitral E wave deceleration time; EDV, end-diastolic volume; EF, ejection fraction; ESV, end-systolic volume; GLS, global longitudinal strain; E/A, mitral E/A ratio; E/e', the ratio between mitral E wave and average septal (sep) and lateral (lat) e'; LAScd, left atrial strain conduit phase; LASct, left atrial strain contraction phase; LASr, left atrial strain reservoir phase; LAVi, left atrial volume index; LVMi, left ventricular mass index; TRV, tricuspid regurgitation velocity.*

5 DISCUSSION

In this thesis, left ventricular and left atrial remodeling and function were studied using currently available noninvasive imaging techniques. The most important variables to evaluate LV remodeling and function are LV volumes and EF. Therefore, the first two studies were focused on methodological aspects of the estimation of these parameters using 3DE, compared with traditional techniques and CMR as a reference standard. LV and LA remodeling and changes in systolic and diastolic LV function and phasic LA function were further explored in Studies III and IV. In these studies, LV and LA remodeling and reverse remodeling in response to alteration in loading conditions were studied using 2DE and 3DE, including strain measurements. The results are discussed below in the context of research in these areas.

5.1 ASSESSMENT OF LV VOLUMES AND EF IN ISCHEMIC HEART DISEASE

Accurate and reproducible measurements of LV volumes and EF are crucial in the diagnostic workup, risk assessment, and follow-up in a wide variety of cardiovascular diseases.[9,35-40] Several imaging modalities are being used to assess LV volumes and EF. For the clinician to make correct judgments on patients' diagnosis and treatment, it is essential to be aware of the performance and the differences in accuracy, precision, and reproducibility between the modalities, particularly if the same patient is examined with different modalities.

In Study I, we compared three different imaging modalities used in clinical practice to evaluate patients with cardiovascular diseases, namely SPECT, 3DE, and CMR, in 15 patients with previous myocardial infarction.

We found that the agreement on LV volume estimations was moderate between all three methods and that there were systematic differences in the LV volume estimates; EDV and ESV measured by CMR were higher compared with the measurements by both SPECT and 3DE. The agreement on EF estimation was good in terms of ICC and without any significant mean differences in the EF estimates; however, the limits of agreement were wide for SPECT vs. 3DE and CMR vs. 3DE, likely highly influenced by the relatively small sample size.

Of note is that although CMR is considered the *de facto* standard for LV volume measurement, the modality is not without its drawbacks. It is not as commonly available as echocardiography and is not appropriate in some cases, e.g., in patients with certain implanted devices. CMR cine images require repeated breath-holds to minimize motion artifacts, and if the patient cannot hold their breath, the accuracy of the LV volume measurements is decreased due to motion blurring. Even when patients can hold their breath, varying diaphragm positions between image acquisitions may cause slice misalignment in the short-axis cine image stack.[82] Furthermore, the retrospective ECG gating used in CMR cine image acquisitions makes the technique susceptible to artifacts caused by arrhythmia.

In SPECT, LV volumes add diagnostic and prognostic information in patients under evaluation for ischemic heart disease; however, SPECT exposes the patient to radiation and is also sensitive to arrhythmia due to the retrospective nature of the ECG-gating technique.

On the other hand, 3DE has the advantage of being a rapid bedside tool without known hazards to the patient. However, the technique used in the present studies required data acquisitions over four to seven consecutive heartbeats, rendering the method susceptible to arrhythmia analogous to CMR and SPECT.

The negative bias of LV volumes obtained using 3DE compared with CMR has been reported previously.[83] In our study, the mean difference in EDV estimation was 64 mL, and the mean difference in ESV estimation was 37 mL. The main reason for the discrepancy is the delineation of fine trabeculations, which are more easily discernable in CMR and by convention included in the LV cavity.[84] Trabeculations are less visible in 3DE and therefore tend to be delineated as part of the LV myocardium.[85] Furthermore, the LV outflow tract is easily visible and included in the LV cavity in CMR. In contrast, it was not included in the 3DE analysis due to restraints in the analysis software.

A previous study compared SPECT, 3DE, and CMR in 30 patients and found that 3DE underestimated LV volumes to a lesser extent than SPECT, which is in contrast with our results.[86] That study used a different 3DE analysis software, which includes the LV outflow tract, and the SPECT examinations were performed using ^{201}Tl, which has been reported to yield less reproducible LV volume estimates than ^{99m}Tc used in our study.[87]

For SPECT, the average underestimate of EDV and ESV compared with CMR was 54 mL and 28 mL, respectively. Others have reported similar findings using the same analysis software.[88-90] There are several possible reasons for the difference in LV volume measurements between the modalities. Analogous to 3DE, trabeculations are not visible in the SPECT images and might be incorporated in the LV wall by the SPECT analysis software. Furthermore, the LV outflow tract was not visible in the SPECT standard views, which means that it was excluded from the volume measurements. Another explanation might be the presence of dropouts in the SPECT images because of infarcted LV myocardium, that will hamper the LV volume estimations. Our sample size was too small to assess whether the infarct size significantly impacted the LV volume estimations. There is also a difference in time resolution between CMR and SPECT that likely affected the results. The CMR images were acquired typically using 25 phases per cardiac cycle, whereas the SPECT images were acquired using eight images per cardiac cycle. This difference should primarily affect the agreement on ESV because the R-wave in the ECG identifies EDV by both methods. Using eight-frame ECG gating has been shown to result in an underestimation of EF by 3.7 percentage points compared with sixteen-frame ECG gating.[71]

In the comparison between 3DE and SPECT, we found no significant differences in the mean estimates of LV volumes and EF. However, although the agreements were moderate to good, the Bland–Altman analyses revealed considerable variability between the methods, with 95%

LOA on EF measurements of ±20%. This result was likely affected by the small sample size, with outliers having a significant influence on the results. Others have reported less variability. In a study including 91 patients with ischemic heart disease, there was no significant bias in the EF measurements between SPECT and 3DE, and the 95% LOA for the difference in EF was ±12%.[91]

The intra- and interobserver agreement on LV volumes and EF were exceptionally good for CMR and SPECT, which is in line with previous reports.[68,86] For SPECT, this finding was related to the high degree of automation in the software used for LV volume and EF measurements. The CMR software was not automated to the same degree. However, the excellent contrast between the blood in the LV cavity and the myocardium facilitates reproducible delineations of the endocardial border. For 3DE, the intraobserver agreement was good, whereas the interobserver agreement was moderate, and the variation was high. In echocardiography, image quality and measurement precision depend on the patient's body composition. Furthermore, the determination of LV volumes is dependent on the experience of the examiners,[85] which possibly played a part in the results of our study.

Echocardiography is the most frequently used noninvasive diagnostic tool for the evaluation of cardiac volumes and function. In Study II, we focused on the performance of 3DE and 2DE, the impact of echocardiographic image quality, and the value of contrast-enhanced echocardiography for the assessment of LV volumes and function in 32 patients with previous myocardial infarction. CMR was used as the reference standard.

The main findings of the study were that all echocardiographic modalities underestimated LV volumes compared with CMR. CE3DE showed the highest agreement with the least bias, and 2DE showed the least agreement and highest bias. 3DE and CE2DE were comparable in terms of agreement and bias of LV volume measurements. Contrast enhancement improved the endocardial border delineation resulting in less negative bias for both 2DE and 3DE regarding LV volumes. In a previous study on the interobserver variability of 3DE volume delineation, the apical cap, the anterior and anterolateral walls, and the basal anteroseptal wall showed the most errors between investigators.[92] In our study, many of these segments showed a significant increase in image quality score after contrast enhancement, which might explain the reduced bias and improved interobserver agreement for CE3DE compared with 3DE. In contrast, the basal inferoseptal, inferior, and inferolateral segments showed a decrease in image quality score in CE3DE compared with 3DE, which was due to a shadowing effect by the contrast agent. This shadowing effect did not significantly impair the volume calculations, most likely because the atrioventricular plane, which is usually visible, aids the definition of the basal part of the LV.

Conversely, contrast enhancement did not improve the agreement with CMR on the estimation of EF for either 3DE or 2DE in the group as a whole. However, when stratified according to image quality, an improvement was observed for 2DE in cases with poor image quality (image quality index < 2), whereas there was no difference between the groups for 3DE, suggesting that contrast enhancement plays a more important role in 2DE than in 3DE. This might be

explained by the 3DE analysis software's ability to "cover" nonvisualized segments using information from the border delineation in adjacent visible segments.[32]

The main advantage of contrast enhancement in our study was the improvement seen in intra- and interobserver agreement, which is an important factor in the serial follow-up of patients.

Our results regarding the underestimation of LV volumes using 2DE and 3DE compared with CMR are consistent with previous reports.[83,93,94] The reasons for the discrepancies are multifactorial. For 2DE, the biplane method of disks used for the volume calculations relies on two orthogonal planes prone to foreshortening errors and relies on geometric assumptions that might not hold up in asymmetrically remodeled left ventricles. On the other hand, 3DE is not hampered by image foreshortening, and the volume calculation *per se* does not rely on geometric assumptions regarding the LV shape. However, the pyramidal 3D shape cannot always accommodate larger ventricles. Indeed, there was a trend toward increased disagreement between 3DE and CMR for larger LV volumes in our study. Furthermore, as discussed above, trabeculations are generally easily discernible in CMR images and are included in the LV cavity by convention. In contrast, in 3DE trabeculations might be lumped together with the myocardium, owing largely to a lower lateral resolution compared with CMR. The result is an underestimation of LV volumes using 3DE. Fortunately, the latter effect is a systematic bias that can be addressed. Using water-filled balloons, the authors of a previous study demonstrated that boundary tracings should not be defined by the innermost echo in 3DE because this resulted in a significant underestimation of the enclosed volume.[85] Newer 3DE analysis software offers the option to adjust the default extension of the algorithm's LV boundary definition into the myocardial wall, and investigators have reported an improved agreement and less bias compared with CMR using this adjustment.[95]

5.2 LV AND LA REMODELING IN VOLUME OVERLOAD

Severe AR results in volume overload of the LV, which leads to increased preload and afterload. As long as the LV is compliant, the LV harbors the volume overload without increasing filling pressure. Over time this process induces progressive LV dilatation associated with increased wall stress, myocyte apoptosis, and increased fibrous content of the myocardium, resulting in increased LV stiffness.[96-99] Eventually, this leads to impaired systolic function. If the processes have gone too far, the detrimental effects on the LV may become irreversible. Thus, LV dimensions and systolic function are well-established predictors of outcome and need for surgery in AR patients.[100-105] Volume overload and increased LV stiffness in AR also affect LV diastolic function, which in turn have an impact on LA size and function. However, LV diastolic function has not been studied as extensively as LV systolic function in patients with AR, and the data on LA function in these patients is limited.[8,106]

Our study found that patients with severe AR had increased LV volumes and LV mass, reduced EF and increased LA volumes compared with controls. One-third of the patients had signs of DD at baseline, compared with none of the controls. The reduction in volume overload

following aortic valve surgery was associated with reductions in LV volumes, LV mass, LA volume, and an increase in the EF estimates. Indices of diastolic function improved in most AR patients, even though 10% were still in DD grade ≥ 2 at follow-up. We observed significant alterations in LA phasic function during the follow-up period with increases in LASr and LASct. In multiple logistic regression analysis, LAScd added significantly to ESVi to predict impaired functional and structural recovery after surgery.

The observation that ESVi was associated with adverse outcome was not surprising, given the abundant evidence of LV dimensions as prognostic markers in AR. However, to the best of our knowledge, LA phasic function dynamics and prognostic value in patients with AR undergoing AVR have not been previously described.

The regurgitation flow in AR is a diastolic process that coincides with LAScd and LASct during the heart cycle. We found a reduction in LASct in patients with AR and DD grade ≥ 2 compared with controls, which indicates a diminished active atrial contraction in these patients. This observation might be explained by increased LV preload imposing an increased afterload on the left atrium. However, increased LV myocardial stiffness likely played an important role – the pattern of LAS phasic function alterations that we observed differs from the pattern reported in acute LV preload changes in healthy volunteers, where all components of LA phasic function were reduced.[107] Furthermore, in a study on healthy athletes, chronic volume load imposed by training was associated with increases in the LA conduit and reservoir phase, whereas the LA contraction phase was not altered, supporting that our finding in patients with AR is a pathological process not solely dependent on LV preload.

A significant association between LA phasic function and DD has been established previously, albeit not in patients with AR.[108] We observed an association between LA phasic function and DD in patients with AR, with lower LASr and LASct values in patients with DD grade ≥ 2 compared with those with DD grade < 2. In parallel, the NTproBNP concentration was 2.3 times higher in the patients with DD grade ≥ 2, suggesting a difference in LV filling pressure between the groups. Therefore, it seems that the substrate for DD exists in AR patients before and may remain after unloading of LV following AVR.

We found a high prevalence of DD in patients with AR. This observation has been made previously, although the diagnostic criteria for DD are not consistent between studies. In a study on 41 patients with AR and depressed systolic LV function, 58% were classified as having pseudo normal or restrictive diastolic dysfunction.[109] In another report, DD grade 2 or 3 was present in 65% of 104 patients with severe AR.[110] At follow-up, 10% of the AR patients in our study were still classified in grade ≥ 2. In a report on a small sample of AR patients undergoing AVR and endomyocardial biopsies, invasively assessed LV stiffness was increased, and LV interstitial fibrosis remained elevated late (mean of seven years) after surgery.[111]

We also measured GLS in the patients with AR. GLS has been shown to be predictive of LV dysfunction, mortality, and the need for surgery in AR patients.[112-115] In a recent study on 865

patients with AR undergoing AVR, lower absolute GLS at baseline was associated with reduced survival.[116] In our study, the GLS estimates did not differ significantly between the AR patients and the controls, and there was no significant change in GLS during the follow-up period. These findings might partly be explained by the complex load dependency of GLS. GLS is positively related to SV and inversely related to EDV,[117,118] which are both increased in AR preoperatively and reduced following AVR, resulting in counteracting effects on GLS. In a previous study, GLS showed a biphasic response following AVR in AR patients, with a decrease at one year after AVR followed by an increase during the following year. The authors suggested that this was due to the Frank–Starling relationship, where decreased preload following AVR results in decreased contraction force and consequently decreased GLS.[119] Another study using myocardial tissue tagging by CMR found a decrease in longitudinal strain following AVR in AR patients. The authors suggested that this might be explained by residual myocardial fibrosis.[120] Conversely, other investigators have proposed to normalize GLS to EDV and accordingly reported an increase in indexed GLS following AVR in patients with AR, driven by the decrease in EDV and not in GLS *per se*.[121] Moreover, signs of decreased systolic function may only be evident during exercise. In a study on 21 patients with severe AR, LV longitudinal function during exercise stress, but not at rest, was associated with reverse remodeling after AVR.[114]

5.3 LV REMODELING IN PRESSURE OVERLOAD

In Study IV, we investigated LV remodeling at baseline and LV reverse remodeling at one year after aortic valve surgery in 120 patients with severe AS, using 2D and 3D speckle-tracking echocardiography. We found that the patients with AS had increased LVMi and reduced GLS as measured using both 2D and 3D strain techniques despite having normal EF. This was accompanied by an increased LV twist. Following AVR, the relief of pressure overload increased 2D GLS and decreased LV twist. LVMi decreased during the one-year follow-up period to a value within normal limits in 80% of the patients. The remaining 20% of cases were categorized as incomplete reverse remodeling (IRR).

5.3.1 LV hypertrophy

AS results in pressure overload of the LV, causing increased systolic LV wall stress. This acts as a stimulus for concentric myocardial hypertrophy, which is considered a compensatory mechanism to maintain wall stress within normal limits.[122] However, there is increasing evidence that the hypertrophic response in AS is heterogenic and that some patients develop excessive LV hypertrophy as a maladaptive rather than a purely compensatory mechanism, with potentially irreversible structural alterations of the LV.[123,124] In a study using CMR to assess remodeling patterns in AS, there was only a weak correlation between AS severity and the degree of LV hypertrophy, suggesting that other factors are involved in the process of LV hypertrophy.[125] This event was also evident in a study on 137 patients with AS, where LV mass was predictive of systolic dysfunction and heart failure, independent of the severity of valvular obstruction.[126] Furthermore, excessive LV hypertrophy was found to be a strong predictor of

increased cardiovascular events in asymptomatic patients with severe AS, independent of other risk factors.[127]

The transition process of LV hypertrophy from an adaptive to a maladaptive state involves myocyte cell death and myocardial fibrosis.[128] In a histopathological study on patients with severe AS stratified according to LV systolic function, interstitial fibrosis was already present in the group with normal EF and was significantly increased in patients with severely depressed EF.[129] These findings were confirmed by a study using CMR to assess fibrosis in AS patients, where interstitial fibrosis, detected by increased extracellular volume, and focal replacement fibrosis were associated with LV hypertrophy and LV dysfunction.[130]

The treatment for symptomatic severe AS is AVR, which relieves the LV of pressure overload, and thus removes one stimulus for LV hypertrophy. Consequently, investigators have consistently reported a decrease in LV mass following AVR, albeit to different degrees related to differences in the follow-up period, comorbidities, echocardiographic techniques, and prosthetic valves used.[131-135] LV mass regression after AVR is an important process that carries prognostic implications because a greater reduction is associated with lower hospitalization rates and improved survival.[136-138] However, although LV hypertrophy is reduced after AVR due to decreased myocyte volume, myocardial fibrosis might persist for years.[139,140]

In Study IV, IRR was present in 20% of patients with AS one year after AVR. The model that was most predictive for IRR was LVMi and 2D GLS. Our results are in line with a previous study of 529 patients undergoing AVR for severe AS, where baseline LVMi was predictive of abnormal LVMi regression at seven-year follow-up.[141] We also confirmed results from a recent study on 152 patients with severe AS undergoing transcatheter aortic valve replacement, where LV mass regression was predicted by baseline LV mass and GLS.[142]

Interestingly, neither PPM nor prosthetic valve size was associated with IRR. This observation might indicate that PPM by our definition (≤ 0.85 cm^2 and mean pressure gradient > 20 mmHg) was not hemodynamically significant in these patients. It is important to note that we did not have information on symptoms or functional status at the follow-up examination, which would have identified patients with clinically significant PPM. Nevertheless, similar results have been reported by others.[131,141]

5.3.2 2D Deformation analysis

LVMi was less likely to normalize after AVR in patients with lower 2D GLS and higher LVMi preoperatively. Moreover, the contribution of 2D GLS to LVMi was significant in the predictive model, suggesting that GLS is an indicator of myocardial systolic functional alteration that is not solely related to LV hypertrophy. A previous report found that longitudinal strain was associated with LV fibrosis irrespective of LV wall thickness in patients with AS, suggesting that GLS might primarily be an indicator of LV fibrosis in these patients.[143]

Conversely, EF was associated with IRR in unadjusted analysis but did not add to LVMi in the predictive model. Indeed, GLS is a well-established measure of longitudinal LV function that

has been shown to be a more sensitive marker of LV functional alterations than EF in several cardiovascular conditions, including AS.[144] In concentric LV hypertrophy, the EF is frequently preserved when the longitudinal function decreases because of an increased wall thickening (i.e., radial motion). The thickening is due to a geometrical relationship between EF and wall thickness in the hypertrophied LV.[43,145,146] Moreover, a decrease in GLS may be compensated by only a small increase in GCS to preserve EF in the hypertrophied LV.[147] Accordingly, we observed reduced 2D GLS despite normal EF in patients with AS. EF estimates were more closely correlated with 3D GCS, 3D GRS, and 3D PTS than with 2D GLS. Moreover, the reduction in pressure overload and regression in LV hypertrophy after AVR was associated with improved 2D GLS during the one-year follow-up period, while the EF was unchanged. The improvement in GLS is in accord with previous studies listed in Table 7. Although the improvement in longitudinal function might be explained by the relief of pressure overload and the regression of LV hypertrophy *per se*, a reduction in LV fibrosis and improved LV microcirculation are likely to be contributing factors here.[148] Separating the effect of contractility from that of load alterations on deformation parameters is not trivial and requires studying the LV performance under varying loading conditions and heart rates.[149] Adjusting LV strain measurements for afterload using stress–strain relationships may provide a more load-independent index of LV systolic performance. In a recent study on patients with severe AS, the end-systolic stress–strain index identified patients with increased myocardial fibrosis and was associated with functional recovery after AVR.[150] Current guidelines incorporate EF in the decision algorithm for valve replacement in patients with severe AS. However, strain imaging appears to be a more sensitive marker of LV dysfunction in these patients and might improve patient selection by identifying patients who would benefit from early intervention.

5.3.3 3D Deformation analysis

The principal tangential strain (PTS) is derived from 3D speckle-tracking analysis and describes myocardial deformation by its principal direction tangential to the endocardial surface.[54] PTS has been proposed to be related to the myofiber geometry in the LV and to provide a simplified LV function assessment.[151] Previous investigators have used 3D strain analysis in studies of healthy athletes and patients with hypertension and found no significant difference in 3D GLS or 3D GCS in these groups compared with controls. However, when they applied principal strain analysis, while differences were observed, they were not in the direction of PTS *per se*, but in its perpendicular direction, which is designated as secondary strain.[151,152] We could not confirm a discriminatory ability of PTS between patients with AS and controls. The 3D-derived strain variables that were significantly altered in AS patients were 3D GLS and LV twist. 3D GLS was associated with IRR in simple regression analysis analogous to 2D GLS; however, it did not add significantly to LVMi in the predictive model in multiple regression analysis. Furthermore, 2D GLS was more sensitive than 3DE for the detection of a small but statistically significant increase in LV longitudinal function after AVR. This was likely explained by a more favorable intraobserver agreement on 2D GLS measurements compared with those obtained by 3D GLS and possibly related to lower spatial and temporal resolution in 3DE compared with 2DE.

LV twist represents rotational deformation that arises from the counterhelical arrangement of the LV myofibers and is important for LV ejection.[153] We confirmed previous observations of increased LV twist in AS patients compared with controls, possibly acting as a compensatory mechanism to maintain stroke volume.[154-156] Unopposed subepicardial rotation due to subendocardial ischemia has also been proposed to explain increased twist in AS.[157] Others have found LV twist to be associated with LV afterload in patients with LV hypertrophy and to correlate with AS severity[154,156] Interestingly, LV twist did not correlate with valvulo-arterial impedance in our study. Nevertheless, there was a reduction in LV twist at the follow-up examination, representing reverse remodeling toward normal myocardial mechanics in AS patients, which is in line with previous reports.[158,159]

There was a consistent bias between the 3D GLS and the 2D GLS estimates at baseline and follow-up. This observation is not surprising given different strain modalities (i.e., 2D myocardial strain and 3D endocardial strain) and different software vendors.[77,160,161] Therefore, a direct comparison of the GLS estimates between the modalities may not be meaningful in the absence of a proper reference standard. However, the difference in absolute estimates does not preclude a comparison between the modalities regarding precision and diagnostic performance.

Table 7 Studies on alterations of LV deformation indices after aortic valve replacement for severe aortic stenosis

Study	Year	n	Patient characteristics	TAVR/ SAVR	Follow-up	Changes relative to baseline measurements
Naeim et al.[181]	2020	80	Preserved EF, reduced EF	TAVR	8 mo	Preserved EF: GLS +10%, LV twist -27%; Reduced EF: GLS +20%, LV twist +58%
Al-Rashid et al.[180]	2020	150		TAVR	3 mo	GLS +23%
Reskovic Luksic et al.[179]	2020	62	Preserved EF	TAVR	3.5 y	GLS N.S., mid-level RS +17%
Dahl Pedersen et al.[178]	2020	499		TAVR	743 d	ABr related to NT-proBNP and mortality risk
Lozano Granero et al.[177]	2019	119		TAVR	1 y	GLS +7%
Alenezi et al.[142]	2019	152		TAVR	1 y	GLS +3%, GLS predictive of LV mass regression
Lozano Granero et al.[176]	2018	92		TAVR	5 d	GLS +9%
Corrigan et al.[175]	2018	123	Reduced EF, preserved EF	TAVR	1 y	GLS +10%
Fries et al.[174]	2017	514		both	5 y	GLS independent predictor of all-cause mortality
Kim et al.[173]	2016	28		TAVR	1 mo	GLS endo +11%, mid +12%, epi +10%; CS N.S.
Kamperidis et al.[172]	2014	68	LFLG AS	TAVR	1 y	GLS +14%
Spethmann et al.[171]	2014	54	Preserved EF, LFLG, reduced EF	TAVR	1 y	GLS +17%
Staron et al.[170]	2013	66	Preserved EF	SAVR	4 mo	LS +27%, CS +11%, ApRot N.S. CS predictive of LV mass regression
Dahl et al.[169]	2012	125	EF>40%	SAVR	4 y	GLS independent predictor of MACEs
Giannini et al.[168]	2011	50	Preserved EF	TAVR	3 mo	LS increase, RS increase, CS increase
Grabskaya et al.[167]	2011	36		SAVR	1 mo	LS +11%, RS + 17%, CS N.S.
Lindqvist et al.[159]	2011	28	Preserved EF	SAVR	6 mo	LV twist -27%
Lindqvist et al.[166]	2010	41	Preserved EF	SAVR	6 mo	Lateral S +25%, Septal S N.S.
Rost et al.[165]	2010	40		SAVR	6 mo	LS +16%, RS +21%, CS +28%
Delgado et al.[164]	2009	73	Preserved EF	SAVR	17 mo	LS +12%, RS +20%, CS +13%
Becker et al.[163]	2007	22		SAVR	6 mo	RS +10%, CS +16%
Poulsen et al.[162]	2007	45	No CAD	SAVR	12 mo	Mean SS +55%

CAD, coronary artery disease; CS, circumferential strain; GLS, global longitudinal strain; LFLG, low-flow low gradient; LS, longitudinal strain; N.S., nonsignificant change; RS, radial strain; S, strain; SAVR, surgical aortic valve replacement; SS, systolic strain; TAVR, transcatheter aortic valve replacement

5.4 LIMITATIONS

5.4.1 Studies I and II

In Study I, the sample size was small, making the statistical analyses sensitive to measurement variability and outliers. There were few women in Studies I and II, but this should have little impact for the purpose of our study because a gender effect on the agreement between the imaging modalities is unlikely. The semiautomated analysis software used for the 3DE analyses was not optimized for contrast-enhanced images, necessitating more manual tracings in these data sets, which might have had a negative impact on the intra- and interobserver agreement for CE3DE compared with 3DE in Study II. The patients were not examined on the same day in all cases in Study II, which might have impacted the agreement between the modalities. However, LV volume alterations generally occur during the first month following a myocardial infarction,[182] and the mean period from the cardiac event to imaging was 11 months in our study. Furthermore, there were no significant changes observed by CMR in the mean EDV and ESV estimates between the examinations at 3 months and at 12 months in the study group from which our sample was drawn.[183] Therefore, we assume that the LV volumes remained stable at the time of echocardiography and CMR, and if not, the bias introduced would be equal for all echocardiographic modalities.

5.4.2 Study III

The assessment of DD remains challenging in AR.[7] The simultaneous diastolic inflow from the LA and the aorta to the LV constitutes a fundamental difference in diastolic filling dynamics compared with other conditions. The mitral inflow pattern might be influenced by an eccentric AR jet, and the relative contribution of AR severity and LV stiffness to LV filling pressures is not readily assessed. However, a previous study assessing diastolic function in AR patients using invasively measured LV pressures found that indices of DD were indeed present in 20 of 22 patients, despite normal EF.[106] Moreover, we found a significant difference in NTproBNP levels between patients classified as DD grade ≥ 2 and DD grade < 2, supporting the validity of the integrative algorithm to differentiate between normal and increased filling pressures in patients with AR. To assess whether the trauma of cardiac surgery *per se* would induce changes in LV function or LAS, a control group was recruited among patients free from significant aortic valve disease who underwent open thoracic surgery for a thoracic aortic aneurysm during the same period. There were no significant changes in LV or LA volumes or function in the control group, suggesting that the alterations observed in the AR patients were not significantly affected by the trauma of surgery. The relatively short follow-up time and small sample size precluded the use of hard outcomes such as mortality or major cardiac events. Instead, we used a composite variable to define impaired LV functional and structural recovery, which might limit the generalizability of the results. Thus, the prognostic implications of LAS in patients with AR merits further studies in larger cohorts.

5.4.3 Study IV

The study was a single-center observational study with a one-year follow-up period. Therefore, we were not able to study hard clinical endpoints such as mortality or longer-term outcome. However, LV mass regression following AVR is a clinically relevant outcome variable proven to have prognostic implications in AS patients.

The controls were not age-matched with the patients, which may have introduced a bias in the comparison of echocardiographic data. However, they did not differ in other possible confounding factors, such as blood pressure or gender. The controls were used to define a normal range for the definition of IRR, and for this purpose, age is not an important factor because the correlation between LVMi and age is weak.[47,184]

We chose to perform LV mass measurements using the biplane method of disks in images derived from 3DE volumes. This methodology has been shown to yield more accurate results and with less interobserver variability than the 2D biplane method.[185] However, to our knowledge, no comprehensive reference ranges using the same approach are available. The reference ranges stated in current guidelines are based on either linear measurement, 2D area–length or truncated ellipsoid technique, or 3D calculations where the entire LV is delineated along with the endo- and epicardium.[45,184,186,187]

Software from different vendors were used for 2D and 3D strain analyses, which might affect the generalizability of the results. This should be considered when comparing the modalities and different studies.

6 CONCLUSIONS

Comparisons of 3DE, SPECT, and CMR showed significant differences between the modalities for LV volume measurements and that both 3DE and SPECT underestimate the LV volumes compared with CMR. Despite the differences between the three modalities for the measurement of LV volumes, the determination of EF showed good agreement between all three modalities. However, the limits of agreement for EF estimation were wide for SPECT vs. 3DE and 3DE vs. CMR.

3DE was more accurate than 2DE for LV volume measurement and showed more favorable intra- and interobserver agreement of EF estimates. Contrast enhancement improved accuracy for both 2DE and 3DE and improved inter-observer variability of EF estimates. Poor image quality had a more negative impact on the accuracy of EF estimates for 2DE than for 3DE. Our results emphasize the importance of using the same technique for longitudinal studies of LV EF and especially LV volumes.

One-third of patients with chronic severe AR had signs of impaired LV diastolic function. Reduction of volume overload following aortic valve surgery improved diastolic LV function, decreased LV and LA volumes, and increased LA reservoir and contractile function. LA conduit strain added incremental prognostic value to the well-established LV end-systolic dimension to predict impaired LV functional and structural recovery following aortic valve surgery. However, further research is needed to establish the role of LA strain in the echocardiographic evaluation of AR patients.

Patients with isolated severe AS had increased LVMi accompanied by an increased LV twist and reduced GLS as measured using both 2D and 3D strain techniques, compared with controls. Aortic valve replacement resulted in relief of pressure overload and was associated with reduced LVMi, improved 2D GLS, and a decrease in LV twist. 2D GLS and LVMi were predictive of incomplete reverse remodeling during the one-year follow-up period after aortic valve replacement. 3D strain parameters did not add discriminatory or predictive information over 2D GLS.

7 POINTS OF PERSPECTIVE

7.1 3D ECHOCARDIOGRAPHIC ASSESSMENT OF LV REMODELING

There is a rapid and continuing development in echocardiographic techniques and quantification software. When Studies I and II were conceptualized in 2007, transthoracic 3DE was still a relatively new technique that required a dedicated and rather bulky 3D transducer and specialized stand-alone analysis software. Since then, there has been a substantial development in probe technology, including improved parallel beamforming and increased data processing power, allowing for real-time full-volume acquisitions with acceptable image and time resolution. Most vendors offer 3D capability in their standard transthoracic echocardiographic probes today, making 3D acquisitions easier to perform and more readily incorporated into standard study protocols. Furthermore, efforts have been made to implement an advanced automatic analysis of 3D data sets, using pattern recognition and artificial intelligence to allow cardiac chamber quantification not only of the LV but also the left atrium and right ventricle. In Study II, we called for improvements in 3D echocardiographic user interfaces and further development in automatic volume detection algorithms, which have mostly been accommodated today.

Nevertheless, 3DE may not be used in everyday practice even when it is available. One reason for this might be the perception that 3DE is sensitive to reduced image quality and the notion that when the 2D imaging is difficult, the 3D imaging will be even worse. One of the main findings in Study II was that the quantification of LV volumes using 3DE was *less* dependent on image quality than 2DE, meaning that reduced image quality in 2D images should not impede the investigator from trying to acquire and analyze 3D data. Another option in cases with reduced image quality is applying contrast enhancement. In Study II, we found that CE2DE was essentially equal to 3DE in terms of accuracy and reproducibility of LV volume measurements. In that study, we pointed out that one crucial factor hampering its use for this purpose was the lack of reference ("normal") ranges. Recently, one study has reported reference values for CE2DE; however, the sample size of 84 patients was moderate, raising questions about this study's generalizability.[169] Thus, the establishment of valid reference values for contrast-enhanced 2DE remains an important subject for future research.

There are still areas in which 2DE outperforms 3DE, such as superior image and time resolution, making 2DE better suited for detailed analysis of cardiac structures and allowing for cardiac motion analysis with higher precision. The latter was evident in Study IV, where we found that 2D-derived GLS was more sensitive than 3D-derived GLS in detecting an increase in LV longitudinal function during the follow-up period. Furthermore, 2D strain measurements added prognostic value independent of LV mass, whereas the 3D strain measurements did not. Thus, until the performance of 3D echocardiographic data acquisition and analysis algorithms improve, the clinical utility of 3D strain over 2D strain will remain to be demonstrated.

7.2 AORTIC VALVE DISEASE

Echocardiography is key in diagnosing patients with aortic valve disease, monitoring disease progression, and determining when to intervene. In severe AS, the indication for aortic valve replacement is well-established as the time point when the patient starts to experience symptoms because the prognosis of symptomatic AS is dismal if left untreated. However, in some patients, alterations in LV structure and function may be present at the time of intervention and persist even aortic valve replacement because they may have been subject to intervention too late. Study IV aimed at contributing to the knowledge about factors determining cardiac recovery after AVR. Although we examined patients already scheduled for aortic valve replacement, our results may apply to patients with AS even before symptoms occur. The benefit of aortic valve replacement in asymptomatic patients with normal EF remains to be shown, making it an exciting field of research, especially in the current era with the increasing adaptation of percutaneous valve replacement.

The situation is somewhat different in patients with AR. These patients often remain asymptomatic for many years despite having severe valve disease. Compared with AS, severe AR does not carry the same mortality rate even when symptomatic, and patients with AR are generally younger. These factors contribute to making the timing of intervention challenging. Accordingly, the current opinion is to intervene “not too early and not too late.” LV size has shown to be prognostic in these patients and is included in the decision algorithm in current guidelines. In Study III, we found that the volume overload associated with AR affects not only the LV size and systolic function but also LV diastolic function and LA function. Moreover, the LA function had incremental prognostic value in our study group. Indeed, the long-term prognostic implications of LA function in patients with AR have not been explored and warrant further studies.

8 ACKNOWLEDGMENTS

This work would not have been possible without the dedication and hard work of all the people involved in the projects. I am incredibly grateful to everyone who has supported me and my work in one way or another during these years.

I would like to extend my sincere thanks to the following people:

My primary supervisor **Kenneth Caidahl** for inspiring my interest in research, and for his patient guidance, support, and persistence throughout the years.

Maria Eriksson, my co-supervisor, for sharing her incredible knowledge in clinical physiology, for her unwavering support, and for always providing inspiration and encouragement through each stage of my journey both as a clinician and a scientist.

Co-supervisor **Martin Ugander** for sharing his great passion for research, showing me that the R&D department is where all the fun takes place, and for teaching me CMR.

Co-supervisor **Per Eriksson** for his valuable support.

Anders Franco-Cereceda for supervising the ASAP study, thereby providing great opportunities for new insights on aortic valve disease and his valuable suggestions as a co-author.

John Pernow for supervising the PROMISE study and for valuable suggestions as a co-author.

Co-author **Natalie Beitner** for the initiation of Study I, her hard work on the data analysis, and collaboration on the manuscript.

Co-author **Ali Ilami** for his dedication and relentless work on the data analysis for Studies III and IV, and always being incredibly helpful and optimistic.

Flemming Larsen and **Maria Eriksson**, former heads of the Department of Clinical Physiology at Karolinska University Hospital, for facilitating my Ph.D. studies, as well as **Mojgan Montakhaby**, head of the Department of Clinical Physiology at Södersjukhuset, for generously granting me time off to finish the thesis.

Peder Sörensson for introducing me to CMR, encouraging both my clinical and scientific work, and for his contributions to Study I and II.

Mahmood Farasati and **Kamel Ramak** for their excellent performance of echocardiographic examinations.

Margareta Ring for assistance with the data collection and data analysis for Studies I and II.

Dianna Bone and **Frederic Bouvier** for assistance with the data collection for Study I**.**

Jonas Selling for valuable statistical assistance.

All **former colleagues** at the Department of Clinical Physiology, Karolinska University Hospital for their support, especially fellow Ph.D. students **Johan Petrini, Anna Asp**, and **Mohamed Yousry**, for cooperation, friendship, and inspiration.

My dear **co-workers** at the **Department of Clinical Physiology, Södersjukhuset** for their friendship, support, and generosity by covering for me while I am off to do research. Special thanks to **Magnus Lundin** for his valuable suggestions for the thesis.

Fellow researchers of the **Karolinska CMR group** and **Kristoffer Lundbäck** for companionship and support.

Finally, my beloved family **Katarina, Oscar** and **Lucas** for being my greatest inspiration; my mother **Britt** and father **Håkan** for all support and keen interest in my scientific endeavor.

The studies were financially supported by the Swedish Heart-Lung Foundation, the Swedish Research Council, the Söderberg Foundation, Karolinska Institutet, Stockholm County Council, and a generous donation from Fredrik Lundberg

9 REFERENCES

1. Grant C, Greene DG, Bunnell IL. Left ventricular enlargement and hypertrophy. A clinical and angiocardiographic study. *Am J Med.* 1965;39(6):895-904.
2. Klabunde RE. *Cardiovascular physiology concepts.* 2nd ed. Philadelphia: Wolters Kluwer Health/Lippincott Williams & Wilkins; 2012.
3. Chirinos JA, Segers P. Noninvasive evaluation of left ventricular afterload: part 2: arterial pressure-flow and pressure-volume relations in humans. *Hypertension.* 2010;56(4):563-570.
4. Kelly RP, Ting CT, Yang TM, et al. Effective arterial elastance as index of arterial vascular load in humans. *Circulation.* 1992;86(2):513-521.
5. Chemla D, Antony I, Lecarpentier Y, Nitenberg A. Contribution of systemic vascular resistance and total arterial compliance to effective arterial elastance in humans. *Am J Physiol Heart Circ Physiol.* 2003;285(2):H614-620.
6. Briand M, Dumesnil JG, Kadem L, et al. Reduced systemic arterial compliance impacts significantly on left ventricular afterload and function in aortic stenosis: implications for diagnosis and treatment. *J Am Coll Cardiol.* 2005;46(2):291-298.
7. Nagueh SF, Smiseth OA, Appleton CP, et al. Recommendations for the Evaluation of Left Ventricular Diastolic Function by Echocardiography: An Update from the American Society of Echocardiography and the European Association of Cardiovascular Imaging. *Eur Heart J Cardiovasc Imaging.* 2016;17(12):1321-1360.
8. Zaid RR, Barker CM, Little SH, Nagueh SF. Pre- and post-operative diastolic dysfunction in patients with valvular heart disease: diagnosis and therapeutic implications. *J Am Coll Cardiol.* 2013;62(21):1922-1930.
9. Baumgartner H, Falk V, Bax JJ, et al. 2017 ESC/EACTS Guidelines for the management of valvular heart disease. *Eur Heart J.* 2017;38(36):2739-2791.
10. Andell P, Li X, Martinsson A, et al. Epidemiology of valvular heart disease in a Swedish nationwide hospital-based register study. *Heart.* 2017;103(21):1696-1703.
11. Nagy E, Eriksson P, Yousry M, et al. Valvular osteoclasts in calcification and aortic valve stenosis severity. *Int J Cardiol.* 2013;168(3):2264-2271.
12. Carabello BA, Paulus WJ. Aortic stenosis. *Lancet.* 2009;373(9667):956-966.
13. Otto CM. Valvular aortic stenosis: disease severity and timing of intervention. *J Am Coll Cardiol.* 2006;47(11):2141-2151.
14. Ross J, Jr., Braunwald E. Aortic stenosis. *Circulation.* 1968;38(1 Suppl):61-67.
15. Schwarz F, Baumann P, Manthey J, et al. The effect of aortic valve replacement on survival. *Circulation.* 1982;66(5):1105-1110.
16. Iung B, Baron G, Butchart EG, et al. A prospective survey of patients with valvular heart disease in Europe: The Euro Heart Survey on Valvular Heart Disease. *Eur Heart J.* 2003;24(13):1231-1243.
17. Sillesen AS, Vøgg O, Pihl C, et al. Prevalence of Bicuspid Aortic Valve and Associated Aortopathy in Newborns in Copenhagen, Denmark. *Jama.* 2021;325(6):561-567.
18. Tornos Mas P, Lansac E. Aortic regurgitation. *ESC CardioMed (3rd edn)* 2020; www.oxfordmedicine.com, 2020.
19. Singh S, Goyal A. The origin of echocardiography: a tribute to Inge Edler. *Tex Heart Inst J.* 2007;34(4):431-438.
20. Edler I, Lindstrom K. The history of echocardiography. *Ultrasound Med Biol.* 2004;30(12):1565-1644.

21. Evangelista A, Flachskampf F, Lancellotti P, et al. European Association of Echocardiography recommendations for standardization of performance, digital storage and reporting of echocardiographic studies. *Eur J Echocardiogr.* 2008;9(4):438-448.

22. Bot H, Delemarre BJ, Visser CA, Dunning AJ. Signal processing in 2 dimensional Doppler echocardiography. *Int J Card Imaging.* 1987;2(3):173-181.

23. Miyatake K, Yamagishi M, Tanaka N, et al. New method for evaluating left ventricular wall motion by color-coded tissue Doppler imaging: in vitro and in vivo studies. *J Am Coll Cardiol.* 1995;25(3):717-724.

24. Edvardsen T, Gerber BL, Garot J, Bluemke DA, Lima JA, Smiseth OA. Quantitative assessment of intrinsic regional myocardial deformation by Doppler strain rate echocardiography in humans: validation against three-dimensional tagged magnetic resonance imaging. *Circulation.* 2002;106(1):50-56.

25. Mor-Avi V, Lang RM, Badano LP, et al. Current and evolving echocardiographic techniques for the quantitative evaluation of cardiac mechanics: ASE/EAE consensus statement on methodology and indications endorsed by the Japanese Society of Echocardiography. *Eur J Echocardiogr.* 2011;12(3):167-205.

26. Matsumoto M, Inoue M, Tamura S, Tanaka K, Abe H. Three-dimensional echocardiography for spatial visualization and volume calculation of cardiac structures. *J Clin Ultrasound.* 1981;9(4):157-165.

27. Stickels KR, Wann LS. An analysis of three-dimensional reconstructive echocardiography. *Ultrasound Med Biol.* 1984;10(5):575-580.

28. Ludomirsky A, Vermilion R, Nesser J, et al. Transthoracic real-time three-dimensional echocardiography using the rotational scanning approach for data acquisition. *Echocardiography.* 1994;11(6):599-606.

29. Sapin PM, Schroeder KD, Smith MD, DeMaria AN, King DL. Three-dimensional echocardiographic measurement of left ventricular volume in vitro: comparison with two-dimensional echocardiography and cineventriculography. *J Am Coll Cardiol.* 1993;22(5):1530-1537.

30. Gopal AS, Keller AM, Rigling R, King DL, Jr., King DL. Left ventricular volume and endocardial surface area by three-dimensional echocardiography: comparison with two-dimensional echocardiography and nuclear magnetic resonance imaging in normal subjects. *J Am Coll Cardiol.* 1993;22(1):258-270.

31. von Ramm OT, Smith SW. Real time volumetric ultrasound imaging system. *J Digit Imaging.* 1990;3(4):261-266.

32. Caiani EG, Corsi C, Zamorano J, et al. Improved semiautomated quantification of left ventricular volumes and ejection fraction using 3-dimensional echocardiography with a full matrix-array transducer: comparison with magnetic resonance imaging. *J Am Soc Echocardiogr.* 2005;18(8):779-788.

33. Deng CX, Lizzi FL. A review of physical phenomena associated with ultrasonic contrast agents and illustrative clinical applications. *Ultrasound Med Biol.* 2002;28(3):277-286.

34. Kurt M, Shaikh KA, Peterson L, et al. Impact of contrast echocardiography on evaluation of ventricular function and clinical management in a large prospective cohort. *J Am Coll Cardiol.* 2009;53(9):802-810.

35. Galderisi M, Lauer MS, Levy D. Echocardiographic determinants of clinical outcome in subjects with coronary artery disease (the Framingham Heart Study). *Am J Cardiol.* 1992;70(11):971-976.

36. White HD, Norris RM, Brown MA, Brandt PW, Whitlock RM, Wild CJ. Left ventricular end-systolic volume as the major determinant of survival after recovery from myocardial infarction. *Circulation.* 1987;76(1):44-51.

37. Sharir T, Germano G, Kang X, et al. Prediction of myocardial infarction versus cardiac death by gated myocardial perfusion SPECT: risk stratification by the amount of stress-induced ischemia and the poststress ejection fraction. *J Nucl Med.* 2001;42(6):831-837.

38. Ponikowski P, Voors AA, Anker SD, et al. 2016 ESC Guidelines for the diagnosis and treatment of acute and chronic heart failure: The Task Force for the diagnosis and treatment of acute and chronic heart failure of the European Society of Cardiology (ESC). Developed with the special contribution of the Heart Failure Association (HFA) of the ESC. *Eur J Heart Fail.* 2016;18(8):891-975.

39. Zamorano JL, Lancellotti P, Rodriguez Munoz D, et al. 2016 ESC Position Paper on cancer treatments and cardiovascular toxicity developed under the auspices of the ESC Committee for Practice Guidelines: The Task Force for cancer treatments and cardiovascular toxicity of the European Society of Cardiology (ESC). *Eur Heart J.* 2016;37(36):2768-2801.

40. Solomon SD, Anavekar N, Skali H, et al. Influence of ejection fraction on cardiovascular outcomes in a broad spectrum of heart failure patients. *Circulation.* 2005;112(24):3738-3744.

41. Lauer MS, Evans JC, Levy D. Prognostic implications of subclinical left ventricular dilatation and systolic dysfunction in men free of overt cardiovascular disease (the Framingham Heart Study). *Am J Cardiol.* 1992;70(13):1180-1184.

42. Wang TJ, Evans JC, Benjamin EJ, Levy D, LeRoy EC, Vasan RS. Natural history of asymptomatic left ventricular systolic dysfunction in the community. *Circulation.* 2003;108(8):977-982.

43. Aurigemma GP, Silver KH, Priest MA, Gaasch WH. Geometric changes allow normal ejection fraction despite depressed myocardial shortening in hypertensive left ventricular hypertrophy. *J Am Coll Cardiol.* 1995;26(1):195-202.

44. Starling MR, Kirsh MM, Montgomery DG, Gross MD. Impaired left ventricular contractile function in patients with long-term mitral regurgitation and normal ejection fraction. *J Am Coll Cardiol.* 1993;22(1):239-250.

45. Lang RM, Badano LP, Mor-Avi V, et al. Recommendations for cardiac chamber quantification by echocardiography in adults: an update from the American Society of Echocardiography and the European Association of Cardiovascular Imaging. *Eur Heart J Cardiovasc Imaging.* 2015;16(3):233-270.

46. Torrent-Guasp F, Ballester M, Buckberg GD, et al. Spatial orientation of the ventricular muscle band: physiologic contribution and surgical implications. *J Thorac Cardiovasc Surg.* 2001;122(2):389-392.

47. Stoylen A, Dalen H, Molmen HE. Left ventricular longitudinal shortening: relation to stroke volume and ejection fraction in ageing, blood pressure, body size and gender in the HUNT3 study. *Open Heart.* 2020;7(2).

48. Carlsson M, Ugander M, Mosen H, Buhre T, Arheden H. Atrioventricular plane displacement is the major contributor to left ventricular pumping in healthy adults, athletes, and patients with dilated cardiomyopathy. *Am J Physiol Heart Circ Physiol.* 2007;292(3):H1452-1459.

49. D'Hooge J, Heimdal A, Jamal F, et al. Regional strain and strain rate measurements by cardiac ultrasound: principles, implementation and limitations. *Eur J Echocardiogr.* 2000;1(3):154-170.

50. Urheim S, Edvardsen T, Torp H, Angelsen B, Smiseth OA. Myocardial strain by Doppler echocardiography. Validation of a new method to quantify regional myocardial function. *Circulation.* 2000;102(10):1158-1164.

51. Kaluzynski K, Chen X, Emelianov SY, Skovoroda AR, O'Donnell M. Strain rate imaging using two-dimensional speckle tracking. *IEEE Trans Ultrason Ferroelectr Freq Control.* 2001;48(4):1111-1123.

52. Voigt JU, Pedrizzetti G, Lysyansky P, et al. Definitions for a common standard for 2D speckle tracking echocardiography: consensus document of the EACVI/ASE/Industry Task Force to standardize deformation imaging. *Eur Heart J Cardiovasc Imaging.* 2015;16(1):1-11.

53. Seo Y, Ishizu T, Enomoto Y, et al. Validation of 3-dimensional speckle tracking imaging to quantify regional myocardial deformation. *Circ Cardiovasc Imaging.* 2009;2(6):451-459.

54. Pedrizzetti G, Kraigher-Krainer E, De Luca A, et al. Functional strain-line pattern in the human left ventricle. *Phys Rev Lett.* 2012;109(4):048103.

55. Owan TE, Hodge DO, Herges RM, Jacobsen SJ, Roger VL, Redfield MM. Trends in prevalence and outcome of heart failure with preserved ejection fraction. *N Engl J Med.* 2006;355(3):251-259.

56. Redfield MM, Jacobsen SJ, Burnett JC, Jr., Mahoney DW, Bailey KR, Rodeheffer RJ. Burden of systolic and diastolic ventricular dysfunction in the community: appreciating the scope of the heart failure epidemic. *JAMA.* 2003;289(2):194-202.

57. Badano LP, Albanese MC, De Biaggio P, et al. Prevalence, clinical characteristics, quality of life, and prognosis of patients with congestive heart failure and isolated left ventricular diastolic dysfunction. *J Am Soc Echocardiogr.* 2004;17(3):253-261.

58. Biesiadecki BJ, Davis JP, Ziolo MT, Janssen PML. Tri-modal regulation of cardiac muscle relaxation; intracellular calcium decline, thin filament deactivation, and cross-bridge cycling kinetics. *Biophys Rev.* 2014;6(3-4):273-289.

59. Maksuti E, Carlsson M, Arheden H, Kovacs SJ, Broome M, Ugander M. Hydraulic forces contribute to left ventricular diastolic filling. *Sci Rep.* 2017;7:43505.

60. Nagueh SF, Appleton CP, Gillebert TC, et al. Recommendations for the evaluation of left ventricular diastolic function by echocardiography. *Eur J Echocardiogr.* 2009;10(2):165-193.

61. Nagueh SF. Non-invasive assessment of left ventricular filling pressure. *Eur J Heart Fail.* 2018;20(1):38-48.

62. Henein MY, Lindqvist P. Diastolic function assessment by echocardiography: A practical manual for clinical use and future applications. *Echocardiography.* 2020;37(11):1908-1918.

63. Andersen OS, Smiseth OA, Dokainish H, et al. Estimating Left Ventricular Filling Pressure by Echocardiography. *J Am Coll Cardiol.* 2017;69(15):1937-1948.

64. Hoit BD. Left atrial size and function: role in prognosis. *J Am Coll Cardiol.* 2014;63(6):493-505.

65. Barbier P, Solomon SB, Schiller NB, Glantz SA. Left atrial relaxation and left ventricular systolic function determine left atrial reservoir function. *Circulation.* 1999;100(4):427-436.

66. Myerson SG, Holloway CJ, Francis JM, Neubauer S. Cardiovascular magnetic resonance (CMR)--an update and review. *Prog Nucl Magn Reson Spectrosc.* 2011;59(3):213-222.

67. American College of Cardiology Foundation Task Force on Expert Consensus D, Hundley WG, Bluemke DA, et al. ACCF/ACR/AHA/NASCI/SCMR 2010 expert consensus document on cardiovascular magnetic resonance: a report of the American College of Cardiology Foundation Task Force on Expert Consensus Documents. *J Am Coll Cardiol.* 2010;55(23):2614-2662.

68. Bellenger NG, Davies LC, Francis JM, Coats AJ, Pennell DJ. Reduction in sample size for studies of remodeling in heart failure by the use of cardiovascular magnetic resonance. *J Cardiovasc Magn Reson.* 2000;2(4):271-278.

69. Abbott BG, Case JA, Dorbala S, et al. Contemporary Cardiac SPECT Imaging-Innovations and Best Practices: An Information Statement from the American Society of Nuclear Cardiology. *J Nucl Cardiol.* 2018;25(5):1847-1860.

70. Grucker D, Florentz P, Oswald T, Chambron J. Myocardial gated tomoscintigraphy with 99Tcm-methoxy-isobutyl-isonitrile (MIBI): regional and temporal activity curve analysis. *Nucl Med Commun.* 1989;10(10):723-732.

71. Germano G, Kiat H, Kavanagh PB, et al. Automatic quantification of ejection fraction from gated myocardial perfusion SPECT. *J Nucl Med.* 1995;36(11):2138-2147.

72. Sorensson P, Saleh N, Bouvier F, et al. Effect of postconditioning on infarct size in patients with ST elevation myocardial infarction. *Heart.* 2010;96(21):1710-1715.

73. Jackson V, Petrini J, Caidahl K, et al. Bicuspid aortic valve leaflet morphology in relation to aortic root morphology: a study of 300 patients undergoing open-heart surgery. *Eur J Cardiothorac Surg.* 2011;40(3):e118-124.

74. Baumgartner H, Hung J, Bermejo J, et al. Recommendations on the Echocardiographic Assessment of Aortic Valve Stenosis: A Focused Update from the European Association of Cardiovascular Imaging and the American Society of Echocardiography. *J Am Soc Echocardiogr.* 2017;30(4):372-392.

75. Zoghbi WA, Adams D, Bonow RO, et al. Recommendations for Noninvasive Evaluation of Native Valvular Regurgitation: A Report from the American Society of Echocardiography Developed in Collaboration with the Society for Cardiovascular Magnetic Resonance. *J Am Soc Echocardiogr.* 2017;30(4):303-371.

76. Cerqueira MD, Weissman NJ, Dilsizian V, et al. Standardized myocardial segmentation and nomenclature for tomographic imaging of the heart. A statement for healthcare professionals from the Cardiac Imaging Committee of the Council on Clinical Cardiology of the American Heart Association. *Circulation.* 2002;105(4):539-542.

77. Badano LP, Kolias TJ, Muraru D, et al. Standardization of left atrial, right ventricular, and right atrial deformation imaging using two-dimensional speckle tracking echocardiography: a consensus document of the EACVI/ASE/Industry Task Force to standardize deformation imaging. *Eur Heart J Cardiovasc Imaging.* 2018;19(6):591-600.

78. Takeuchi M, Nishikage T, Mor-Avi V, et al. Measurement of left ventricular mass by real-time three-dimensional echocardiography: validation against magnetic resonance and comparison with two-dimensional and m-mode measurements. *J Am Soc Echocardiogr.* 2008;21(9):1001-1005.

79. Heiberg E, Sjogren J, Ugander M, Carlsson M, Engblom H, Arheden H. Design and validation of Segment--freely available software for cardiovascular image analysis. *BMC Med Imaging.* 2010;10:1.

80. Landis JR, Koch GG. The measurement of observer agreement for categorical data. *Biometrics.* 1977;33(1):159-174.

81. Bland JM, Altman DG. Statistical methods for assessing agreement between two methods of clinical measurement. *Lancet.* 1986;1(8476):307-310.

82. Holst K, Fyrdahl A, Caidahl K, Ugander M, Sigfridsson A. Projection-based respiratory-resolved left ventricular volume measurements in patients using free-breathing double golden-angle 3D radial acquisition. *Magma.* 2019;32(3):331-341.

83. Dorosz JL, Lezotte DC, Weitzenkamp DA, Allen LA, Salcedo EE. Performance of 3-dimensional echocardiography in measuring left ventricular volumes and ejection fraction: a systematic review and meta-analysis. *J Am Coll Cardiol.* 2012;59(20):1799-1808.

84. Kawel-Boehm N, Maceira A, Valsangiacomo-Buechel ER, et al. Normal values for cardiovascular magnetic resonance in adults and children. *J Cardiovasc Magn Reson.* 2015;17(1):29.

85. Mor-Avi V, Jenkins C, Kuhl HP, et al. Real-time 3-dimensional echocardiographic quantification of left ventricular volumes: multicenter study for validation with magnetic resonance imaging and investigation of sources of error. *JACC Cardiovasc Imaging.* 2008;1(4):413-423.

86. Chan J, Jenkins C, Khafagi F, Du L, Marwick TH. What is the optimal clinical technique for measurement of left ventricular volume after myocardial infarction? A comparative study of 3-dimensional echocardiography, single photon emission computed tomography, and cardiac magnetic resonance imaging. *J Am Soc Echocardiogr.* 2006;19(2):192-201.

87. Hyun IY, Kwan J, Park KS, Lee WH. Reproducibility of Tl-201 and Tc-99m sestamibi gated myocardial perfusion SPECT measurement of myocardial function. *J Nucl Cardiol.* 2001;8(2):182-187.

88. Persson E, Carlsson M, Palmer J, Pahlm O, Arheden H. Evaluation of left ventricular volumes and ejection fraction by automated gated myocardial SPECT versus cardiovascular magnetic resonance. *Clin Physiol Funct Imaging.* 2005;25(3):135-141.

89. Bax JJ, Lamb H, Dibbets P, et al. Comparison of gated single-photon emission computed tomography with magnetic resonance imaging for evaluation of left ventricular function in ischemic cardiomyopathy. *Am J Cardiol.* 2000;86(12):1299-1305.

90. Bavelaar-Croon CD, Kayser HW, van der Wall EE, et al. Left ventricular function: correlation of quantitative gated SPECT and MR imaging over a wide range of values. *Radiology.* 2000;217(2):572-575.

91. Lipiec P, Wejner-Mik P, Krzeminska-Pakula M, et al. Gated 99mTc-MIBI single-photon emission computed tomography for the evaluation of left ventricular ejection fraction: comparison with three-dimensional echocardiography. *Ann Nucl Med.* 2008;22(8):723-726.

92. Papachristidis A, Galli E, Geleijnse ML, et al. Standardized Delineation of Endocardial Boundaries in Three-Dimensional Left Ventricular Echocardiograms. *J Am Soc Echocardiogr.* 2017;30(11):1059-1069.

93. Jenkins C, Bricknell K, Chan J, Hanekom L, Marwick TH. Comparison of two- and three-dimensional echocardiography with sequential magnetic resonance imaging for evaluating left ventricular volume and ejection fraction over time in patients with healed myocardial infarction. *Am J Cardiol.* 2007;99(3):300-306.

94. Pouleur AC, le Polain de Waroux JB, Pasquet A, et al. Assessment of left ventricular mass and volumes by three-dimensional echocardiography in patients with or without wall motion abnormalities: comparison against cine magnetic resonance imaging. *Heart.* 2008;94(8):1050-1057.

95. Tamborini G, Piazzese C, Lang RM, et al. Feasibility and Accuracy of Automated Software for Transthoracic Three-Dimensional Left Ventricular Volume and Function Analysis: Comparisons with Two-Dimensional Echocardiography, Three-Dimensional Transthoracic Manual Method, and Cardiac Magnetic Resonance Imaging. *J Am Soc Echocardiogr.* 2017;30(11):1049-1058.

96. Liu SK, Magid NR, Fox PR, Goldfine SM, Borer JS. Fibrosis, myocyte degeneration and heart failure in chronic experimental aortic regurgitation. *Cardiology.* 1998;90(2):101-109.

97. Borer JS, Truter S, Herrold EM, et al. Myocardial fibrosis in chronic aortic regurgitation: molecular and cellular responses to volume overload. *Circulation.* 2002;105(15):1837-1842.

98. Taniguchi K, Nakano S, Kawashima Y, et al. Left ventricular ejection performance, wall stress, and contractile state in aortic regurgitation before and after aortic valve replacement. *Circulation.* 1990;82(3):798-807.

99. Moorjani N, Westaby S, Narula J, et al. Effects of left ventricular volume overload on mitochondrial and death-receptor-mediated apoptotic pathways in the transition to heart failure. *Am J Cardiol.* 2009;103(9):1261-1268.

100. Dujardin KS, Enriquez-Sarano M, Schaff HV, Bailey KR, Seward JB, Tajik AJ. Mortality and morbidity of aortic regurgitation in clinical practice. A long-term follow-up study. *Circulation.* 1999;99(14):1851-1857.

101. Verseckaite R, Mizariene V, Montvilaite A, et al. The predictive value of left ventricular myocardium mechanics evaluation in asymptomatic patients with aortic regurgitation and preserved left ventricular ejection fraction. A long-term speckle-tracking echocardiographic study. *Echocardiography.* 2018;35(9):1277-1288.

102. Bonow RO, Lakatos E, Maron BJ, Epstein SE. Serial long-term assessment of the natural history of asymptomatic patients with chronic aortic regurgitation and normal left ventricular systolic function. *Circulation.* 1991;84(4):1625-1635.

103. Chaliki HP, Mohty D, Avierinos JF, et al. Outcomes after aortic valve replacement in patients with severe aortic regurgitation and markedly reduced left ventricular function. *Circulation.* 2002;106(21):2687-2693.

104. Henry WL, Bonow RO, Borer JS, et al. Observations on the optimum time for operative intervention for aortic regurgitation. I. Evaluation of the results of aortic valve replacement in symptomatic patients. *Circulation.* 1980;61(3):471-483.

105. Tornos P, Sambola A, Permanyer-Miralda G, Evangelista A, Gomez Z, Soler-Soler J. Long-term outcome of surgically treated aortic regurgitation: influence of guideline adherence toward early surgery. *J Am Coll Cardiol.* 2006;47(5):1012-1017.

106. Villari B, Hess OM, Kaufmann P, Krogmann ON, Grimm J, Krayenbuehl HP. Effect of aortic valve stenosis (pressure overload) and regurgitation (volume overload) on left ventricular systolic and diastolic function. *Am J Cardiol.* 1992;69(9):927-934.

107. Genovese D, Singh A, Volpato V, et al. Load Dependency of Left Atrial Strain in Normal Subjects. *J Am Soc Echocardiogr.* 2018;31(11):1221-1228.

108. Singh A, Addetia K, Maffessanti F, Mor-Avi V, Lang RM. LA Strain for Categorization of LV Diastolic Dysfunction. *JACC Cardiovasc Imaging.* 2017;10(7):735-743.

109. Cayli M, Kanadasi M, Akpinar O, Usal A, Poyrazoglu H. Diastolic function predicts outcome after aortic valve replacement in patients with chronic severe aortic regurgitation. *Clin Cardiol.* 2009;32(8):E19-23.

110. Ma W, Zhang W, Shi W, Kong Y, Ma X. Left Ventricular Diastolic Function After Aortic Valve Replacement for Chronic Aortic Regurgitation. *Ann Thorac Surg.* 2018;106(1):24-29.

111. Villari B, Sossalla S, Ciampi Q, et al. Persistent diastolic dysfunction late after valve replacement in severe aortic regurgitation. *Circulation.* 2009;120(23):2386-2392.

112. Alashi A, Mentias A, Abdallah A, et al. Incremental Prognostic Utility of Left Ventricular Global Longitudinal Strain in Asymptomatic Patients With Significant Chronic Aortic Regurgitation and Preserved Left Ventricular Ejection Fraction. *JACC Cardiovasc Imaging.* 2018;11(5):673-682.

113. Ewe SH, Haeck ML, Ng AC, et al. Detection of subtle left ventricular systolic dysfunction in patients with significant aortic regurgitation and preserved left ventricular ejection fraction: speckle tracking echocardiographic analysis. *Eur Heart J Cardiovasc Imaging.* 2015;16(9):992-999.

114. Forsberg LM, Nylander E, Tamas E. Exercise echocardiography predicts postoperative left ventricular remodeling in aortic regurgitation. *Scand Cardiovasc J.* 2014;48(1):4-12.

115. Olsen NT, Sogaard P, Larsson HB, et al. Speckle-tracking echocardiography for predicting outcome in chronic aortic regurgitation during conservative management and after surgery. *JACC Cardiovasc Imaging.* 2011;4(3):223-230.

116. Alashi A, Khullar T, Mentias A, et al. Long-Term Outcomes After Aortic Valve Surgery in Patients With Asymptomatic Chronic Aortic Regurgitation and Preserved LVEF: Impact of Baseline and Follow-Up Global Longitudinal Strain. *JACC Cardiovasc Imaging.* 2020;13(1 Pt 1):12-21.

117. Burns AT, La Gerche A, D'Hooge J, MacIsaac AI, Prior DL. Left ventricular strain and strain rate: characterization of the effect of load in human subjects. *Eur J Echocardiogr.* 2010;11(3):283-289.

118. Weidemann F, Jamal F, Sutherland GR, et al. Myocardial function defined by strain rate and strain during alterations in inotropic states and heart rate. *Am J Physiol Heart Circ Physiol.* 2002;283(2):H792-799.

119. Vollema EM, Singh GK, Prihadi EA, et al. Time course of left ventricular remodelling and mechanics after aortic valve surgery: aortic stenosis vs. aortic regurgitation. *Eur Heart J Cardiovasc Imaging.* 2019;20(10):1105-1111.

120. Pomerantz BJ, Wollmuth JR, Krock MD, et al. Myocardial systolic strain is decreased after aortic valve replacement in patients with aortic insufficiency. *Ann Thorac Surg.* 2005;80(6):2186-2192.

121. Smedsrud MK, Pettersen E, Gjesdal O, et al. Detection of left ventricular dysfunction by global longitudinal systolic strain in patients with chronic aortic regurgitation. *J Am Soc Echocardiogr.* 2011;24(11):1253-1259.

122. Grossman W, Jones D, McLaurin LP. Wall stress and patterns of hypertrophy in the human left ventricle. *J Clin Invest.* 1975;56(1):56-64.

123. Grossman W, Paulus WJ. Myocardial stress and hypertrophy: a complex interface between biophysics and cardiac remodeling. *J Clin Invest.* 2013;123(9):3701-3703.

124. Rassi AN, Pibarot P, Elmariah S. Left ventricular remodelling in aortic stenosis. *Can J Cardiol.* 2014;30(9):1004-1011.

125. Dweck MR, Joshi S, Murigu T, et al. Left ventricular remodeling and hypertrophy in patients with aortic stenosis: insights from cardiovascular magnetic resonance. *J Cardiovasc Magn Reson.* 2012;14:50.

126. Kupari M, Turto H, Lommi J. Left ventricular hypertrophy in aortic valve stenosis: preventive or promotive of systolic dysfunction and heart failure? *Eur Heart J.* 2005;26(17):1790-1796.

127. Cioffi G, Faggiano P, Vizzardi E, et al. Prognostic effect of inappropriately high left ventricular mass in asymptomatic severe aortic stenosis. *Heart.* 2011;97(4):301-307.

128. You J, Wu J, Zhang Q, et al. Differential cardiac hypertrophy and signaling pathways in pressure versus volume overload. *Am J Physiol Heart Circ Physiol.* 2018;314(3):H552-H562.

129. Hein S, Arnon E, Kostin S, et al. Progression from compensated hypertrophy to failure in the pressure-overloaded human heart: structural deterioration and compensatory mechanisms. *Circulation.* 2003;107(7):984-991.

130. Chin CWL, Everett RJ, Kwiecinski J, et al. Myocardial Fibrosis and Cardiac Decompensation in Aortic Stenosis. *JACC Cardiovasc Imaging.* 2017;10(11):1320-1333.

131. Bech-Hanssen O, Caidahl K, Wall B, Myken P, Larsson S, Wallentin I. Influence of aortic valve replacement, prosthesis type, and size on functional outcome and ventricular mass in patients with aortic stenosis. *J Thorac Cardiovasc Surg.* 1999;118(1):57-65.

132. Gelsomino S, Frassani R, Morocutti G, et al. Time course of left ventricular remodeling after stentless aortic valve replacement. *Am Heart J.* 2001;142(3):556-562.

133. Kuhl HP, Franke A, Puschmann D, Schondube FA, Hoffmann R, Hanrath P. Regression of left ventricular mass one year after aortic valve replacement for pure severe aortic stenosis. *Am J Cardiol.* 2002;89(4):408-413.

134. Lund O, Erlandsen M. Changes in left ventricular function and mass during serial investigations after valve replacement for aortic stenosis. *J Heart Valve Dis.* 2000;9(4):583-593.

135. Maselli D, Pizio R, Bruno LP, Di Bella I, De Gasperis C. Left ventricular mass reduction after aortic valve replacement: homografts, stentless and stented valves. *Ann Thorac Surg.* 1999;67(4):966-971.

136. Ali A, Patel A, Ali Z, et al. Enhanced left ventricular mass regression after aortic valve replacement in patients with aortic stenosis is associated with improved long-term survival. *J Thorac Cardiovasc Surg.* 2011;142(2):285-291.

137. Chau KH, Douglas PS, Pibarot P, et al. Regression of Left Ventricular Mass After Transcatheter Aortic Valve Replacement: The PARTNER Trials and Registries. *J Am Coll Cardiol.* 2020;75(19):2446-2458.

138. Izumi C, Kitai T, Kume T, et al. Effect of Left Ventricular Reverse Remodeling on Long-term Outcomes After Aortic Valve Replacement. *Am J Cardiol.* 2019;124(1):105-112.

139. Villari B, Vassalli G, Monrad ES, Chiariello M, Turina M, Hess OM. Normalization of diastolic dysfunction in aortic stenosis late after valve replacement. *Circulation.* 1995;91(9):2353-2358.

140. Everett RJ, Tastet L, Clavel MA, et al. Progression of Hypertrophy and Myocardial Fibrosis in Aortic Stenosis: A Multicenter Cardiac Magnetic Resonance Study. *Circ Cardiovasc Imaging.* 2018;11(6):e007451.

141. Hanayama N, Christakis GT, Mallidi HR, et al. Determinants of incomplete left ventricular mass regression following aortic valve replacement for aortic stenosis. *J Card Surg.* 2005;20(4):307-313.

142. Alenezi F, Fudim M, Rymer J, et al. Predictors and Changes in Cardiac Hemodynamics and Geometry With Transcatheter Aortic Valve Implantation. *Am J Cardiol.* 2019;123(5):813-819.

143. Weidemann F, Herrmann S, Stork S, et al. Impact of myocardial fibrosis in patients with symptomatic severe aortic stenosis. *Circulation.* 2009;120(7):577-584.

144. Potter E, Marwick TH. Assessment of Left Ventricular Function by Echocardiography: The Case for Routinely Adding Global Longitudinal Strain to Ejection Fraction. *JACC Cardiovasc Imaging.* 2018;11(2 Pt 1):260-274.

145. Dumesnil JG, Shoucri RM. Effect of the geometry of the left ventricle on the calculation of ejection fraction. *Circulation.* 1982;65(1):91-98.

146. Wandt B, Bojo L, Tolagen K, Wranne B. Echocardiographic assessment of ejection fraction in left ventricular hypertrophy. *Heart.* 1999;82(2):192-198.

147. Stokke TM, Hasselberg NE, Smedsrud MK, et al. Geometry as a Confounder When Assessing Ventricular Systolic Function: Comparison Between Ejection Fraction and Strain. *J Am Coll Cardiol.* 2017;70(8):942-954.

148. Rajappan K, Rimoldi OE, Dutka DP, et al. Mechanisms of coronary microcirculatory dysfunction in patients with aortic stenosis and angiographically normal coronary arteries. *Circulation.* 2002;105(4):470-476.

149. Bombardini T. Myocardial contractility in the echo lab: molecular, cellular and pathophysiological basis. *Cardiovasc Ultrasound.* 2005;3:27.

150. Slimani A, Melchior J, de Meester C, et al. Relative Contribution of Afterload and Interstitial Fibrosis to Myocardial Function in Severe Aortic Stenosis. *JACC Cardiovasc Imaging.* 2020;13(2 Pt 2):589-600.

151. Pedrizzetti G, Sengupta S, Caracciolo G, et al. Three-dimensional principal strain analysis for characterizing subclinical changes in left ventricular function. *J Am Soc Echocardiogr.* 2014;27(10):1041-1050 e1041.

152. Stefani L, De Luca A, Toncelli L, Pedrizzetti G, Galanti G. 3D Strain helps relating LV function to LV and structure in athletes. *Cardiovasc Ultrasound.* 2014;12:33.

153. Ingels NB, Jr., Hansen DE, Daughters GT, 2nd, Stinson EB, Alderman EL, Miller DC. Relation between longitudinal, circumferential, and oblique shortening and torsional deformation in the left ventricle of the transplanted human heart. *Circ Res.* 1989;64(5):915-927.

154. Santoro A, Alvino F, Antonelli G, et al. Left ventricular twisting modifications in patients with left ventricular concentric hypertrophy at increasing after-load conditions. *Echocardiography.* 2014;31(10):1265-1273.

155. Tumenbayar M, Yamaguchi K, Yoshitomi H, Endo A, Tanabe K. Increased apical rotation in patients with severe aortic stenosis assessed by three-dimensional speckle tracking imaging. *J Echocardiogr.* 2018;16(1):28-33.

156. van Dalen BM, Tzikas A, Soliman OI, et al. Left ventricular twist and untwist in aortic stenosis. *Int J Cardiol.* 2011;148(3):319-324.

157. Popescu BA, Calin A, Beladan CC, et al. Left ventricular torsional dynamics in aortic stenosis: relationship between left ventricular untwisting and filling pressures. A two-dimensional speckle tracking study. *Eur J Echocardiogr.* 2010;11(5):406-413.

158. Holmes AA, Taub CC, Garcia MJ, Shan J, Slovut DP. Increased apical rotation in severe aortic stenosis is associated with reduced survival: a speckle-tracking study. *J Am Soc Echocardiogr.* 2015;28(11):1294-1301.

159. Lindqvist P, Zhao Y, Bajraktari G, Holmgren A, Henein MY. Aortic valve replacement normalizes left ventricular twist function. *Interact Cardiovasc Thorac Surg.* 2011;12(5):701-706.

160. Mirea O, Pagourelias ED, Duchenne J, et al. Intervendor Differences in the Accuracy of Detecting Regional Functional Abnormalities: A Report From the EACVI-ASE Strain Standardization Task Force. *JACC Cardiovasc Imaging.* 2018;11(1):25-34.

161. Truong VT, Phan HT, Pham KNP, et al. Normal Ranges of Left Ventricular Strain by Three-Dimensional Speckle-Tracking Echocardiography in Adults: A Systematic Review and Meta-Analysis. *J Am Soc Echocardiogr.* 2019;32(12):1586-1597 e1585.

162. Poulsen SH, Sogaard P, Nielsen-Kudsk JE, Egeblad H. Recovery of left ventricular systolic longitudinal strain after valve replacement in aortic stenosis and relation to natriuretic peptides. *J Am Soc Echocardiogr.* 2007;20(7):877-884.

163. Becker M, Kramann R, Dohmen G, et al. Impact of left ventricular loading conditions on myocardial deformation parameters: analysis of early and late changes of myocardial deformation parameters after aortic valve replacement. *J Am Soc Echocardiogr.* 2007;20(6):681-689.

164. Delgado V, Tops LF, van Bommel RJ, et al. Strain analysis in patients with severe aortic stenosis and preserved left ventricular ejection fraction undergoing surgical valve replacement. *Eur Heart J.* 2009;30(24):3037-3047.

165. Rost C, Korder S, Wasmeier G, et al. Sequential changes in myocardial function after valve replacement for aortic stenosis by speckle tracking echocardiography. *Eur J Echocardiogr.* 2010;11(7):584-589.

166. Lindqvist P, Bajraktari G, Molle R, et al. Valve replacement for aortic stenosis normalizes subendocardial function in patients with normal ejection fraction. *Eur J Echocardiogr.* 2010;11(7):608-613.

167. Grabskaya E, Becker M, Altiok E, et al. Impact of transcutaneous aortic valve implantation on myocardial deformation. *Echocardiography.* 2011;28(4):397-401.

168. Giannini C, Petronio AS, Talini E, et al. Early and late improvement of global and regional left ventricular function after transcatheter aortic valve implantation in patients with severe aortic stenosis: an echocardiographic study. *Am J Cardiovasc Dis.* 2011;1(3):264-273.

169. Dahl JS, Videbaek L, Poulsen MK, Rudbaek TR, Pellikka PA, Moller JE. Global strain in severe aortic valve stenosis: relation to clinical outcome after aortic valve replacement. *Circ Cardiovasc Imaging.* 2012;5(5):613-620.

170. Staron A, Bansal M, Kalakoti P, et al. Speckle tracking echocardiography derived 2-dimensional myocardial strain predicts left ventricular function and mass regression in aortic stenosis patients undergoing aortic valve replacement. *Int J Cardiovasc Imaging.* 2013;29(4):797-808.

171. Spethmann S, Baldenhofer G, Dreger H, et al. Recovery of left ventricular and left atrial mechanics in various entities of aortic stenosis 12 months after TAVI. *Eur Heart J Cardiovasc Imaging.* 2014;15(4):389-398.

172. Kamperidis V, Joyce E, Debonnaire P, et al. Left ventricular functional recovery and remodeling in low-flow low-gradient severe aortic stenosis after transcatheter aortic valve implantation. *J Am Soc Echocardiogr.* 2014;27(8):817-825.

173. Kim HJ, Lee SP, Park CS, et al. Different responses of the myocardial contractility by layer following acute pressure unloading in severe aortic stenosis patients. *Int J Cardiovasc Imaging.* 2016;32(2):247-259.

174. Fries B, Liu D, Gaudron P, et al. Role of Global Longitudinal Strain in the Prediction of Outcome in Patients With Severe Aortic Valve Stenosis. *Am J Cardiol.* 2017;120(4):640-647.

175. Corrigan FE, Zhou X, Lisko JC, et al. Mean Aortic pressure gradient and global longitudinal strain recovery after transcatheter aortic valve replacement - A retrospective analysis. *Hellenic J Cardiol.* 2018;59(5):268-271.

176. Lozano Granero VC, Fernández Santos S, Fernández-Golfín C, et al. Immediate improvement of left ventricular mechanics following transcatheter aortic valve replacement. *Cardiol J.* 2018;25(4):487-494.

177. Lozano Granero VC, Fernández Santos S, Fernández-Golfín C, et al. Sustained Improvement of Left Ventricular Strain following Transcatheter Aortic Valve Replacement. *Cardiology.* 2019;143(1):52-61.

178. Dahl Pedersen AL, Povlsen JA, Dybro A, et al. Prevalence and Prognostic Implications of Increased Apical-to-Basal Strain Ratio in Patients with Aortic Stenosis Undergoing Transcatheter Aortic Valve Replacement. *J Am Soc Echocardiogr.* 2020;33(12):1465-1473.

179. Reskovic Luksic V, Postolache A, Martinez C, et al. Global and regional myocardial function and outcomes after transcatheter aortic valve implantation for aortic stenosis and preserved ejection fraction. *J Cardiovasc Med (Hagerstown).* 2020;21(3):238-245.

180. Al-Rashid F, Totzeck M, Saur N, et al. Global longitudinal strain is associated with better outcomes in transcatheter aortic valve replacement. *BMC Cardiovasc Disord.* 2020;20(1):267.

181. Naeim HA, Abuelatta R, Alatawi FO, Khedr L. Assessment of Left Ventricular Mechanics in Patients with Severe Aortic Stenosis after Transcatheter Aortic Valve Implantation: 2-D Speckle Tracking Imaging Study. *J Saudi Heart Assoc.* 2020;32(2):248-255.

182. Carrabba N, Parodi G, Valenti R, Migliorini A, Bellandi B, Antoniucci D. Prognostic value of reverse left ventricular remodeling after primary angioplasty for STEMI. *Atherosclerosis.* 2012;222(1):123-128.

183. Sörensson P. *Effects of postconditioning in ST-elevation myocardial infarction: Assessment of myocardium at risk and infarct size* [Thesis for doctoral degree]. Stockholm: Department of Medicine, Karolinska Institutet; 2011.

184. Mizukoshi K, Takeuchi M, Nagata Y, et al. Normal Values of Left Ventricular Mass Index Assessed by Transthoracic Three-Dimensional Echocardiography. *J Am Soc Echocardiogr.* 2016;29(1):51-61.

185. Mor-Avi V, Sugeng L, Weinert L, et al. Fast measurement of left ventricular mass with real-time three-dimensional echocardiography: comparison with magnetic resonance imaging. *Circulation.* 2004;110(13):1814-1818.

186. Muraru D, Badano LP, Peluso D, et al. Comprehensive analysis of left ventricular geometry and function by three-dimensional echocardiography in healthy adults. *J Am Soc Echocardiogr.* 2013;26(6):618-628.

187. Fukuda S, Watanabe H, Daimon M, et al. Normal values of real-time 3-dimensional echocardiographic parameters in a healthy Japanese population: the JAMP-3D Study. *Circ J.* 2012;76(5):1177-1181.